

AD-A174 634

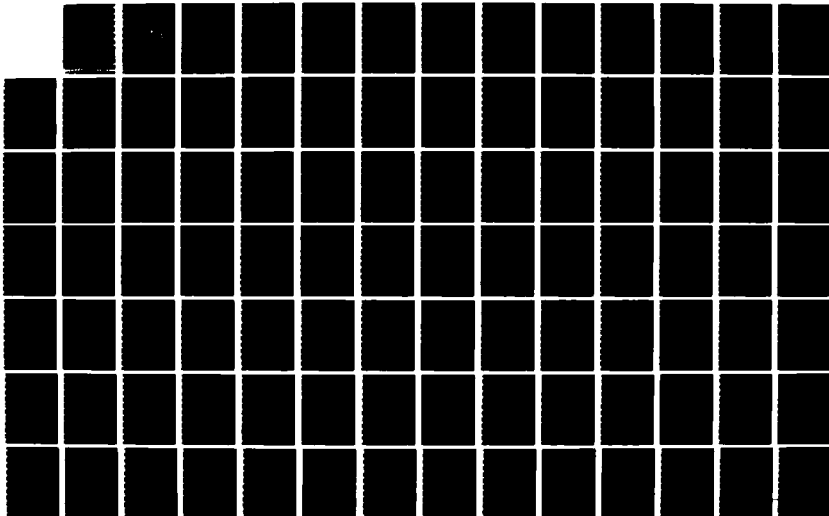
SHORE WAVE MODULATION DUE TO INFRAGRAVITY WAVES IN THE
NEARSHORE ZONE WITH APPLICATIONS(U) NAVAL POSTGRADUATE
SCHOOL MONTEREY CA S M ABDELRAHMAN SEP 86

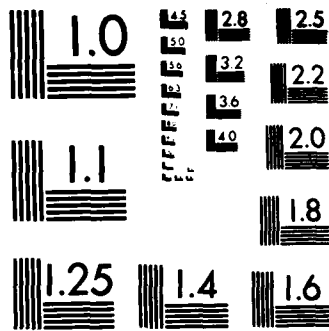
1/2

UNCLASSIFIED

F/G 8/3

NL





MICROCOPY RESOLUTION TEST CHART
NATIONAL BUREAU OF STANDARDS-1963-A

2

AD-A174 634

NAVAL POSTGRADUATE SCHOOL

Monterey, California



DTIC
ELECTE
DEC 3 1986
S B D

THESIS

SHORE WAVE MODULATION DUE TO
INFRAGRAVITY WAVES IN THE
NEARSHORE ZONE, WITH APPLICATIONS

by

Saad M.M. Abdelrahman

September 1986

Dissertation Supervisor: E.B. Thornton

Approved for public release; distribution is unlimited.

DTIC FILE COPY

86 12 02 141

REPORT DOCUMENTATION PAGE

1a REPORT SECURITY CLASSIFICATION Unclassified			1b. RESTRICTIVE MARKINGS		
2a SECURITY CLASSIFICATION AUTHORITY			3 DISTRIBUTION/AVAILABILITY OF REPORT Approved for public release; distribution is unlimited		
2b DECLASSIFICATION/DOWNGRADING SCHEDULE			4 PERFORMING ORGANIZATION REPORT NUMBER(S)		
4 PERFORMING ORGANIZATION REPORT NUMBER(S)			5 MONITORING ORGANIZATION REPORT NUMBER(S)		
6a. NAME OF PERFORMING ORGANIZATION Naval Postgraduate School		6b OFFICE SYMBOL (if applicable) 68	7a. NAME OF MONITORING ORGANIZATION Naval Postgraduate School		
6c ADDRESS (City, State, and ZIP Code) Monterey, California 93943-5000			7b. ADDRESS (City, State, and ZIP Code) Monterey, California 93943-5000		
8a NAME OF FUNDING/SPONSORING ORGANIZATION		8b OFFICE SYMBOL (if applicable)	9. PROCUREMENT INSTRUMENT IDENTIFICATION NUMBER		
8c ADDRESS (City, State, and ZIP Code)			10 SOURCE OF FUNDING NUMBERS		
		PROGRAM ELEMENT NO	PROJECT NO	TASK NO	WORK UNIT ACCESSION NO
11 TITLE (Include Security Classification) SHORT WAVE MODULATION DUE TO INFRAGRAVITY WAVES IN THE NEARSHORE ZONE, WITH APPLICATIONS.					
12 PERSONAL AUTHOR(S) Abdelrahman, Saad M.M.					
13a TYPE OF REPORT Ph.D. Dissertation		13b TIME COVERED FROM TO		14 DATE OF REPORT (Year, Month, Day) 1986 September	15 PAGE COUNT 129
16 SUPPLEMENTARY NOTATION					
17 COSATI CODES			18 SUBJECT TERMS (Continue on reverse if necessary and identify by block number)		
FIELD	GROUP	SUB-GROUP	Infragravity, Sediment transport		
			Longshore Current, Surf zone dynamics.		
19 ABSTRACT (Continue on reverse if necessary and identify by block number) The omni-present low frequency wave motion(30-300 sec) contains a substantial fraction of the total wave energy inside the surf zone. A more complete description of nearshore wave processes considers incident short period waves superposed on, and interacting with, long standing waves. The wind waves are modulated in amplitude, wavenumber and direction due to relatively slowly varying depth changes caused by the long waves. The energy in the wind wave band is enhanced by side band growth at the sum and difference frequencies of short and long waves (order 15% at the shoreline). The modulation is identified in the analysis of field data as a positive correlation between the long waves and the wind wave envelope near the shoreline. Considering oblique incident waves, a steady longshore current showing a non-vanishing current at the shoreline is found as a result of the non-linear interaction between monochromatic incident and infragravity waves. An analytical solution describing the unsteadiness of the longshore current is developed.					
20 DISTRIBUTION/AVAILABILITY OF ABSTRACT <input checked="" type="checkbox"/> UNCLASSIFIED/UNLIMITED <input type="checkbox"/> SAME AS RPT <input type="checkbox"/> DTIC USERS			21 ABSTRACT SECURITY CLASSIFICATION Unclassified		
22a NAME OF RESPONSIBLE INDIVIDUAL E. B. THORNTON			22b TELEPHONE (Include Area Code) (408)646-2847	22c OFFICE SYMBOL 68Tm	

Applying the derived longshore current solution, longshore sediment transport is reformulated to include the infragravity waves, giving improved comparisons with field measurements.



Accession For	
NTIS GRA&I	<input checked="" type="checkbox"/>
DTIC TAB	<input type="checkbox"/>
Unannounced	<input type="checkbox"/>
Justification	
By	
Distribution/	
Availability Codes	
Dist	Avail and/or Special
A-1	

Approved for public release; distribution is unlimited

Short Wave Modulation Due to Infragravity Waves
in the Nearshore Zone, With Applications

by

Saad M.M. Abdelrahman
Ministry of Maritime Transport, Egypt
M.S. Physical Oceanography, Naval Postgraduate School, 1983

Submitted in partial fulfillment of the
requirements for the degree of

DOCTOR OF PHILOSOPHY IN OCEANOGRAPHY

from the

NAVAL POSTGRADUATE SCHOOL
September 1986

Author: Saad M.M. Abdelrahman
SAAD M.M. ABDELRAHMAN

Approved by:

C.H. Wash
C.H. WASH
Professor of Meteorology

C.N.K. Mooers
C.N.K. MOOERS
Professor of Oceanography

A.L. Schoenstadt
A.L. SCHOENSTADT
Professor of Mathematics

R.W. Garwood, Jr.
R.W. GARWOOD, JR.
Professor of Oceanography

E.B. Thornton
E.B. THORNTON
Professor of Oceanography
Dissertation Supervisor

Approved by: E.B. Thornton
E.B. THORNTON, Acting Chairman, Department of Oceanography

Approved by: D.A. Schradly
D.A. SCHRADY, Academic Dean

ABSTRACT

The omni-present low frequency wave motion (30-300 sec) contains a substantial fraction of the total wave energy inside the surf zone. A more complete description of nearshore wave processes considers incident short period wind waves superposed on, and interacting with, long standing waves. The wind waves are modulated in amplitude, wavenumber and direction due to relatively slowly varying depth changes caused by the long waves. The energy in the wind wave band is enhanced by side band growth at the sum and difference frequencies of short and long waves (order 15% at the shoreline). The modulation is identified in the analysis of field data as a positive correlation between the long waves and the wind wave envelope near the shoreline. Considering oblique incident waves, a steady longshore current showing a non-vanishing current at the shoreline is found as a result of the non-linear interaction between monochromatic incident and infragravity waves. An analytical solution describing the unsteadiness of the longshore current is developed. Applying the derived longshore current solution, longshore sediment transport is reformulated to include the infragravity waves, giving improved comparisons with field measurements.

TABLE OF CONTENTS

I.	INTRODUCTION	11
II.	WAVES IN THE NEARSHORE ZONE	21
	A. SHORT PERIOD WAVES	21
	B. LONG PERIOD WAVES	26
	1. Infragravity Wave Models	26
	2. Generation of Infragravity waves	29
III.	SHORT WAVE MODULATION DUE TO LONG WAVES	33
	A. CHANGES IN THE WAVE AMPLITUDE	33
	1. Determination of the Modulated Wave Profile	34
	B. CHANGES IN THE WAVE KINEMATICS	38
	1. Background on Wave Kinematics	38
	2. Kinematics of waves on current	41
	3. Applications	43
	C. CHANGES IN WAVE ENERGY AND MOMENTUM FLUX	49
	1. Background	49
	2. Mass and Momentum Fluxes	54
IV.	DATA ANALYSIS	61
	A. DESCRIPTION OF THE FIELD SITES	61
	B. DATA ANALYSIS	63
	1. Spectral Analysis	64
	2. Cross-Correlation Analysis	70
V.	APPLICATIONS	87
	A. WAVE SETUP AND SETDOWN	87
	1. Background	87
	2. Changes in Setup and Setdown Due to the Presence of Long Waves	89

B.	LONGSHORE CURRENT	93
1.	Background	93
2.	Wave Refraction and Radiation Stress	94
3.	Bottom Shear Stress	95
4.	Longshore Current Models	99
C.	LONGSHORE SEDIMENT TRANSPORT	107
1.	Longshore Sediment Transport due to short and long waves	113
D.	MODEL VALIDATION	114
VI.	SUMMARY AND CONCLUSIONS	118
	BIBLIOGRAPHY	121
	INITIAL DISTRIBUTION LIST	127

LIST OF TABLES

I.	CROSS-CORRELATION BETWEEN THE WAVE ENVELOPE AND LOW FREQUENCY MOTION AT EACH INSTRUMENT (10 NOV., 1978, T.P.)	80
II.	CROSS-CORRELATION BETWEEN THE WAVE ENVELOPE AND LOW FREQUENCY MOTION AT EACH INSTRUMENT (21 NOV., 1978, T. P.)	81
III.	CROSS-CORRELATION BETWEEN THE WAVE ENVELOPE AND LOW FREQUENCY MOTION AT EACH INSTRUMENT (4 FEB., 1980, S.B.)	82
IV.	CROSS-CORRELATION BETWEEN THE WAVE ENVELOPE AND LOW FREQUENCY MOTION AT EACH INSTRUMENT (6 FEB., 1980, S. B.)	83

LIST OF FIGURES

1.1	Surf zone regions and coordinate system	12
1.2	Cross-shore velocity spectra on 20 Nov., 1978, Torrey Pines (after Guza and Thornton, 1985b)	14
1.3	Root mean square wave height H_{rms} vs offshore distance x . Solid curve represents a short wave model and the stars are laboratory data showing non-zero wave height at the shoreline (after Battjes and Stive, 1985)	16
1.4	Longshore current distribution using empirical orthogonal function analysis. The first eignfunction contains most of the variance (after Guza et al., 1986)	18
1.5	Distribution of longshore velocity and sediment transport across the surf zone (after Zenkovich, 1960)	20
2.1	Wave heights inside the surf zone defining breaker index and showing saturation (after Thornton and Guza, 1982)	25
2.2	Modes of edge waves and reflected waves, ϕ is the velocity potential	30
2.3	Dispersion relations for infragravity waves	32
3.1	Wavenumber modulation factor m_k vs non-dimensional distance x/x_b , where x_b is the surf zone width	37
3.2	Behaviour of the Bessel functions $J_0(m_k)$ (solid curve) and $J_1(m_k)$ (dashed curve) across the surf zone	39
3.3	Amplitude square spectra of the modulated short wave at offshore distance: (a) $x = 40.0$ m (b) $x = 0.5$ m	41
3.4	Spatial changes in the wavenumber of short period waves due to the presence of zero mode edge wave	50
3.5	Theoretical wave model to predict energy inside the surf zone, (a)potential energy (b)kinetic energy (c)total energy	55
4.1	Schematic diagram of short and long wave models outside and inside the surf zone	62
4.2	Normalized power spectra at different locations in 10 Nov., T.P., showing an onshore relative increase in the infragravity energy level	65
4.3	Normalized power spectra at different locations in 3 Feb., S.B	67
4.4	Normalized power spectra at different locations in 4 Feb., S.B	68
4.5	Normalized spectra showing significant peaks at frequencies of dominant long wave f_l , short wave f_s and side bands	69
4.6	Spectral time series of current meter CODx with 50% overlapping calculated from four hour record, (4 Feb., 1980, Santa Barbara)	71
4.7	Spatial distribution of band passed velocity variance in 20 Nov., 1978. Low is ($0 < f < 0.05$ Hz) and high is ($0.05 < f < .5$ Hz) (after Guza and Thornton, 1985b)	73

4.8	Segment of the time series for the wave envelope (solid curve) and the associated low frequency (dotted curve) for wave staff W38 (inside the surf zone) in 21 Nov., 1978, Torrey Pines	74
4.9	Segment of the time series for the wave envelope (solid curve) and the associated low frequency (dotted curve) for current meter C07x (outside the surf zone) in 4 Feb., 1980, Santa Barbara	75
4.10	The cross-correlation function for W38, 21 Nov., 1978, Torrey Pines. A positive maximum correlation (.49) corresponds to -4.0 time lag	77
4.11	The cross-correlation function for C07x, 4 Feb., 1980, Santa Barbara. A negative maximum correlation (.29) corresponds to +3.0 time lag	78
4.12	Spatial distribution of cross-correlation coefficients showing a dominant negative correlation outside the surf zone and a positive correlation inside the surf zone. B. L. is the breakcrline	84
4.13	Spatial distribution of cross-correlation coefficients showing a dominant negative correlation outside the surf zone and a positive correlation after midsurf zone	85
4.14	Theoretical model to examine the positive correlation between the wave envelope and the associated low frequency motion within the surf zone, (a) segment of time series (b) cross-correlation function	86
5.1	Wave setup due to both incident and infragravity waves compared with Longuet-Higgins and Stewart model (1962)	92
5.2	Gradient of the longshore current forcing across the surf zone	96
5.3	Unsteady longshore current distribution, at time (a) $t =$ long wave period (b) $t = 1/2$ long wave period	104
5.4	Time variability of the longshore current (a) $x = 2.0$ m (b) $x = 1.0$ m	106
5.5	Steady longshore Current models, with and without lateral mixing term, compared with Longuet-Higgins model (1970a)	108
5.6	Measured longshore sediment transport rate i_y distribution, Santa Barbara (after White and Inman, 1986)	115
5.7	Longshore sediment transport distribution model due to both short and long waves showing a bimodal structure	117

ACKNOWLEDGEMENTS

The author wishes to express sincere thanks and appreciation to professor Edward B. Thornton for providing encouragement, guidance and invaluable advice which invariably motivated the author to continue and finish this work. I express also my appreciation to Dr. C. S. Wu for the time of discussions with me. The assistance of Ms. Donna Burych in providing the processed data is gratefully recognized. Furthermore, appreciation to all my doctoral committee members is expressed for their invaluable discussions.

This dissertation was partially supported by the Office of Naval Research, Coastal Sciences Branch, under Contract NR 388-114.

I. INTRODUCTION

Sea waves are generated by wind, and as they propagate towards the shore they deform due to shoaling and may refract if they are oblique to the bottom contours or if they meet a current. The waves grow in height until they become unstable and break, dissipating their energy. The processes of breaking waves on a sloping bottom make the surf zone an extremely dynamic area where different observable phenomenae take place, such as longshore current, sediment transport and wave runup (setup and swash). Due to this complexity, the proper modeling of wave motion in the nearshore zone has been the goal of many investigators, and yet much remains to be done before a satisfactory understanding is achieved.

The surf zone can be characterized dynamically by three regions: the outer, the inner, and the runup region (Svendson et al., 1978), (see Fig 1.1). The outer region follows the breaking point and is dominated by incident breaking waves. The breaking waves are of either the plunging or spilling type, and are characterized by a rapid transition of wave shape with a horizontal surface roller. In the inner region, the wave forms break down into smaller scales of random and turbulent nature and eventually become similar to moving bores, or hydraulic jumps. The run-up region is characterized by wave setup and swash oscillation running up and down the beach face. In all regions, the wave height and the water motion are strongly locally controlled by the depth. The depth controlled waves are referred to as "saturated."

In general, surf zone dynamics are found to differ dramatically between reflective (steep) beaches and dissipative (gentle slope) beaches (Bradshaw, 1980). Typical features of the reflective beaches are high reflection of incident waves, collapsing or surging breakers on the beach face, and subharmonic resonances (e.g. Guza and Davis, 1974; Guza and Inman, 1975; Huntley and Bowen, 1975b, 1978; Wright et al., 1979). Dissipative beaches are dominated by spilling breakers, pronounced low frequency oscillations and the presence of multiple parallel longshore bars (e.g. Huntley and Bowen, 1975a; Short, 1975; Sasaki and Horikawa, 1975; Holman et al., 1978; Symonds et al., 1982). This study will focus on the dynamics of dissipative beaches in which the inner region is assumed to be a transition region between regions dominated by incident breaking waves and low frequency swash.

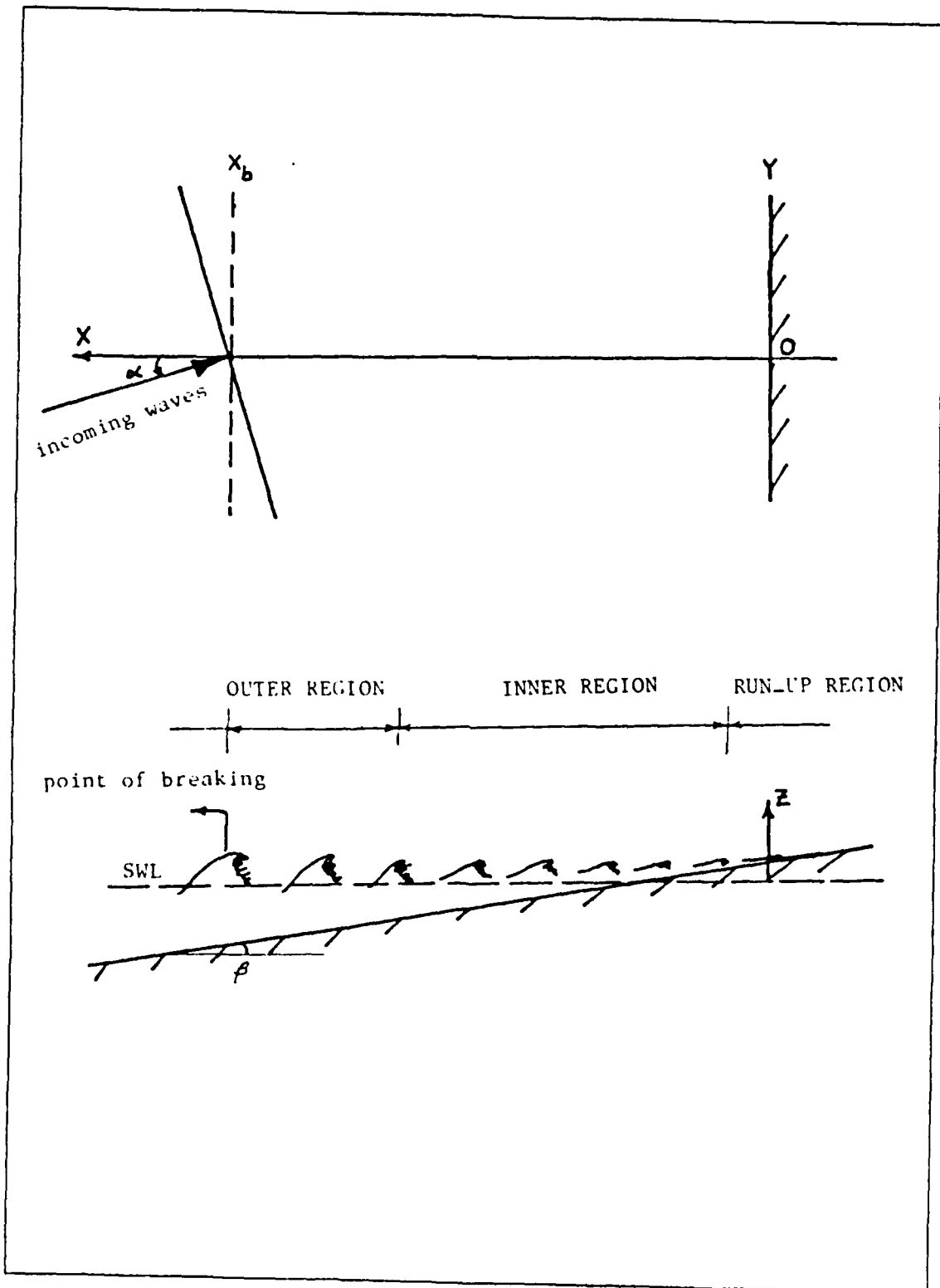


Figure 1.1 Surf zone regions and coordinate system.

In the past decade, considerable attention in the literature of beach and nearshore dynamics has been devoted to the kinematics of low frequency waves. These waves, which have periods ranging from 30-300 sec, are referred to as "infragravity waves." The observations show that the dominant wave motion closer to the shore is not normally at the incident wave frequency band. It is also found that the low frequency wave energy in the very nearshore region contains a substantial fraction of the total wave energy (Inman, 1968 a,b; Suhayda, 1974; Goda, 1975; Huntley and Bowen, 1975b; Sasaki and Horikawa, 1975,1978; Huntley, 1976; Wright et al., 1978,1979,1982; Bradshaw 1980; Holman, 1981; Huntley et al., 1981; Guza and Thornton, 1982,1985a,1985b; and others), (see Fig 1.2 for example). The valley in the energy spectra, where the energy level reaches minimum, suggests an empirical cutoff frequency around 0.03 Hz that separates the two wave bands. Therefore, a complete description of the wave field in the surf zone should include two relatively separated bands of wave frequencies : (1) incident sea-swell waves (short period waves) with periods of 1-30 sec, and (2) infragravity waves (long period waves) with periods of 30-300 sec, which no longer can be neglected inside the surf zone.

Prior to the 1950's, the incident wave characteristics were the main concern when measuring and analyzing waves in the nearshore zone. Munk (1949) and Tucker (1950) were the first to point out the existence and significance of low frequency motion and called the phenomenon "surf beat." More recently, with renewed interest in nearshore processes and with major improvements in the instrumentation, it has become apparent that the low frequency wave energy can be as important as the incident wave energy when approaching the shoreline. Another motivation for the study of the infragravity waves is the coupling between the infragravity length scales (order of hundreds of meters) and the length scales associated with most of the rhythmic beach features such as sand bars, beach cusps and crescentic bars. Many investigators have related the beach morphology changes to the existence of low frequency motions by which a mechanism of forming and maintaining such topographic features is provided (Bowen and Inman, 1971; Guza and Inman, 1975; Bowen, 1980; Holman and Bowen, 1982; Bowen and Huntley, 1984; and others).

In analyzing surf zone data, there are often anomalous patterns of water motion closer to the shoreline when compared with present short wave models. For example, the spatial distribution of wave height measured in both the laboratory and field often shows unexpected wave height at the shoreline (e.g. Suhayda and Pettigrew, 1977;

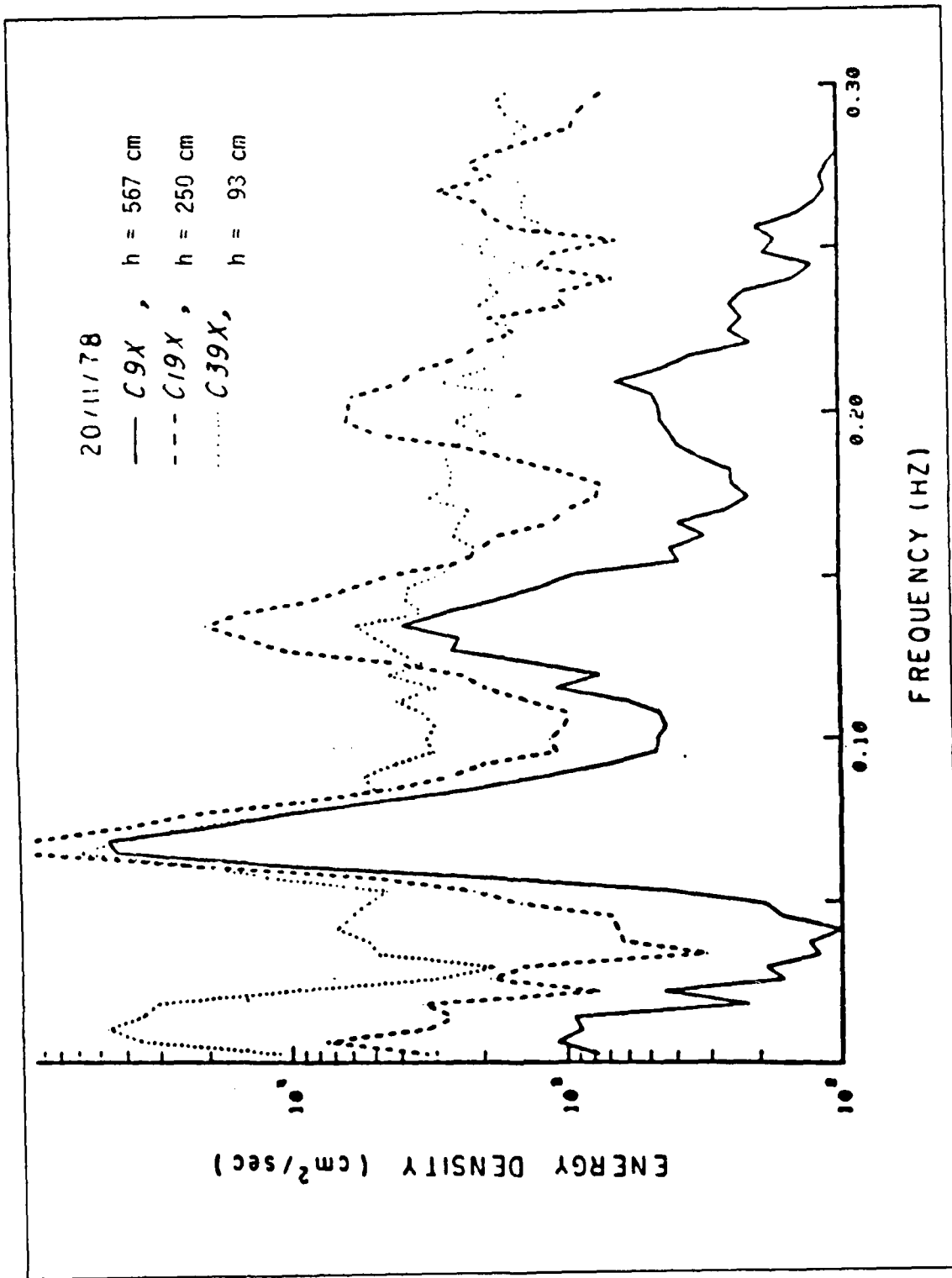


Figure 1.2 Cross-shore velocity spectra on 20 Nov., 1978, Torrey Pines (after Guza and Thornton, 1985b).

Battjes and Stive, 1985), (see for example Fig 1.3). Bowen, et al. (1968), in measuring the setup, found a residual wave height always present at the shoreline and modified their setup formula at the beach face to fit the data. Suhayda and Pettigrew (1977) measured the average wave velocity across the nearshore zone and found it to decrease shoreward until the sea-swash limit of the run-up zone was reached, and then to increase onshore, supporting Waddell's measurement (1973). Thus, the wave height and celerity do not vanish at the vicinity of the shoreline, invalidating the widely applied short wave saturation assumption.

The assumptions of wave saturation and steady state conditions for both monochromatic and random waves, results in a zero current at the shoreline. In addition, the steady longshore current assumption is often unrealistic, especially with the presence of irregular oscillating waves (Wood and Meadows, 1975). This is often seen in field data that show longshore velocity oscillations at longer wave periods than for incident waves (e.g. Holman and Bowen, 1984; Guza and Thornton, 1985a; Oltman-Shay and Guza, 1986). Using an empirical orthogonal function (EOF) analysis on 64 data sets covering a wide variety of wave conditions, Guza et al. (1986) obtained objectively best fit to the longshore current distribution. The analysis showed the "classical parabolic" shape for the longshore current distribution (Bowen, 1969) over most of the surf zone, but with significant residual velocity at the shoreline (Fig. 1.4). In the analysis of the same data, Wu et al., (1985) found a poor agreement between longshore current theory with velocity going to zero at the shoreline and data closer to the shoreline. All present models predict zero current at the shoreline, and no model is available to explain the unsteadiness of longshore current.

Improving the longshore current description is important because it provides the driving means of transporting sediment alongshore (Longuet-Higgins, 1972). The available longshore sediment transport models (e.g. Bijker, 1971; Thornton, 1973; Komar, 1977; Sawaragi and Deguchi, 1979; Bailard, 1981), all show a longshore transport maximum closer to the breakerline, which agrees with the longshore current distribution. The shortcoming of these models is their failure to predict any moving sand at the shoreline regardless of the wave conditions. Zenkovich (1960) measured the suspended sediment transport distribution across the surf zone using fluorescent sand tracers. Sand transport was found greater over bars where energy dissipation is a maximum due to wave breaking and also at the shoreline, (see Fig 1.5). Measuring longshore sand transport distribution using sand tracers, Kraus et al. (1981) found a

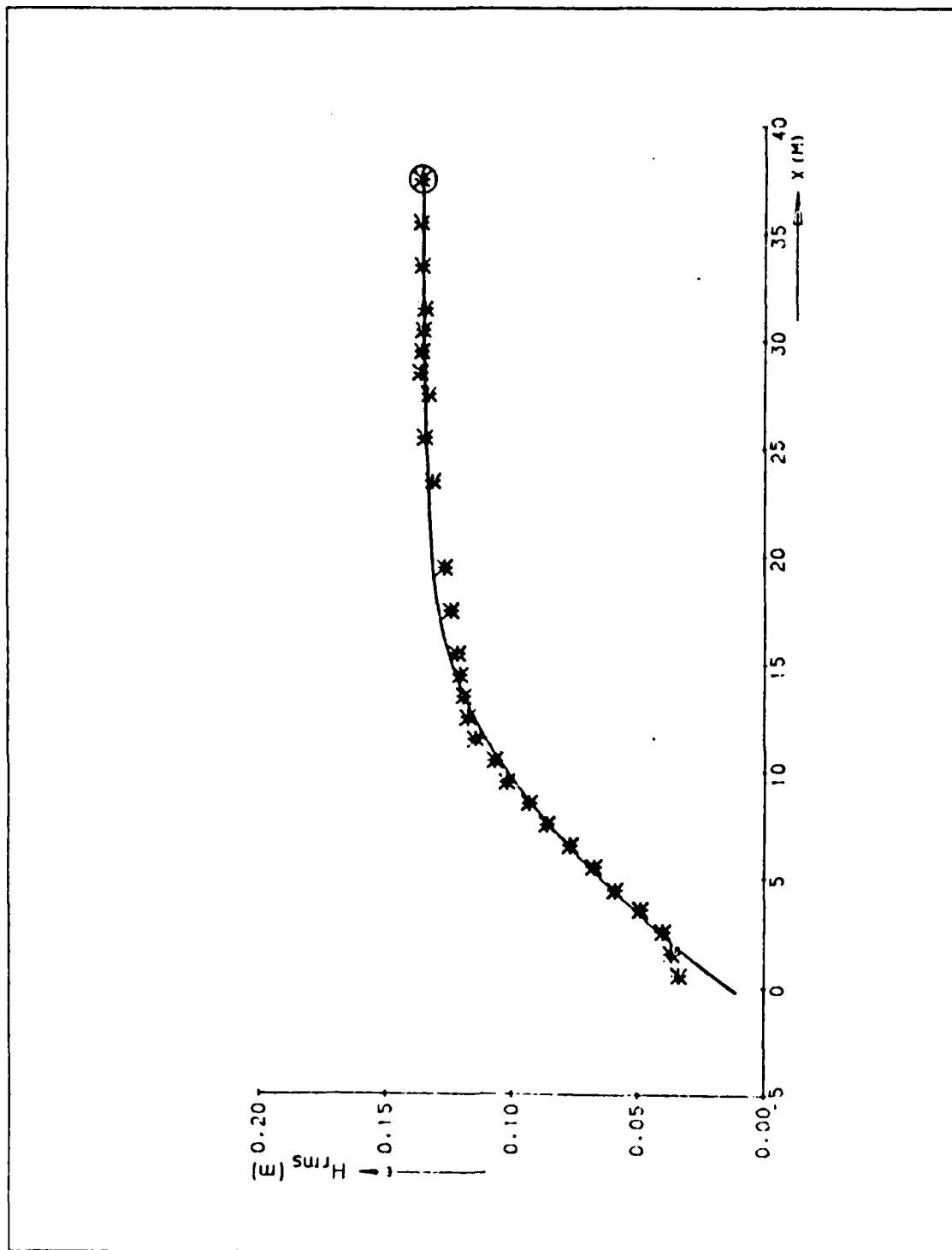


Figure 1.3 Root mean square wave height H_{rms} vs offshore distance x . Solid curve represents a short wave model and the stars are laboratory data showing non-zero wave height at the shoreline (after Battjes and Stive, 1985).

distinct bimodal distribution having maxima at the breakerline and near the shoreline. The same results were obtained by Downing (1984) when measuring the suspended longshore sediment distribution. Abdelrahman (1983) compared longshore sediment transport at Santa Barbara beach with his predicted longshore sediment transport model based on the widely accepted energetic concept by Bagnold (1963). The model did not predict the large transport in the vicinity of the shoreline since theoretical short wave description gives zero amplitude at the shoreline. It was suggested a primary cause of these differences was the presence of infragravity waves, which have not been taken into consideration before.

In recognition of the importance of the infragravity waves in the surf zone, an obvious next improvement in the description of waves kinematics is to combine the infragravity waves with the incident sea-swell. As a result, the incident waves would be modulated in amplitude, wavenumber and direction. The purpose of this dissertation is to improve the understanding of nearshore processes by generating and applying such a composite wave description.

As will be seen, the interaction of the short waves with the long waves results in energy not only at their respective frequencies, but energy transferred to side bands of the incident waves at the sum and difference frequencies. It is the energy and momentum at the side bands that is primarily responsible for the inner surf zone dynamics. The dynamical changes are demonstrated by the successful treatment of using the first order wave description in the momentum flux equation to obtain a second order dynamical effect. However, inclusion of infragravity waves does not mean introducing more independent parameters since the infragravity wave energy is assumed related to the incident wave field.

In the following chapter, a description for the short and long period waves is presented. The short period waves are described by linear (Airy) theory, while the long period waves on a sloping bottom are described by either cross-shore standing waves (2-D) or edge waves (3-D). In chapter 3, the changes in the amplitude and wavenumber of the short waves superposed on long waves are discussed. An analytical expression describing the modulated surface elevation of the short waves is developed along with their energy and momentum. Changes in the wave kinematics are considered with the long period waves treated as a slowly varying current. In chapter 4, narrow banded wave data are analyzed to examine the hypothesis of short wave modulation by the long waves. The dynamical effects of considering the infragravity

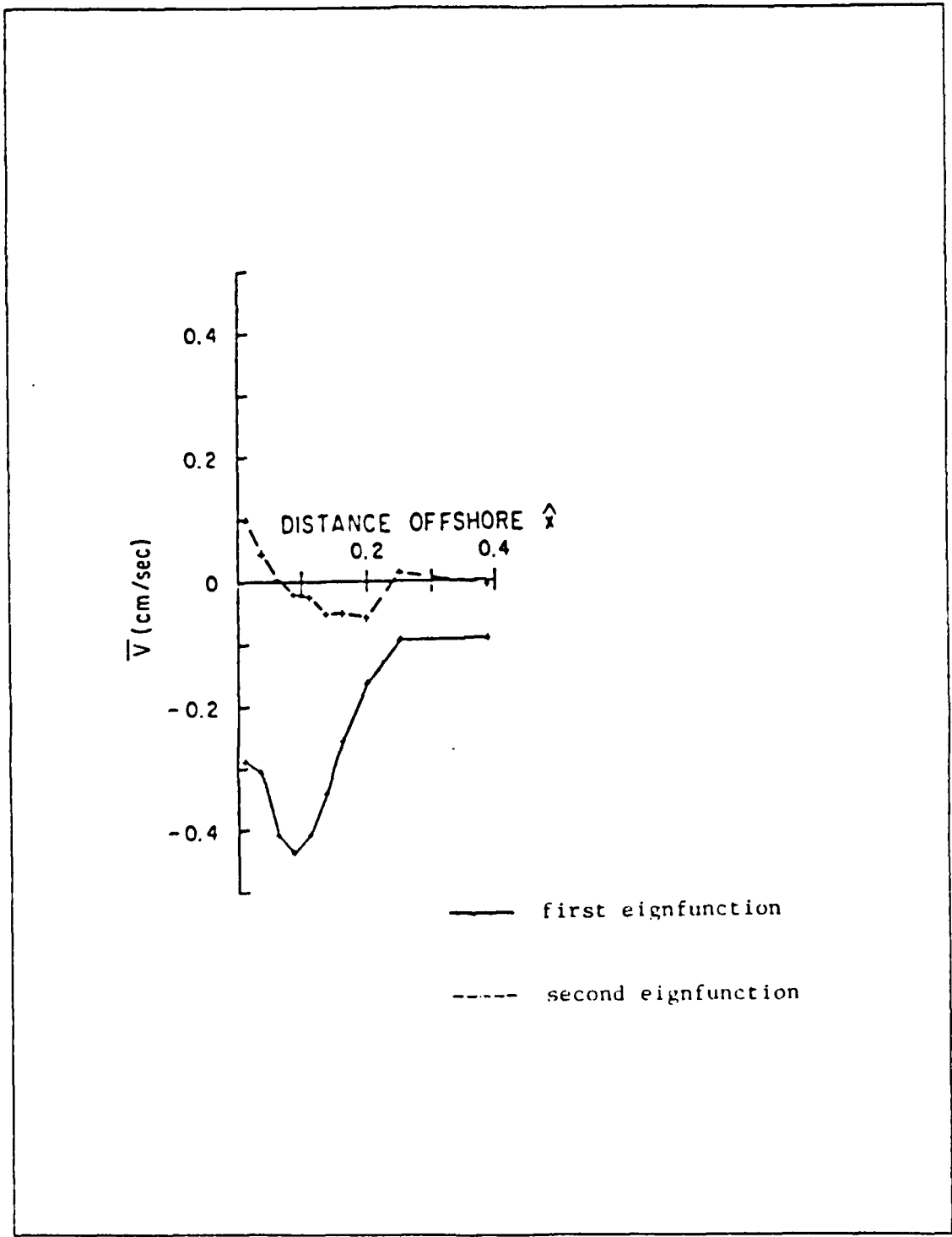


Figure 1.4 Longshore current distribution using empirical orthogonal function analysis. The first eigfunction contains most of the variance (after Guza et al., 1986).

waves inside the surf zone are investigated. Analytical models for calculating wave setup, longshore current and sediment transport are developed in chapter 5. An analytical solution to the unsteady longshore current is derived. Model validation and comparison with other models are included in chapter 5. The conclusions of this study are presented in chapter 6.

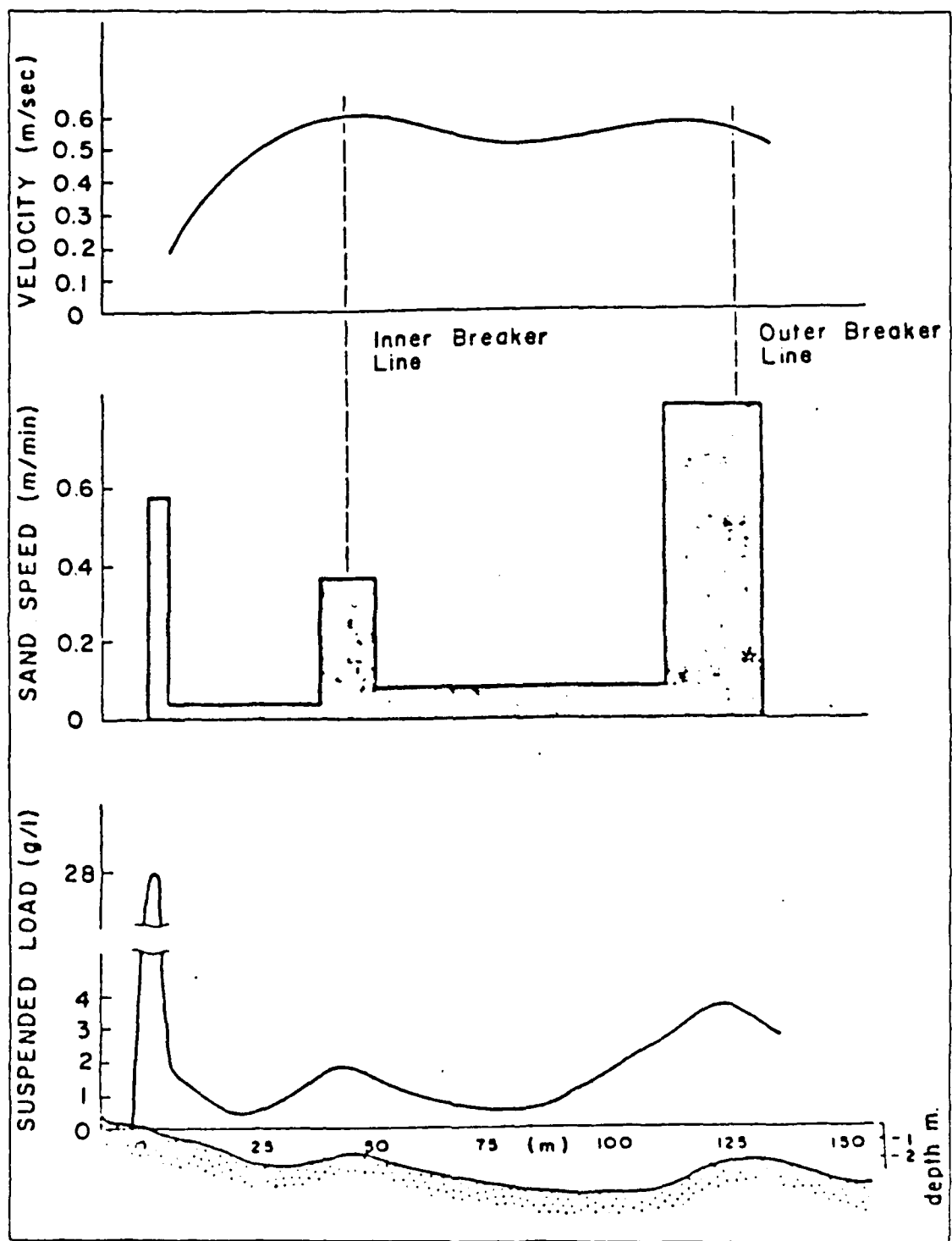


Figure 1.5 Distribution of longshore velocity and sediment transport across the surf zone (alter Zenkovich, 1960).

II. WAVES IN THE NEARSHORE ZONE

A wave record of incoming waves usually contains short period waves (1-30 sec) and long waves (30-300 sec). To study first order modulations of short waves superimposed on long waves, the principle of superposition is applied. Therefore, the non-linear wave theories are excluded in this study. A chosen Cartesian coordinate system is illustrated in Fig. 1.1 where the positive X-axis is directed offshore, the positive Z-axis is vertically upward and Y is alongshore. This coordinate system is convenient for describing the offshore decay of the standing long waves. Linear descriptions of both sea-swell and infragravity waves are discussed separately. Short waves are derived from linear wave theory over a flat bottom, then using shallow water approximation to describe short waves in the nearshore zone. Infragravity waves are derived from shallow water equations on a sloping bottom.

A. SHORT PERIOD WAVES

In general, waves in a viscous fluid propagate over irregular topography of varying permeability. In most cases, the main body of the fluid motion is reasonably assumed irrotational since the viscous effects are usually limited to a thin boundary layer near the surface and the bottom. Surface waves are considered a boundary value problem.

Linear wave theory (small amplitude waves) is considered a first order approximation to the theoretical description of wave behaviour. It is assumed that the wave amplitude, a , is very small compared to both the wavelength L and the local water depth h , ($a \ll L$ and $a \ll h$). The fluid is assumed incompressible, homogenous, inviscid and also irrotational, by which a velocity potential ϕ should exist to represent the field of the flow:

$$\vec{u} = -\nabla\phi \quad (2.1)$$

where \vec{u} is the velocity vector. Equation 2.1 satisfies the continuity equation $\nabla \cdot \vec{u} = 0$, by which the governing differential equation (Laplace equation) is obtained:

$$\nabla^2 \phi = 0 \quad \left\{ \begin{array}{l} -h \leq z \leq \eta \\ -\infty \leq x \leq \infty \end{array} \right. \quad (2.2)$$

With the proper kinematical and dynamical free surface and rigid flat bottom boundary conditions, the method of separation of variables is used to solve equation 2.2. Then, the velocity potential is given by

$$\phi = -\frac{ag}{\omega} \frac{\cosh k(h+z)}{\sinh kh} \cos(kx + \omega t) \quad (2.3)$$

where a is the wave amplitude, $\omega = (2\pi/T)$ is the radial frequency, and $k = (2\pi/L)$ is the wavenumber. The surface elevation η is periodic in both space and time.

$$\eta = a \cos(k_i x_i + \omega t), \quad i = 1, 2 \quad (2.4)$$

where $i = 1, 2$ refers to conditions in the X and Y-directions. The description of the wave motion is completed by the dispersion relationship,

$$\omega^2 = gk \tanh kh \quad (2.5)$$

which arises from the dynamical free surface boundary conditions. The horizontal velocity under the wave is given by

$$u = a \frac{\cosh k(h+z)}{\sinh kh} \cos(kx + \omega t) \quad (2.6)$$

and the vertical velocity

$$W = a\omega \frac{\sinh k(h+z)}{\sinh kh} \sin(kx + \omega t) \quad (2.7)$$

Swell waves propagating from deep water are nearly sinusoidal with long low crests. As waves approach shallow water, they start to feel the bottom and deform at relative depth $h/L < 1/2$. The wavelength decreases while the wave height generally increases, and the wave period remains invariant. The hyperbolic functions have convenient deep and shallow water asymptotes by which an approximate solution can be obtained. In shallow water, the linear gravity waves are non-dispersive since the dispersion relationship reduces to

$$\omega^2 = g k^2 h \quad (2.8)$$

and the horizontal and vertical velocities simplify to

$$u = a \sqrt{g/h} \cos(kx + \omega t) \quad (2.9)$$

$$W = a\omega \left(1 + \frac{z}{h}\right) \sin(kx + \omega t) \quad (2.10)$$

On dissipative beaches, long crested swell waves break when the wave steepness increases and the velocity of the water particles at the crest exceeds the phase speed of the wave form. In the inner surf zone, bores retain their relatively long crested form and progressively decrease in height as they advance onshore. Due to turbulence and non-linearities associated with the breaking process, the motion of the water particles after breaking can no longer be described analytically. As a first approximation, the

wave or bore height, H , at any location inside the surf zone is limited by the local depth according to the saturation assumption, i.e.

$$H = 2\gamma h \quad (2.11)$$

where γ is a constant of order unity. This relation holds for spilling breakers, the most common breaker type on natural beaches. The breaker index γ is important in describing the breaking waves used in longshore current and sediment transport models. This linear relationship is expected on dimensional grounds (Longuet-Higgins, 1972) and gives a reasonable description of laboratory results for monochromatic waves (e.g. Galvin and Eagleson, 1965) and field measurements during conditions of both broad and narrow spectral distributions of wave energy (Thornton and Guza, 1982), (Fig. 2.1).

Very close to the shoreline in the run-up region, the fluctuating component of the wave runup about the mean water level is known as "swash oscillation." Miche (1951) hypothesized that monochromatic waves within the surf zone may be composed of both a progressive component, which is dissipated onshore and has zero shoreline amplitude, and a standing component, which has its maximum amplitude at the shoreline. Many laboratory studies (Moraes, 1970; Battjes, 1974; Guza and Bowen, 1976; Van Dorn, 1976) report that the shoreline swash amplitude a_s is limited by the swash parameter ϵ_s ,

$$\epsilon_s = \frac{a_s^2}{g\beta^2} \quad (2.12)$$

where $\tan \beta$ is the beach slope and ϵ_s varies from one experiment to the other in the range from 1 to 3. Guza and Thornton (1982) attributed this variation to the ill-defined nature of the backwash (run-down). Hunt (1959) related the total runup R^V , defined as the sum of setup and half the swash amplitude, to the surf similarity ξ_0 with an empirical constant M :

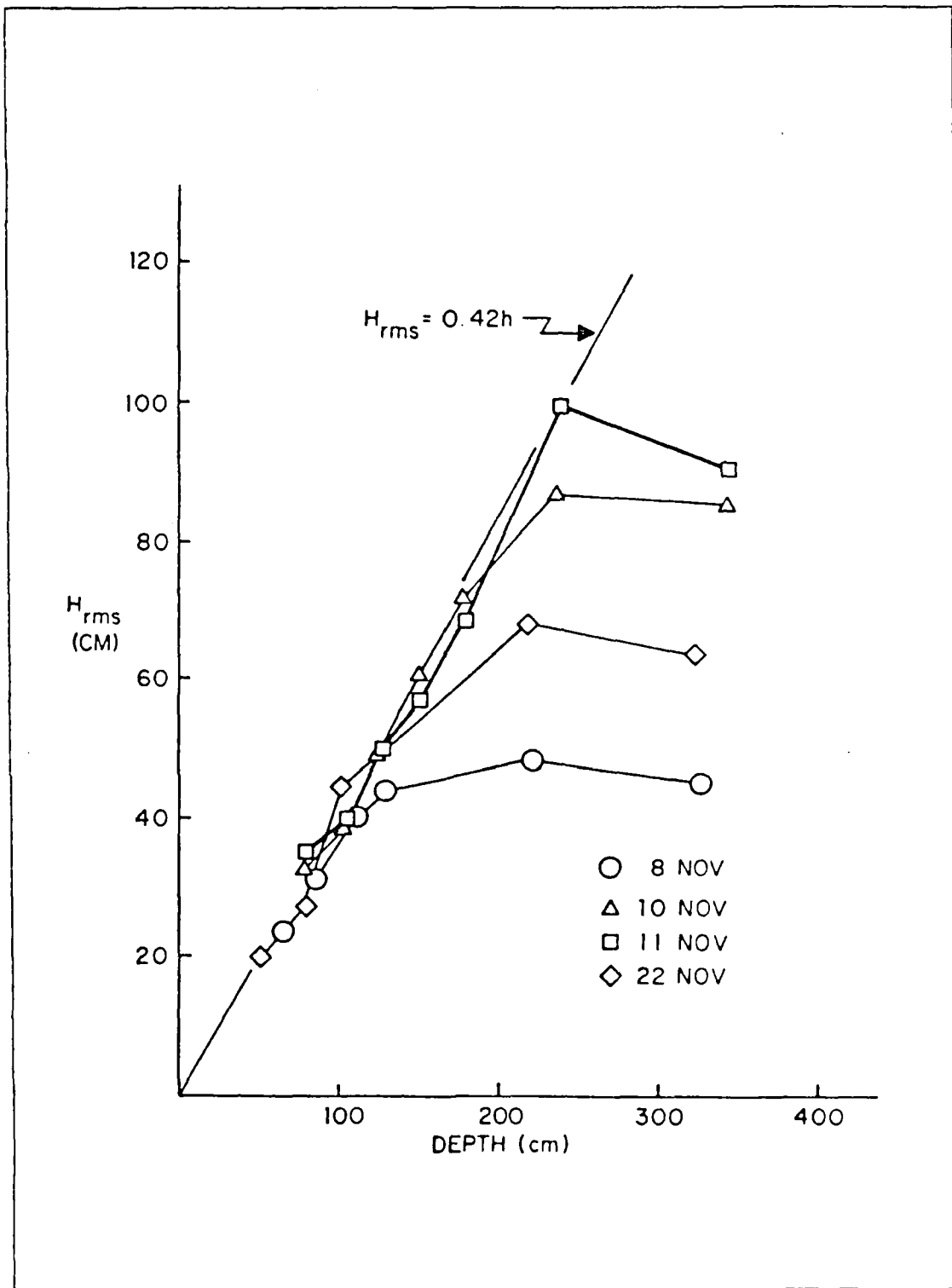


Figure 2.1 Wave heights inside the surf zone defining breaker index and showing saturation (after Thornton and Guza, 1982).

$$R^V / H_{sig} = M \xi_0 = M \tan \beta / \sqrt{(H_0, L_0)} \quad (2.13)$$

where H_{sig} is the significant wave height and the subscript 0 denotes the deep water conditions.

Huntley et al. (1977) showed a swash "saturation" condition at incident wave frequency, i.e. with increasing wave height, the steady set-up will increase but the swash amplitude will not. Guza and Thornton (1982) found a ω^{-3} spectral decay at incident wave frequencies, indicating that energy levels are independent of incident wave height, although Huntley et al. (1977) have shown ω^{-4} dependency. The swash saturation condition is found to be true for both monochromatic and random swash fluctuations (Guza et al., 1984). Swash at low frequency is found to be unsaturated, i.e. the swash amplitude increases with increasing incident wave height. Most of the low frequency energy is found to have infragravity wave periods. Thus swash spectra show a saturated region at incident wave frequency and an unsaturated region at low frequencies that dominates the whole spectrum.

To evaluate the amount of runup, swash studies have been mainly concerned with measuring the swash amplitude at the shoreline without putting much emphasis on the generation and types of the dominant low frequency motions. It is of interest now to investigate the forms of this low frequency water motion that give maximum amplitude at the shoreline.

B. LONG PERIOD WAVES

The long period waves presented in this work are limited to waves having a time scale of 30-300 seconds where gravity is the primary restoring force.

1. Infragravity Wave Models

The principal wave types that may contribute to the low frequency motion on beaches can be summarized by their mathematical formulation as follows:

- (i) 2-D model : the wave motion is mainly in the cross-shore direction and is known as surf beat or "leaky modes".
- (i) 3-D model : the wave motion has longshore variation and is known as edge waves or "trapped modes".

The mathematical forms of both waves are derived from the linear shallow water wave equation on a sloping bottom

$$\frac{\partial^2 \phi}{\partial t^2} - g \left\{ \frac{\partial}{\partial x} \left(h \frac{\partial \phi}{\partial x} \right) + \frac{\partial}{\partial y} \left(h \frac{\partial \phi}{\partial y} \right) \right\} = 0 \quad (2.14)$$

In the 2-D model, the wave energy is reflected offshore and the solution obtained is a standing wave expressed in terms of the zero order Bessel function of the first kind, J_0 , (Lamb, 1932; Fredrichs, 1948)

$$\phi(x, t) = -\frac{ag}{\omega} J_0(\chi) \sin \omega t \quad (2.15)$$

where $\chi = (4\omega^2 x / g \tan \beta)^{1/2}$ and a is the amplitude at the shoreline. It is noted that the Bessel function of the second kind, Y_0 , is excluded since it is unbounded as waves approach the shoreline. The surface elevation and the associated orbital velocities are given by

$$\eta(x, t) = a J_0(\chi) \cos \omega t \quad (2.16)$$

$$u(x, t) = a \sqrt{g/h} J_1(\chi) \sin \omega t \quad (2.17)$$

$$w(x, t) = -a\omega J_0(\chi) \sin \omega t \quad (2.18)$$

In the 3-D models, the edge waves are free waves that propagate along the coast with their energy trapped onshore by refraction, i.e. they do not radiate energy

offshore. Stokes (1846) was the first to provide an analytical solution to describe edge waves using a small amplitude wave assumption. Eckart (1951) solved equation 2.14 analytically in terms of Laguerre polynomials $L_n(2k_y x)$. The solution of progressive edge waves is

$$\phi_n = \frac{ag}{\omega_n} e^{-k_y x} L_n(2k_y x) \cos(k_y y - \omega_n t) \quad (2.19)$$

where k_y is the longshore wavenumber, and n is an integer number which represents the edge wave mode number. Each discrete mode contains finite energy, and the n -th mode edge wave will have n zero-crossings after which the amplitude decays exponentially. Edge waves obtained by Eckart (1951) must satisfy the dispersion relationship,

$$\omega_n^2 = g k_y (2n+1) \tan \beta \quad (2.20)$$

which requires $(2n+1)\tan\beta \ll 1$ to insure that the solution achieves its limiting value as $k_y x \rightarrow \infty$ while still in shallow water.

Ursell (1952) was able to obtain a set of "exact" edge wave solutions on a sloping bottom using the small amplitude wave theory without recourse to the shallow water approximation. His solution satisfies a slightly different dispersion relationship

$$\omega_n^2 = g k_y \sin(2n+1)\beta \quad (2.21)$$

and the solution lies within the range $((2n+1)\beta) \leq \pi/2$ to insure a cutoff mode for a given beach slope. Ursell (1952) showed that Stokes'(1846) edge wave solution is only the zero mode of his solution. For gentle beach slopes and low mode numbers, both dispersion relationships 2.20 and 2.21 are in agreement, suggesting that the shallow water approximation is appropriate under these conditions, (Guza and Davis, 1974). It

is noted that the approximate Eckart (1951) solution is more commonly used in comparisons with field data due to its simpler mathematical formulation. In the field data analysis, a difficulty in discriminating between leaky and edge wave modes for small offshore distances arises because of the similarity of their cross-shore structures. Also, both waves have maximum amplitude at the shoreline. Fig. 2.2 shows such similarities between higher mode edge waves and reflected waves.

In summary, the low frequency motions may be classified as edge waves, leaky modes, forced waves or a combination as shown in Fig 2.3, (after Symonds, 1982). A complete set of free wave solutions of discrete edge waves occurs for $\omega^2 < gk_y$ while a continuum of leaky mode exists for $\omega^2 > gk_y$. It is noted that the forced waves may lie between the edge wave modes, but they do not satisfy the dispersion relationship and are weaker than the free modes since edge waves may grow resonantly as they are excited.

2. Generation of Infragravity waves

Munk (1949) and Tucker (1950) suggested that the long period waves may be caused by an excess of mass carried forward by groups of high swell. The swell waves are assumed to be destroyed on the beach, and the excess mass transport is reflected back as a free long wave. They tested this hypothesis by comparing offshore pressure records, delayed by the calculated travel time of the incident wave envelope. Tucker (1950) observed a negative maximum correlation between incident wind wave groups and the infragravity waves at a time lag equivalent to the travel time of a forced wave moving with the wind wave group velocity and traveling back upon reflection as a free wave.

Longuet-Higgins and Stewart (1962) showed that the variations in the radiation stress due to incident wave grouping drive a forced wave such that a depression of the mean water level (MWL) will occur under incident high waves, and a corresponding rise in MWL occurs under low waves. This forced oscillation of second order is associated with groups until the incident waves break onshore and release a free wave offshore, which theoretically supports the above observation.

Gallagher (1971) suggested edge wave excitation through a non-linear interaction whereby two incident waves can transfer energy into an edge wave if the difference frequency and longshore wavenumber of the two interacting wind waves satisfy the edge wave dispersion relationship, equation 2.21. This resonance has been observed in the laboratory (Bowen and Guza, 1978).

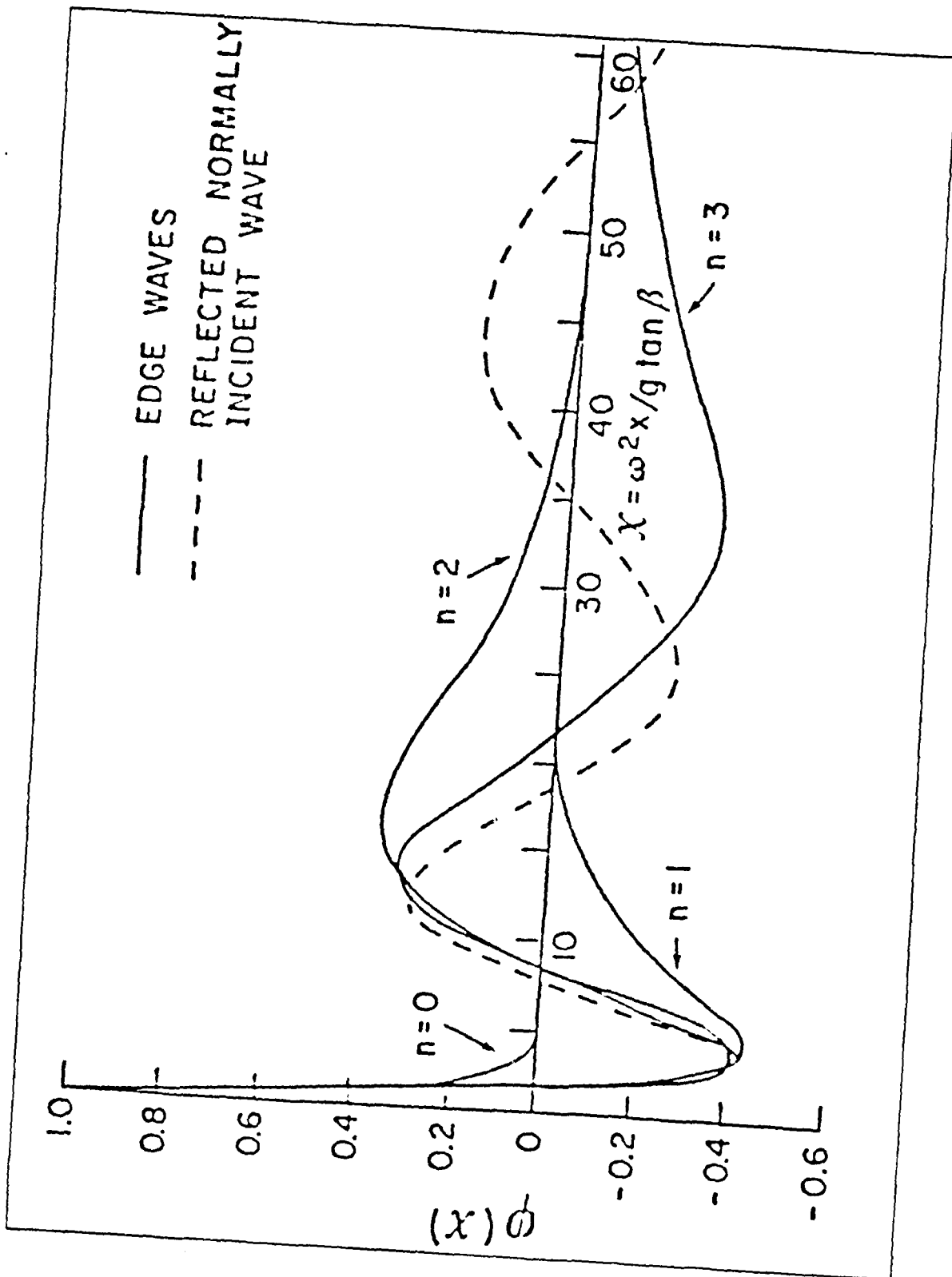


Figure 2.2 Modes of edge waves and reflected waves, ϕ is the velocity potential.

Incident waves may transfer energy to either leaky or trapped modes through many possible interactions. One of these is given by Guza and Davis (1974) where energy is transferred into edge wave modes through a non-linear interaction involving a normally incident standing wave on a sloping bottom. Bowen and Guza (1978) showed energy transferred into leaky modes ($\omega^2 > gk_y$) by edge waves.

Another mechanism for low frequency wave generation is suggested by collision between the stronger component of backwash and the shoreward moving bores that results in roll waves which last for few seconds. On analyzing swash data, Waddell (1973) found that the collision between uprush and backrush plays an important role in reducing the extent of swash runup waves. Furthermore, he suggested that water percolation into the beach serves as a low-pass filter affecting the swash frequency. Bradshaw (1980) suggested bore-bore capture as a mechanism for long wave generation in the swash zone. Mase and Iwagaki (1984) showed a considerable shoreward decrease in the ratio between the number of runup waves to the incident waves.

Symonds et al. (1982) developed a 2-D model for generating long waves which is forced by a time-varying break-point caused by the groupness of the incident wave field. The generated free long wave at the group frequency has a standing wave structure shoreward of the breakpoint and an outgoing progressive wave structure seaward of the breakpoint.

In the above survey, both short and long wave models are described separately showing different characteristics. It is of interest now to combine the two waves and study the changes in the incident wave (short wave) field due to the presence of longer period waves.

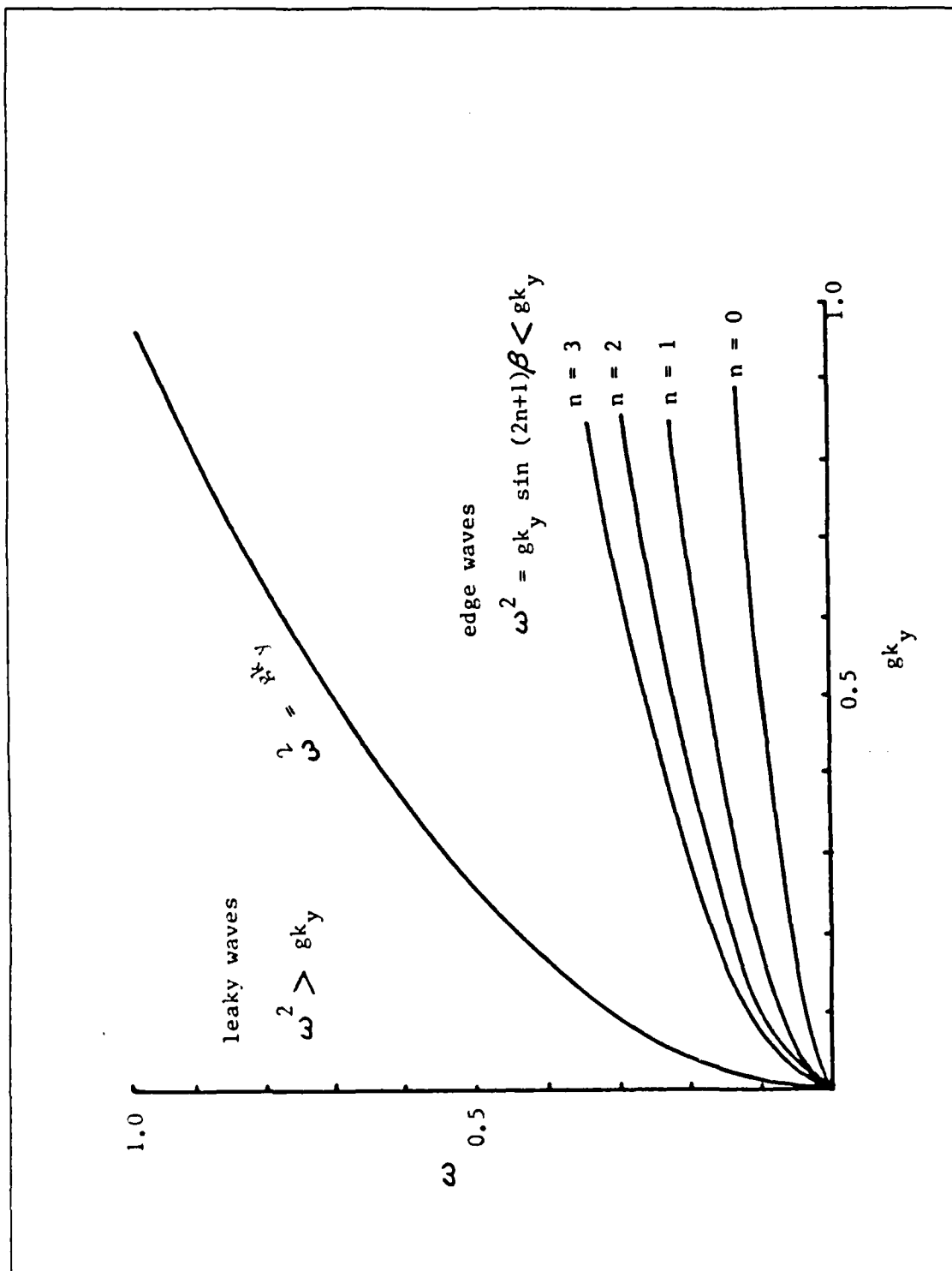


Figure 2.3 Dispersion relations for infragravity waves.

III. SHORT WAVE MODULATION DUE TO LONG WAVES

When short period waves ride on much longer waves, they are modulated in amplitude, wavelength and direction. Their amplitude tends to increase at the crests of the long waves and decrease at the troughs. The changes in wavenumber and direction depend mainly on kinematical considerations. In this chapter, the changes in wavelength, direction and amplitude are investigated. A development for the corresponding changes in energy and momentum flux then follows.

A. CHANGES IN THE WAVE AMPLITUDE

The amplitude modulation of a short progressive wave riding on a much longer wave was pointed out by Unna (1942, 1947). Unna (1947) showed a contraction of the wavelength and an increase in the amplitude of short waves at the long wave crests.

Longuet-Higgins and Stewart (1960) used a perturbation analysis to examine the non-linear interaction between short and long progressive waves over a horizontal bottom. They described the surface elevation

$$\eta = a_s \sin \psi_s + a_\ell \sin \psi_\ell \quad (3.1)$$

where $\psi = (kx - \omega t + \theta)$, is the phase function and θ the phase shift. The subscripts s and ℓ refer to the short and long wave respectively. Using Stokes' method of approximation to the second order, they derived a general form for the modulated surface elevation

$$\eta' = a_s (1 + P) \sin \psi_s + a_s Q \cos \psi_s \quad (3.2)$$

where $P = a_\ell k_\ell \sin \psi_\ell$ and $Q = -a_\ell k_s \cos \psi_\ell$. Using the first term in the right hand side of equation 3.2, Longuet-Higgins and Stewart expressed the modulated short wave amplitude as

$$a' = a_s \left\{ 1 + a_2 k_2 \left(\frac{3}{4} \coth k_2 h + \frac{1}{4} \tanh k_2 h \right) \sin \psi_2 \right\} \quad (3.3)$$

and a modulation in the short wave wavenumber, k' , as

$$k' = k_s \left\{ 1 + a_2 k_2 \coth k_2 h \sin \psi_2 \right\} \quad (3.4)$$

In shallow water, equations 3.3 and 3.4 reduce to

$$a' = a_s \left\{ 1 + \frac{3}{4} \frac{a_2}{h} \sin \psi_2 \right\} \quad (3.5)$$

$$k' = k_s \left\{ 1 + \frac{a_2}{h} \sin \psi_2 \right\} \quad (3.6)$$

These amplitude and wavenumber modulations are explained by the work done by the long waves against the momentum of the short waves. This work is converted into short wave energy and therefore produces a steepening of the short wave at the crests of the long waves, i.e., the energy is redistributed along the wavelength of the long wave. Longuet-Higgins and Stewart (1960) came up with equations similar to 3.3 and 3.4 for a progressive short wave superposed on a long period standing wave in which a_1 was described as $2a_1$.

1. Determination of the Modulated Wave Profile

It is of interest now to show that the refractive changes in amplitude and wavenumber due to the non-linear interaction may result in a modulated short wave expressed as an infinite sum of components at different frequencies. Then, the properties of the modulated wave are investigated to provide a better understanding of the modulation process. The procedure is to let the modulated short wave, designated by primes, propagate in the same wave direction and satisfy

$$\eta' = a' \sin(k'x - \omega't) \quad (3.7)$$

Substituting equations 3.3 and 3.4 into equation 3.7, and letting $\omega' = \omega_s$, yields

$$\eta' = a' \sin(\psi_s + m_k \sin \psi_\ell) \quad (3.8)$$

where $m_k = a_\ell k_\ell k_s \times \coth k_\ell h$ is defined as a non-dimensional wavenumber (wavenumber modulation factor). Equation 3.8 is a general form of amplitude and wavenumber modulation. Equation 3.8 reduces to the simple form $\eta' = a' \sin \psi_s$ when $m_k \ll 1$. Expanding equation 3.8 using trigonometric identities, gives

$$\eta' = a' \{ \sin \psi_s \cos(m_k \sin \psi_\ell) + \cos \psi_s \sin(m_k \sin \psi_\ell) \} \quad (3.9)$$

Using Fourier series expansions to express the sinusoidal arguments (Abramowitz and Stegun, 1964), gives

$$\eta' = a' \sum_{n=-\infty}^{\infty} J_n(m_k) \sin(\psi_s + n\psi_\ell) \quad (3.10)$$

In the above analysis no assumptions have been made regarding either applicable regions or the initial properties of the two interacting waves. Equation 3.10 offers a means of expressing the modulated short waves as a combination of spectral components based on monochromatic input. The short wave is viewed now as a carrier subjected to a simultaneous amplitude and phase modulation, (Panter, 1965). Changing the limits of summation, equation 3.10 becomes

$$\begin{aligned} \eta' = & a' J_0(m_k) \sin \psi_s \quad (3.11) \\ & + a' \sum_{n=1}^{\infty} J_n(m_k) \{ \sin(\psi_s + n\psi_\ell) + (-1)^n \sin(\psi_s - n\psi_\ell) \} \end{aligned}$$

The first term has the form of the solution for waves at the incident wave frequency propagating on a sloping bottom but with a different Bessel argument (see equation 2.16). The remaining terms represent the side bands at sum and difference frequencies ($\psi_s \pm n\psi_\ell$) where they are phase locked. This solution is dependent on the argument m_k and converges rapidly as n increases.

In shallow water, the Bessel function argument m_k reduces to $2(a_\ell/h)k_s x$ for the case of progressive short waves superposed on long standing waves. The argument m_k is found to increase onshore (Fig 3.1), where the computed values of m_k are evaluated until closer to the shore ($x = 1$ cm) before m_k reaches ∞ . Due to the onshore increase of m_k , $J_n(m_k)$ decreases onshore, oscillating rapidly and reaches zero at the shoreline (Fig 3.2). Note the difference in behaviour of the Bessel functions in equation 3.11 and 2.15, where the Bessel argument allows the amplitude of the long standing wave to reach a maximum at the shoreline. For breaking short waves on a long period standing wave, the depth limited breakers is utilized to describe $a_s (= \gamma h)$ in equation 3.5. Substituting a' into 3.11, yields

$$\eta' = \gamma h [J_0(m_k) \sin \psi_s + \frac{3}{4} \frac{a_\ell}{h} J_1(m_k) \cos \psi_s] \\ + \gamma h [J_n(m_k) \{ \sin(\psi_s + n\psi_\ell) - (-1)^n \sin(\psi_s - n\psi_\ell) \} \\ - \frac{3}{8} \frac{a_\ell}{h} (J_{n-1}(m_k) - J_{n+1}(m_k)) \{ \cos(\psi_s + n\psi_\ell) - (-1)^n \cos(\psi_s - n\psi_\ell) \}] \quad (3.12)$$

Two distinct features of this solution are demonstrated in the amplitude squared spectra (Fig 3.3). First, symmetric side bands are generated about the carrier (Fig 3.3 a). The second feature is the transfer of short wave energy to the upper and lower side bands as the depth decreases (Fig 3.3 b), which causes broadening of the wave spectra. It is also noted that the amplitude of the spectral components decrease shoreward. The instabilities associated with the side bands generation are attributed to their spatial structure and phase variation. It is shown that the side bands energy is modified by the decreasing depth. The modulation may contribute to the infragravity waves by strengthening the low frequency energy component closer to the shoreline, which has previously been observed. Waddell (1973) presents evidence of nonlinear transfer of energy from high to low frequency due to collision, where successive bores begin to overrun each other. However, Huntley and Bowen (1975b) suggested that energy transfers are due to the interaction of many irregular spaced breakers in the surf zone.

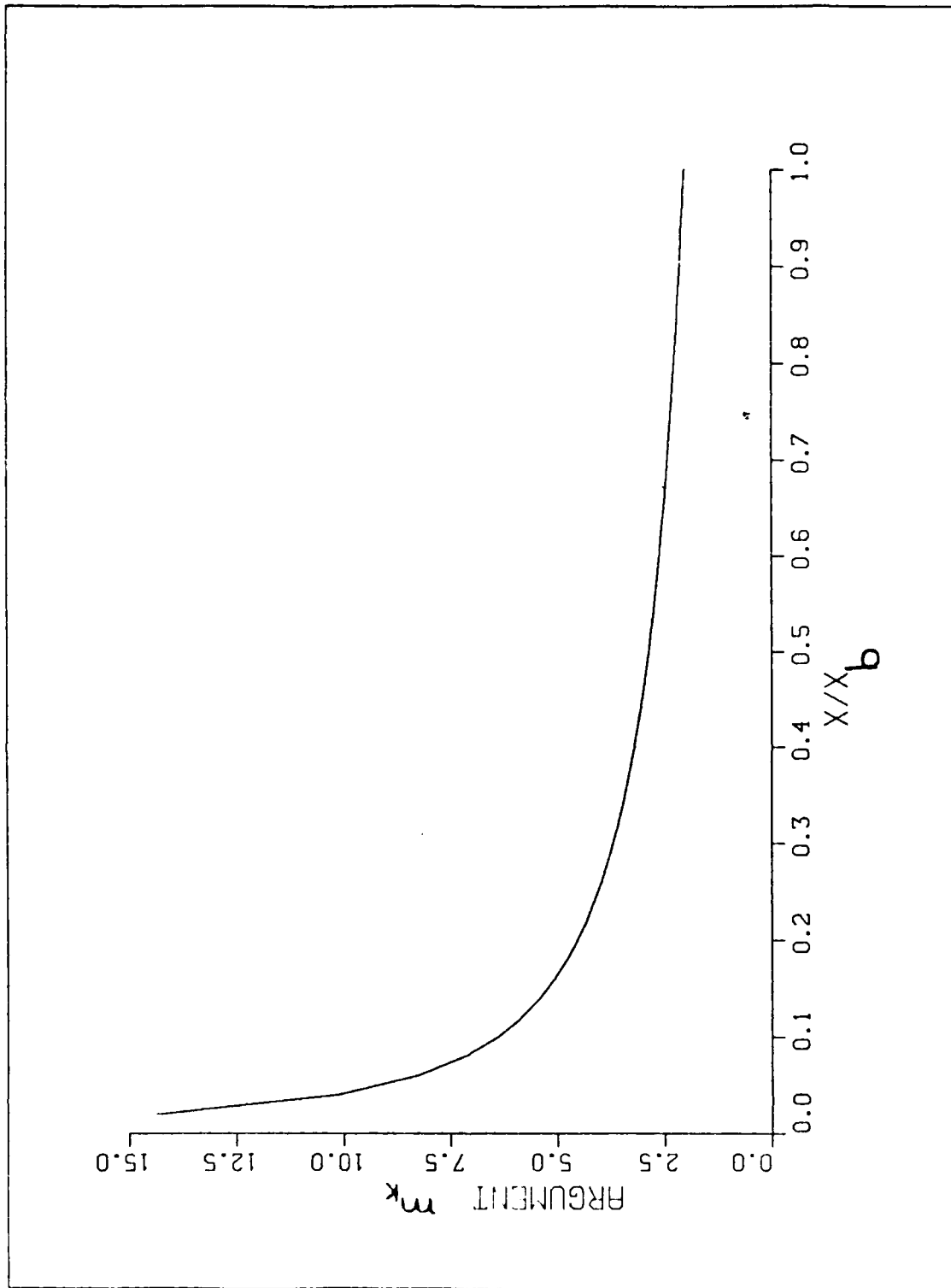


Figure 3.1 Wavenumber modulation factor m_k vs non-dimensional distance x/x_b , where x_b is the surf zone width.

Sawaragi and Iwata (1974) studied experimentally the wave transformation after breaking and observed energy transfer from the carrier into higher frequency waves by an unknown mechanism. The present analysis may be used to illustrate some of these findings. Equation 3.11 shows that the beach does not eliminate the incident wave frequency and that the modulated wave energy components and the incident wave frequency vary spatially.

B. CHANGES IN THE WAVE KINEMATICS

1. Background on Wave Kinematics

At any instant of time, a wave front is defined by the phase function $\psi = \text{constant}$, which is the equation of a family of parallel planes with normal vector k . As time increases, these planes move with the phase speed in the direction k .

In general, the dispersion of the wave motion may be written

$$\omega = \omega(k, h) \quad (3.13)$$

where the frequency varies with both the wavenumber and the local water depth. The local wavenumber and frequency are defined by the gradient of the slowly varying phase function in space and time:

$$\vec{k} = \nabla\psi \quad (3.14)$$

$$\omega = -\frac{\partial\psi}{\partial t} \quad (3.15)$$

Since the curl of a gradient is zero, it follows immediately from equation 3.14 that the local wavenumber vector in space is irrotational, i.e.,

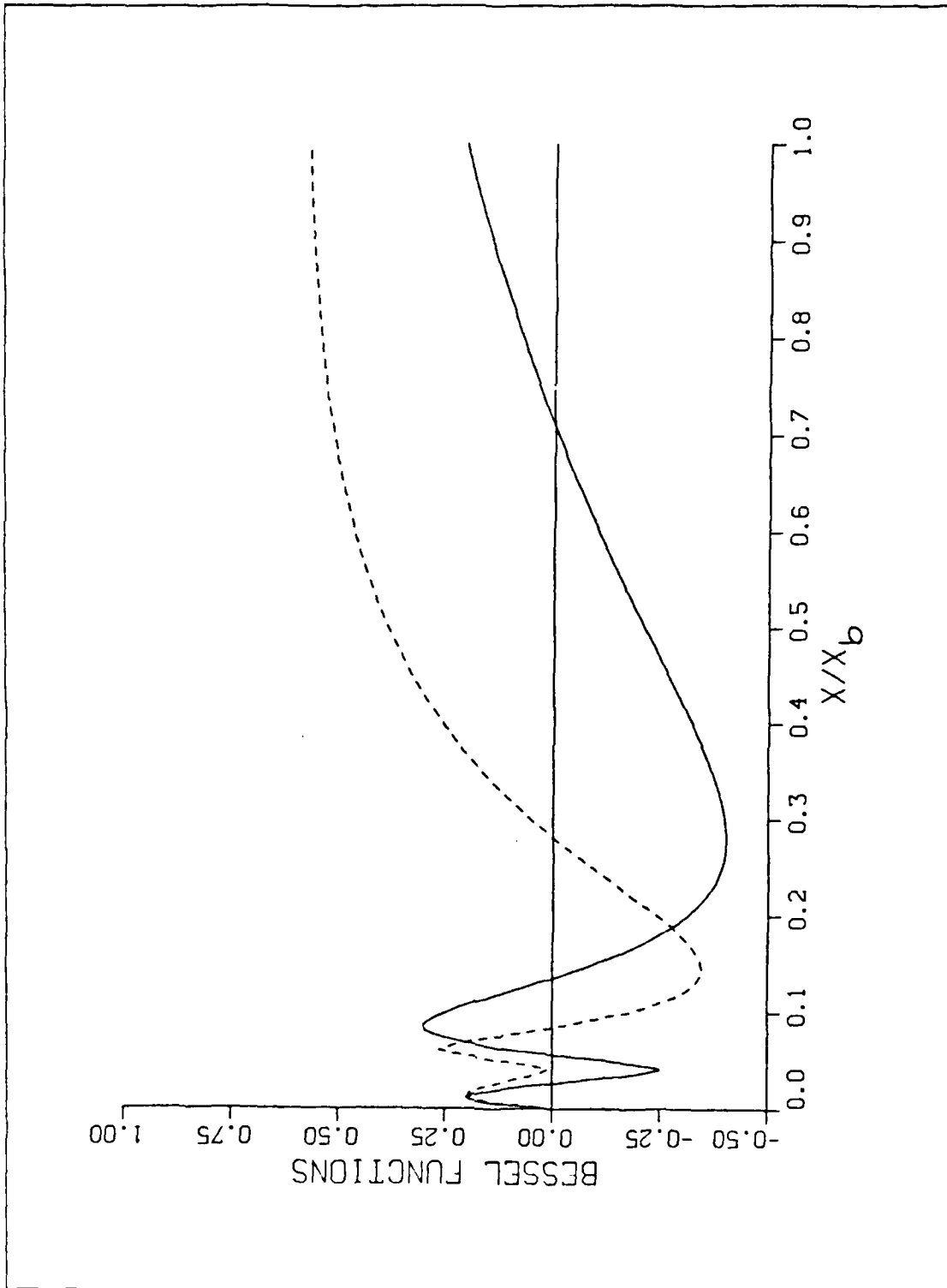


Figure 3.2 Behaviour of the Bessel functions $J_0(m_k)$ (solid curve) and $J_1(m_k)$ (dashed curve) across the surf zone.

$$\nabla \times \vec{k} = 0 \quad (3.16)$$

Cross differentiating equations 3.14 and 3.15 to eliminate ψ yields

$$\frac{\partial \vec{k}}{\partial t} + \nabla \omega = 0 \quad (3.17)$$

Equation 3.17 is known as the kinematical conservation of wave density, where the rate of change of wavenumber is balanced by the convergence of the frequency. Sometimes 3.17 is also called the "conservation of crests equation," since the crests are neither created nor destroyed and their total number must be conserved.

Rewriting equation 3.17 in tensor notation and expanding the convergence term using the dispersion relationship in equation 3.13 gives

$$\frac{\partial k_i}{\partial t} + \frac{\partial \omega}{\partial k_j} \left(\frac{\partial k_j}{\partial x_i} \right) + \frac{\partial \omega}{\partial h} \frac{\partial h}{\partial x_i} = 0, \quad i = 1, 2 \quad (3.18)$$

Equation 3.18 can be rewritten as

$$\frac{\partial k_i}{\partial t} + c_{g_j} \frac{\partial k_i}{\partial x_j} + \frac{\partial \omega}{\partial h} \frac{\partial h}{\partial x_i} = 0, \quad i = 1, 2 \quad (3.19)$$

where $\partial k_j / \partial x_i = \partial k_i / \partial x_j$ from equation 3.16, and the group velocity is defined by

$$c_{g_i} = \frac{\partial \omega}{\partial k_j} \quad (3.20)$$

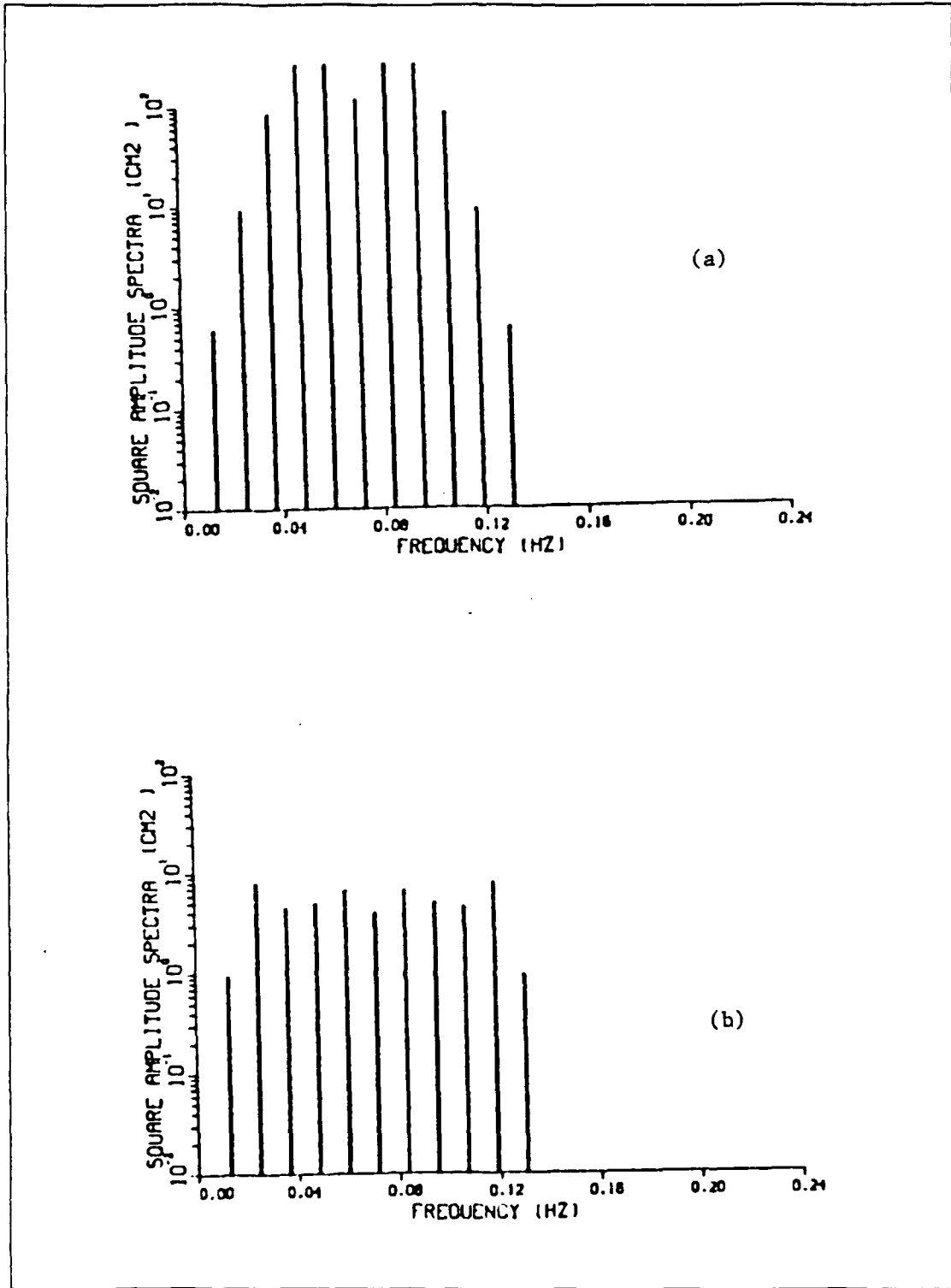


Figure 3.3 Amplitude square spectra of the modulated short wave at offshore distance: (a) $x = 40.0$ m (b) $x = 0.5$ m.

2. Kinematics of waves on current

In studying the problem of short gravity waves superposed on waves of a much longer wavelength and period, the long wave may be modeled as a slowly varying current $U(x,t)$, (e.g. Longuet-Higgins and Stewart, 1960, 1961; Garrett and Smith, 1976). A coordinate system that moves with the current velocity is chosen, by which the observed frequency ω' , passing a fixed point, is given by

$$\omega' = \omega_s + \vec{k}_s \cdot \vec{U}_l \quad (3.21)$$

where ω_s is the intrinsic frequency, (Ursell, 1960; Whitham, 1960). The subscripts s and l refer to short and long wave properties. The second term on the right hand side of 3.21 is due to the relative motion of short waves with respect to the chosen coordinate and is known as the doppler shift effect.

The short wave will be modulated by the presence of the current, and therefore the modulated short wave (denoted by primes) is assumed to satisfy equation 3.17, i.e.,

$$\frac{\partial k'}{\partial t} + \nabla \omega' = 0 \quad (3.22)$$

where k' , the observed (modulated) wavenumber, is unknown and assumed unsteady. The observed frequency ω' is given by equation 3.21. Expanding equation 3.22 gives

$$\frac{\partial k'_i}{\partial t} + c_{g_j} \frac{\partial k'_i}{\partial x_j} + \frac{\partial \omega}{\partial h} \frac{\partial h}{\partial x_i} + \frac{\partial k'_i U_i}{\partial x_i} = 0 \quad (3.23)$$

where the quantities k'_i , c_{g_j} and ω are for the short waves, and U is the current (long waves).

Assuming a steady intrinsic short wave train; i.e., $\partial k_s / \partial t = 0$, equation 3.23 may be simplified by the use of equation 3.19 to give

$$\frac{\partial k'_i}{\partial t} + \frac{\partial k_{s_i} U_i}{\partial x_i} = 0 \quad (3.24)$$

which describes the kinematic conservation of the modulated wave density.

3. Applications

The following analyses demonstrate the efficiency and simplicity of equation 3.24 in examining the wavenumber changes of short waves riding on a current of longer period. Two different bottom topographies are considered: flat bottom and plane sloping bottom. Different current models are applied.

a. Waves on a Current in Water of Constant Depth

The current will be modeled as a progressive or standing long period wave.

i. Current as a progressive long wave

The short wave is assumed to propagate over a flat bottom and to be parallel to the long wave (collinear) in the X-direction. The current U is described by the orbital velocity of a progressive long period wave,

$$U_\ell = a_\ell \omega_\ell \frac{\cosh k_\ell (h+z)}{\sinh k_\ell h} \sin \psi_\ell \quad (3.25)$$

which corresponds to a free surface elevation, $\eta_\ell = a_\ell \sin \psi_\ell$. Substituting into equation 3.24 gives

$$\frac{\partial k'_i}{\partial t} + k_{s_x} \left[a_\ell \omega_\ell k_\ell \frac{\cosh k_\ell (h+z)}{\sinh k_\ell h} \sin \psi_\ell \right] = 0 \quad (3.26)$$

Equation 3.26 is easily integrated over time to give

$$k'_i - k_{s_x} k_\ell a_\ell \frac{\cosh k_\ell (h+z)}{\sinh k_\ell h} \cos \psi_\ell = \text{Constant} \quad (3.27)$$

where the constant is evaluated at $U = 0$, so that $k' = \text{constant} = k_s$, i.e. the wavenumber will not change if there is no current. Then, the general solution is obtained such that

$$k' = k_{s_x} \left[1 + \frac{U}{c_\lambda} \right] \quad (3.28)$$

which describes the wavenumber changes due to the non-linear interaction between the short wave and a progressive long wave using a kinematic approach. Evaluating equation 3.25 at the free surface, $z = 0$, equation 3.28 may be written

$$k' = k_s (1 + a_\lambda k_\lambda \coth k_\lambda h \sin \psi_\lambda)$$

It is interesting that the above result, obtained from the first principles of kinematical conservation, is the same equation as (3.4) obtained by Longuet-Higgins and Stewart (1960) using a lengthy second order perturbation analysis scheme.

ii. Current as a long standing wave

For the flat bottom case, equation 3.24 reduces to

$$\frac{\partial k'}{\partial t} + k_{s_i} \frac{\partial U_i}{\partial x_i} = 0 \quad (3.29)$$

The current U is described by the orbital velocity of a linear standing wave

$$U = a_\lambda \omega_\lambda k_\lambda \frac{\cosh k_\lambda (h+z)}{\sinh k_\lambda h} \sin k_\lambda x \sin \omega_\lambda t \quad (3.30)$$

which varies only in the x -direction. Applying equations 3.29 for both x and y directions yields

$$\frac{\partial k'_x}{\partial t} + k_{s_x} a_\lambda k_\lambda \omega_\lambda \frac{\cosh k_\lambda (h+z)}{\sinh k_\lambda h} \cos k_\lambda x \sin \omega_\lambda t = 0 \quad (3.31)$$

$$\frac{\partial k'_y}{\partial t} = 0$$

Integrating over time gives

$$\left\{ \begin{array}{l} k'_x - k_{s_x} k_\lambda \frac{\cosh k_\lambda (h+z)}{\sinh k_\lambda h} \eta_\lambda = \text{Constant} \\ k'_y = k_{s_y} = \text{Constant} \end{array} \right. \quad (3.32)$$

Equation 3.32 indicates that the wavenumber component alongshore is always constant since no longshore component of the current exists.

The constant in (3.32) can be evaluated at any node where $\eta_\lambda = 0$. At these locations, it is assumed that the wavenumber does not change, i.e. $k'_x = k_{s_x}$. Substituting into equation 3.32, a general solution is obtained:

$$\left\{ \begin{array}{l} k'_x = k_{s_x} \{1 + a_\lambda k_\lambda \coth k_\lambda h \cos k_\lambda x \cos \omega_\lambda t\} , \\ k'_y = k_{s_y} = \text{Constant} . \end{array} \right. \quad (3.33)$$

Therefore the wavenumber component in the x direction is always modulated in time and space, while the longshore wavenumber component is always constant. As a result, the wavenumber vector changes in time and space; i.e. the waves are refracted.

It is clear that if the waves are parallel to the current, i.e. collinear in x-direction, then $k_y = 0$ and the solution reduces to the first equation in 3.33 .

b. Waves on Current in Water of Variable Depth

A reasonable model to describe the current on a sloping bottom is the orbital velocity of either a cross-shore long standing wave or edge waves. Collinear and oblique incident waves on a current are included. Let us assume a plane sloping bottom for simplicity of analysis.

i. Current as a cross-shore long standing wave

On a sloping bottom, the horizontal velocity of a standing wave is described by equation 2.17 . Recalling the equation for wave density conservation (3.24),

$$\frac{\partial k'_i}{\partial t} + k_{s_i} \frac{\partial U}{\partial x_i} + U \frac{\partial k_{s_i}}{\partial x_i} = 0 \quad (3.34)$$

which requires specifying $\partial U / \partial x$ and $\partial k_{s_i} / \partial x_i$. The gradient of the current velocity becomes

$$\frac{\partial U}{\partial x} = -\left\{ \frac{U}{x} + \frac{1}{h} \frac{\partial \eta_l}{\partial t} \right\} \quad (3.35)$$

Using the dispersion relationship in shallow water to differentiate the wavenumber components gives

$$\frac{\partial k_{s_x}}{\partial x} = -k_{s_x} \left\{ \tan \alpha \frac{d\alpha}{dx} + \frac{1}{2x} \right\} \quad (3.36)$$

and $\partial k_y / \partial y = 0$, since the dispersion relationship is independent of y as the depth contours are assumed straight and parallel. Applying Snell's law to describe the change in the angle of approach with x , $\partial \alpha / \partial x$ gives

$$\frac{d\alpha}{dx} = \frac{1}{2h} \tan \alpha \tan \beta \quad (3.37)$$

Substituting into 3.36, gives

$$\frac{\partial k_{s_x}}{\partial x} = -\frac{k_{s_x}}{2x} (\sec^2 \alpha) \quad (3.38)$$

Substituting into 3.34 using 3.35 and 3.38

$$\frac{\partial k'_x}{\partial t} + k_{s_x} \left[-\frac{U}{x} - \frac{1}{h} \frac{\partial \eta_l}{\partial t} \right] - U \left[\frac{k_{s_x} \sec^2 \alpha}{2x} \right] = 0 \quad (3.39)$$

$$\frac{\partial k'_y}{\partial t} = 0$$

from which $\partial k'_y / \partial y = 0$ and, therefore, $k'_y = k_y = \text{constant}$. Integrating equation 3.39 over time gives

$$k'_x - \frac{k_{sx}}{x} \int^t U dt \left[1 + \frac{\sec^2 \alpha}{2} \right] - k_{sx} \frac{\eta_\ell}{h} = \text{Constant} \quad (3.40)$$

since

$$\int U dt = -(1/\omega^2) \partial U / \partial t + \text{constant}$$

Therefore, equation 3.40 becomes

$$k'_x - \frac{k_{sx}}{x\omega_\ell^2} \frac{\partial U}{\partial t} \left[1 + \frac{\sec^2 \alpha}{2} \right] - k_{sx} \frac{\eta_\ell}{h} = \text{Constant} \quad (3.41)$$

The constant in 3.41 can be evaluated at $x = \infty$ where current vanishes, i.e. $\eta_\ell = 0$ and $U = 0$, which gives $k'_x = \text{constant} = k_{sx}$. Then, for a steady oblique wave train, the general solution is given by

$$k'_x = k_{sx} \left[1 + \frac{\eta_\ell}{h} - \frac{1}{x\omega_\ell^2} \left(1 + \frac{\sec^2 \alpha}{2} \right) \frac{\partial U}{\partial t} \right] \quad (3.42)$$

If the waves and the current are collinear ($\alpha = 0$), equation 3.42 reduces to

$$\begin{cases} k'_x = k_{sx} \left[1 + \frac{\eta_\ell}{h} - \frac{3}{2} \frac{1}{x\omega_\ell^2} \frac{\partial U}{\partial t} \right] \\ k'_y = k_y = \text{Constant} \end{cases} \quad (3.43)$$

This equation shows the dependence of the wavenumber changes on the surface elevation and on the acceleration of the current.

ii. Current as an Edge Wave

In the 3-D model the long wave is described by an edge wave. A zero mode edge wave is used to simplify the analysis where the Laguerre polynomial equals unity. The horizontal velocity components are given as

$$U = \frac{a_{\ell} g k_{y\ell}}{\omega_{\ell}} e^{-k_{y\ell} x} \sin(k_{y\ell} y - \omega_{\ell} t) \quad (3.44)$$

$$V = \frac{a_{\ell} g k_{y\ell}}{\omega_{\ell}} e^{-k_{y\ell} x} \cos(k_{y\ell} y - \omega_{\ell} t) \quad (3.45)$$

A steady short wave train riding on an edge wave will satisfy the wave density conservation equation (3.24). Substituting into equation 3.24, using equations 3.38 and 3.39, gives

$$\frac{\partial k'_x}{\partial t} - U \left[k_{s_x} k_{y\ell} + \frac{k_{s_x}}{2x} \sec^2 \alpha \right] = 0 \quad (3.46)$$

$$\frac{\partial k'_y}{\partial t} + k_{s_y} k_{\ell y} U = 0 \quad (3.47)$$

Integrating both 3.46 and 3.47 with respect to time gives

$$k'_x + k_{s_x} \left[\left(\frac{k_{\ell y}}{\omega_{\ell}} \right) V + \frac{\sec^2 \alpha}{2x \omega_{\ell}} V \right] = \text{Constant} \quad (3.48)$$

The constant in 3.48, can be evaluated when $x \rightarrow \infty$ where both U and V go to zero and $k'_x = k_{s_x}$. This leads to

$$k'_x = k_{sx} \left\{ 1 + \frac{V}{C_{\lambda_y}} \left[1 + \frac{\sec^2 \alpha}{2 \times k_{\lambda_y}} \right] \right\} \quad (3.49)$$

$$k'_y = k_{sy} \left\{ 1 + \frac{V}{C_{\lambda}} \right\} \quad (3.50)$$

Since edge waves are progressive in the alongshore direction, equation 3.50 is similar to 3.28 where the current was modeled as a progressive wave. The changes in the wavenumber and direction of short waves riding on zero mode edge waves are demonstrated in Fig 3.4 . The modulation in the wavenumber increases onshore where the wavelength goes to zero. Increasing the angle of wave incidence is shown to increase the wavenumber modulation.

C. CHANGES IN WAVE ENERGY AND MOMENTUM FLUX

1. Background

A wave train composed of a group of individual waves propagates with the group velocity at which the total energy is transmitted. Energy is usually expressed in terms of average energy over a complete wavelength per unit surface area. The total energy of any wave system is the sum of both the potential and kinetic energy.

The average potential energy E_p per unit surface area is given by

$$E_p = \frac{1}{2} \frac{\rho g}{TL} \int_t^{t+T} \int_x^{x+L} \eta^2 dx dt \quad (3.51)$$

The average kinetic energy E_k per unit surface area is estimated by

$$E_k = \frac{1}{2} \frac{\rho}{2TL} \int_t^{t+T} \int_x^{x+L} \int_{-h}^{\eta=0} (u^2 + v^2 + w^2) dz dx dt \quad (3.52)$$

For linear progressive surface gravity waves, the average total energy E_T is

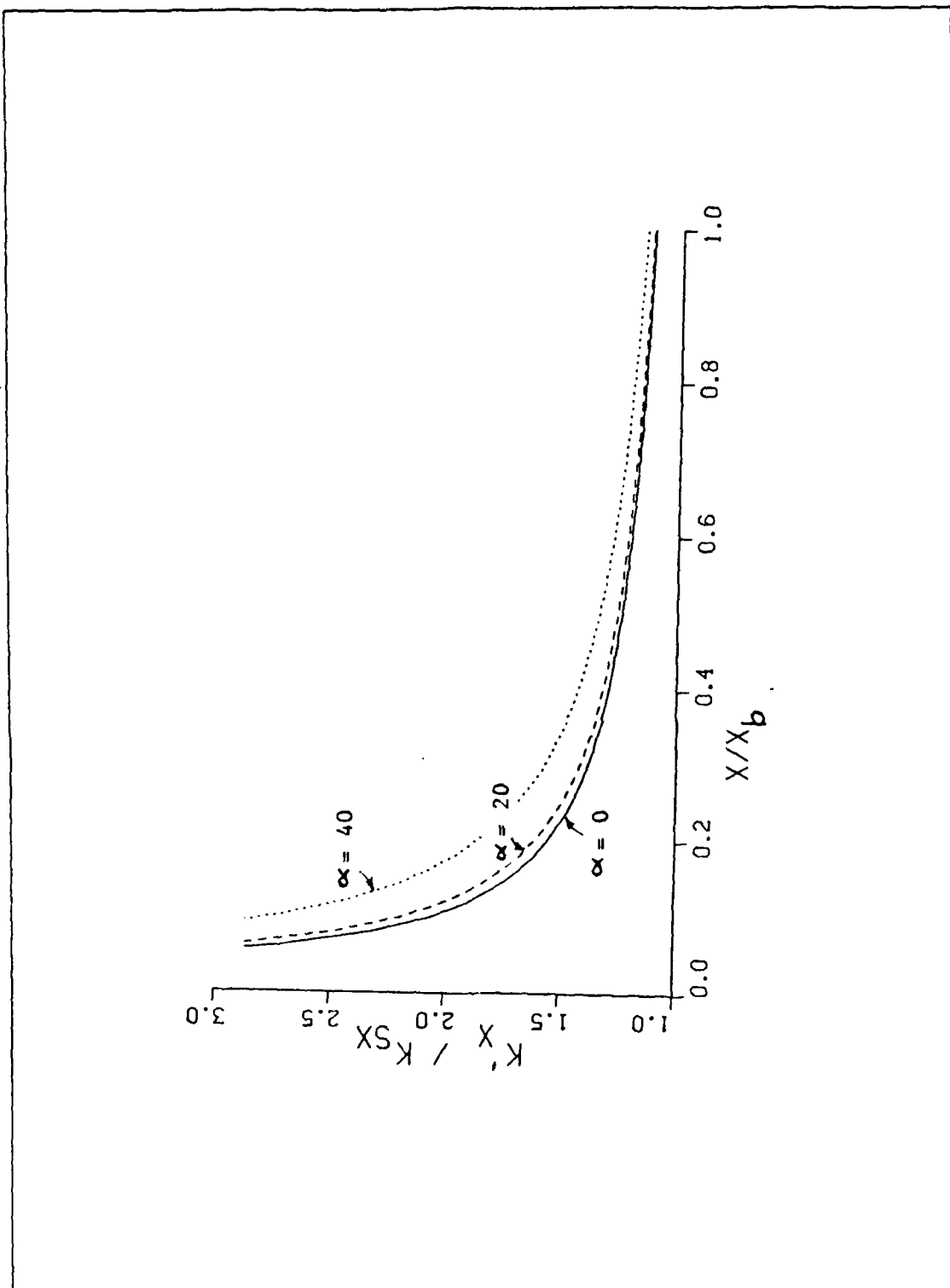


Figure 3.4 Spatial changes in the wavenumber of short period waves due to the presence of zero mode edge wave.

$$E_T = \frac{1}{2} \rho g a^2 \quad (3.53)$$

which is equally partitioned between the potential and the kinetic energy.

a. First Order Sea-Swell Energy Modulation

Short period waves riding on much longer wave can be examined using the principle of superposition. First order modulations are examined using the linear description of both waves. The linear theory is recognized as a reasonable approximation for its successful use in describing many observed phenomena even within the surf zone, (Bowen et al., 1968; Guza and Thornton, 1980). The total surface elevation may then be expressed as

$$\eta_T = \eta_s + \eta_l \quad (3.54)$$

where the subscripts s and l refer to sea-swell waves and long period waves (infragravity waves) respectively. Inside the surf zone, short waves break, dissipating their energy onshore. The depth-controlled wave breaking model is adopted (equation 2.11) to describe first order short wave dissipation with zero amplitude at the intersection of the mean water level (MWL) with the beach. The depth in equation 2.11 is modified to include the slowly varying depth changes due to the presence of the long wave,

$$a_s = \gamma (h + \eta_l) \quad (3.55)$$

where η_l is the surface elevation of low frequency wave motion on a sloping beach and is described by either a long standing wave or an edge wave. The objective of this approach is to examine a first order energy perturbation (second order in amplitude) due to the presence of long waves. In the 2-D model, the long wave is modeled as a long standing wave. The potential energy for the combined short and long waves is

calculated by substituting the combined surface elevation given by equation 3.54 into equation 3.51 . The kinetic energy (equation 3.52) is similarly calculated using the total horizontal velocity,

$$u_T = u_s + u_\lambda \quad (3.56)$$

where

$$u_s = \gamma (h + \eta_\lambda) \sqrt{g/h} \cos \omega_s t \quad (3.57)$$

and u_l is given by 2.17 . It is assumed that the vertical velocities in shallow water are small compared with the horizontal velocities, i.e., $w \ll u$. The total energy E_T averaged over short and long wave periods is the sum of both the potential and kinetic energy and is given by

$$\begin{aligned} E_T = & \frac{1}{2} \rho g [(\gamma h)^2]_{\omega_s} + \frac{1}{2} a_\lambda^2 (J_0^2(\chi) + J_1^2(\chi)) |_{\omega_\lambda} \\ & + \frac{1}{4} \gamma^2 a_\lambda^2 J_0^2(\chi) |_{(\omega_s + \omega_\lambda)} \\ & + \frac{1}{4} \gamma^2 a_\lambda^2 J_0^2(\chi) |_{\omega_s - \omega_\lambda} \end{aligned} \quad (3.58)$$

The total averaged energy in equation 3.58 is represented by four terms at frequency bands $\omega_s, \omega_l, (\omega_s + \omega_l)$ and $(\omega_s - \omega_l)$. The first term in right hand side is identified as the short wave contribution if the short waves were considered alone. Similarly, the second term represents the contribution from the long waves alone. The third term is due to the nonlinear interaction between the short wave and the long wave and is represented by two side bands at the sum and difference between short and long wave frequencies.

b. Model Parameters and Preliminary Results

Energy calculations for the combined short and long waves requires specifying the two parameters γ and a_1 in equation 3.58 . The breaker index γ , which relates the breaking wave amplitude to the local water depth, is taken to be .20 when using the root mean square wave height (Thornton and Guza, 1982). The second parameter, the long standing wave amplitude, is defined as the vertical excursion of the low frequency swash oscillation at the shoreline. Earlier work by Munk (1949) and Tucker (1950) showed the infragravity wave height to be 10 percent of the incident wave height, with both quantities measured in 15 m water depth. Goda (1975) measured infragravity wave heights in 1 m water depth and found them to be 20-40 percent of the offshore incident wave height. Guza and Thornton (1982) measured infragravity run-up height in Torrey Pines to be 70 percent of the wind wave heights measured in 10 m water depth. Holman and Bowen (1984) measured the significant runup height, defined as the significant vertical excursion of water level at the shoreline, and found it to be 60 percent of the incident significant wave height at the breakerline. Guza and Thornton (1985a) analyzed data acquired from three different experiments and found that the significant vertical swash excursion on the average was equal to the incident significant wind wave height measured in 10 m depth

$$R^V = H_{sig} \quad (3.59)$$

Therefore, the amplitude of the long wave a_2 is taken as $.50 H_{sig}$. This result will be used here since equation 3.59 is weighted over three different beaches and incorporates the Santa Barbara data, which are considered in the present analysis.

Data acquired at the Leadbetter Beach experiment in Santa Barbara during 1980 are utilized to specify the parameters of the energy model. The best fit to the beach profile assuming a plane sloping beach is found to be 1:25 with a surf zone width of 50 m. The characteristic periods for both the short and long waves as determined from the spectral analysis of current meter records are 14 and 85 seconds respectively. These are typical values for the data acquired on February 4 (narrow banded waves). The model results are shown in Fig 3.5 . The potential energy for long waves is shown to reach a maximum at the shoreline with a magnitude comparable to the maximum

short wave potential energy at the breakerline (Fig 3.5 a). The kinetic energy for both short and long waves decays shoreward (Fig 3.5 b). The total averaged energy decays onshore, with short waves dissipating all their energy at the shoreline where the long waves have their maximum energy (Fig3.5 c). The two side band components show a steady growth (order of 15 percent) in total energy in the vicinity of the shoreline.

2. Mass and Momentum Fluxes

a. Background

The changes in the mass and the momentum fluxes are required to specify the driving forces for predicting the surf zone dynamics. Conservation equations developed by Phillips (1966) are followed, in which the terms representing the mean and fluctuating quantities have been separated. These equations are applicable to wave motion as well as general turbulent motion. No restrictions are placed on the wave slopes and/or amplitudes through the use of these equations.

The conservation of total mass per unit area can be expressed

$$\frac{\partial \rho D}{\partial t} + \frac{\partial M_i}{\partial x} = 0, \quad i = 1, 2 \quad (3.60)$$

where i, j refer to horizontal coordinates, D is the total averaged depth of water, which may include the wave setup, and M_i is the total mass flux defined as

$$M_i = \int_{-h}^{\eta} \overline{\rho u_i} dz, \quad i = 1, 2 \quad (3.61)$$

where u_i is the total horizontal velocity that contains a mean quantity and a fluctuating quantity due to the waves. The overbar denotes, at this stage, averaging in time over the short wave periods, but not so long as to exclude the long waves.

The momentum flux equations are derived from the horizontal momentum equations integrated over depth, averaged over time and using the free surface and bottom boundary conditions:

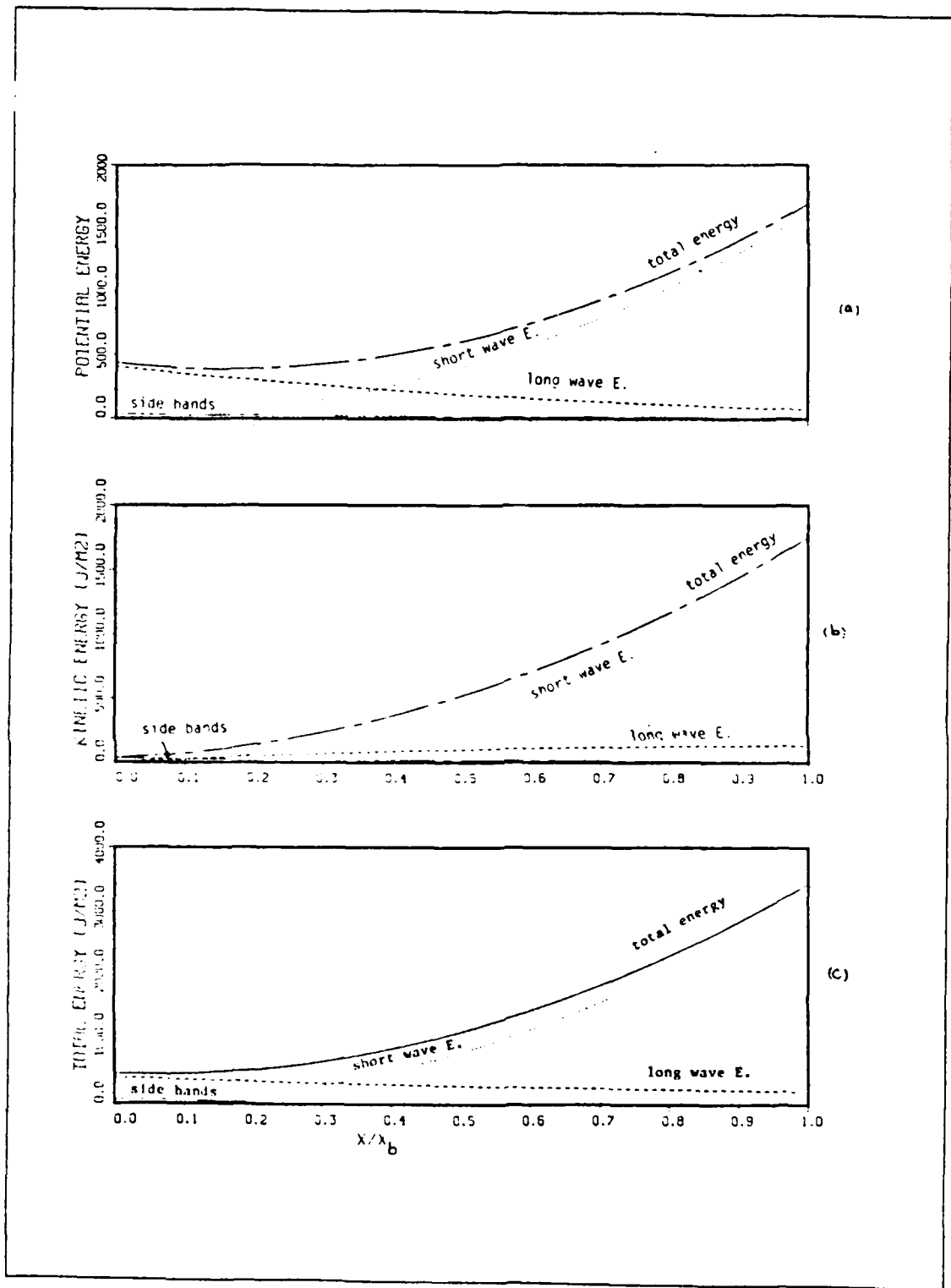


Figure 3.5 Theoretical wave model to predict energy inside the surf zone, (a) potential energy (b) kinetic energy (c) total energy.

$$\frac{\partial M_i}{\partial t} + \frac{\partial}{\partial x_j} \{ U_i M_j + S_{ij} \} = -\rho g D \frac{\partial \eta}{\partial x_i} + R_i \quad (3.62)$$

The first term on the right hand side is the change in the mean hydrostatic pressure due to the slope of the mean free water surface, and R_i is the mean shear stress term. The first term on the left hand side is the local change in horizontal momentum flux; the second term contains the mean momentum flux $U_i M_j$ and the excess momentum due to the wave presence S_{ij} , which was termed the "radiation stress" tensor by Longuet-Higgins and Stewart (1961, 1962). The advantage of using the "radiation stress" technique to solve physical problems is that the second order effects are obtained using first order wave theory, and therefore some non-linear wave properties, such as setup and surf beat, can be explained easily. The radiation stress for a progressive linear waves is given by

$$S_{ij} = \int_{-h}^{\eta} (\rho u_i u_j + p \delta_{ij}) dz - \frac{1}{2} \rho g D^2 \delta_{ij} - \frac{M_i M_j}{\rho D} \quad (3.63)$$

where δ is the Kronecker delta. The third term can be neglected since it is of higher order in deep water and has a negligible contribution in shallow water. Evaluating all terms in equation 3.63, the excess momentum tensor for a linear progressive wave is

$$S_{ij} = \frac{E c}{c} \frac{k_i k_j}{k^2} + \frac{1}{2} E \left[2 \frac{c_g}{c} - 1 \right] \delta_{ij}, \quad i = 1, 2 \quad (3.64)$$

where k_x, k_y are the wavenumber components and are used in the expression to indicate the directions $k_x/k = \cos \alpha$ and $k_y/k = \sin \alpha$.

These expressions are also a good first approximation for slowly varying depth if a and k are interpreted as the local values corresponding to the local depth h (Mei, 1983). In shallow water, the group velocity c_g equals the phase speed c and the radiation stress components are approximated by

$$S_{xx} = \frac{E}{2} [2 \cos^2 \alpha + 1] \quad (3.65)$$

$$S_{yy} = \frac{E}{2} [2 \sin^2 \alpha + 1] \quad (3.66)$$

$$S_{yx} = E \sin \alpha \cos \alpha \quad (3.67)$$

As expected, for a standing wave on a flat bottom, the radiation stress components are exactly twice the values of a progressive wave (Longuet-Higgins and Stewart, 1960).

b. Changes in The Radiation Stresses Due to the Long Waves

The objective now is to rederive the excess momentum due to combined short and long waves to develop explicit formulae. The short waves are assumed to arrive obliquely at an angle α , measured counter-clockwise between the wave ray and the positive X-axis. The long waves are modeled as a normally incident standing wave on a plane sloping bottom. The procedure of calculating the momentum flux components due to the presence of both the short and long waves is to substitute into the general formulation 3.63, which is applicable to all kinds of steady and unsteady flow. In the following development, the terms second order in amplitude (first order in energy and momentum) are retained, and all the higher order terms are neglected. Then, the resulting expressions are averaged over the long wave period to eliminate the time dependence of the obtained formulae.

The radiation stress component S_{xx} , defined as the flux of onshore directed momentum, is given from equation 3.63 as

$$S_{xx} = \int_{-h}^0 \overline{(\rho u u + P)} dz - \frac{1}{2} \rho g D^2 \quad (3.68)$$

The first term under the integral is the product of the total horizontal wave velocities, which can be obtained by summing equations 2.6 and 2.17. The limits of integration

are taken from the bottom to the still water level (SWL) at $\eta = 0$, which is consistent with the analysis being second order in wave slope. Integrating over depth and averaging in time over long wave periods yields

$$\int_{-h}^0 \overline{\rho u_{\tau} u_{\tau}} dz = \frac{1}{2} \rho g \{ \gamma^2 h^2 + a_{\lambda}^2 \left(\frac{\gamma^2 J_0^2(\chi)}{2} + J_1^2(\chi) \right) \} \quad (3.69)$$

The pressure term in equation 3.68 is obtained by integrating the vertical momentum equation (neglecting the vertical stresses) from any depth z to the free surface (see Phillips, 1966), which gives

$$P|_z = \rho \left\{ \int_z^{\eta} g dz + \frac{\partial}{\partial t} \int_z^{\eta} w dz + \frac{\partial}{\partial x_j} \int_z^{\eta} u_j w dz - \rho w_{\tau}^2 \right\} \quad (3.70)$$

The first term is the hydrostatic pressure. Integrating from the bottom to the free surface and averaging over short and long wave periods gives

$$\text{term 1} = \frac{1}{2} \rho g \left\{ \frac{\gamma^2 h^2}{2} + (\eta+h)^2 + \frac{1}{2} \left(\frac{\gamma^2}{2} + 1 \right) a_{\lambda}^2 J_0^2(\chi) \right\} \quad (3.71)$$

The second term is similarly evaluated, but it was found to vanish when averaged over the long wave period. The third and fourth terms give

$$\text{term 3} = -\frac{1}{4} \rho h a_{\lambda}^2 \omega_{\lambda}^2 [J_0^2(\chi) - J_1^2(\chi)] \quad (3.72)$$

$$+ \frac{1}{4} \rho \omega_{\lambda} \tan \beta \sqrt{gh} a_{\lambda}^2 J_0(\chi) J_1(\chi)$$

(3.73)

$$\text{term 4} = \rho h \left\{ \frac{7}{6} \omega_s^2 \gamma^2 (h^2 + \frac{a_{\lambda}^2 J_0^2(\cdot)}{2}) + \omega_{\lambda}^2 \frac{a_{\lambda}^2 J_0^2(\cdot)}{2} \right\}$$

The time averaged radiation stress S_{xx} is obtained by adding equations 3.69, 3.71, 3.72 and 3.73 :

$$\begin{aligned}
 S_{xx} = & \frac{1}{4} \rho g \{ 3 \bar{\gamma}^2 h^2 + (1 + \frac{3 \bar{\gamma}^2}{2}) a_\lambda^2 J_0^2(\chi) + 2 a_\lambda^2 J_1^2(\chi) \} \\
 & + \frac{1}{4} \rho \omega_\lambda a_\lambda^2 (\tan \beta \sqrt{gh} J_0(\chi) J_1(\chi)) + \frac{7}{6} \rho \omega_s^2 \bar{\gamma}^2 h^3 \\
 & + \frac{\rho}{2} a_\lambda^2 h \{ \frac{\omega_\lambda^2}{2} (J_0^2(\chi) + J_1^2(\chi)) + \frac{7}{6} \omega_s^2 J_0^2(\chi) \}
 \end{aligned} \tag{3.74}$$

The first term on the right hand side is identified as the short wave contribution if considered alone, which is in agreement with equation 3.64 obtained by Longuet-Higgins and Stewart (1962). The second and the third terms are the contributions by the long waves and the side bands.

The transverse component of radiation stress, S_{yx} , is defined as the onshore flux of longshore momentum across a vertical plane any distance offshore. This component can be calculated from the direct evaluation of the momentum flux as the product of the total horizontal velocities, u_T and v_T ,

$$S_{yx} = \int_{-h}^{\eta_\lambda} u_T v_T dz \tag{3.75}$$

A cross-shore long wave is considered for simplicity, i.e. no longshore velocity component, while an oblique short wave is considered. Then, equation 3.75 becomes

$$S_{yx} = \rho \int_{-h}^{\eta} (u_s \cos \alpha + u_\lambda) u_s \sin \alpha dz \tag{3.76}$$

The transverse component S_{yx} is the driving force for the longshore current inside the surf zone. When considering the cross-shore long waves, the primary change in S_{yx} arises from the amplitude modulation of the short waves, which is a function of the

long waves. Integrating equation 3.76 over depth and averaging over the short wave period gives the time dependent form,

$$S_{yx} = \frac{1}{2} \rho g \{ \gamma^2 (h + \eta_2)^2 \} \sin \alpha \cos \alpha \quad (3.77)$$

Averaging over the long wave period to eliminate the time dependency, the transverse component S_{yx} inside the surf zone is

$$S_{yx} = \frac{1}{2} \rho g \{ \gamma^2 h^2 + \frac{1}{2} \gamma^2 a_2^2 J_0^2(\chi) \} \sin \alpha \cos \alpha \quad (3.78)$$

The first term on the right hand side is in agreement with equation 3.67, while the second term can be identified as side bands. In equation 3.78, it is noted that the cross-shore long wave by itself does not contribute to S_{yx} , but their interaction with the short wave results in the side bands that increase the S_{yx} term.

IV. DATA ANALYSIS

The analysis of field data is performed to test the hypotheses that the nearshore dynamics are due to both the short and long waves. Outside the surf zone, waves arriving in groups cause a change in MWL (Fig. 4.1) and drive a forced long wave (Longuet-Higgins and Stewart, 1962). At the breaker zone, the short waves break and their heights become depth dependent, obeying the saturation curve. The water depth is modified by the presence of the long waves. Therefore, the short waves are expected to be modulated by the infragravity waves inside the surf zone. The experiments are briefly discussed, followed by analyzed results.

A. DESCRIPTION OF THE FIELD SITES

Two experiments were performed as a part of the Nearshore Sediment Transport Study (NSTS). The objective of NSTS was to develop an improved engineering formula to predict sediment transport on beaches. Field sites were selected for their simple topography of straight and parallel depth contours, which match the assumptions often used for nearshore dynamics. The first experiment was located at Torrey Pines Beach (T.P.), San Diego, California and conducted for one month in November, 1978. Torrey Pines is a gently sloping beach ($\tan \beta = 0.002$) with nearly straight and parallel contours. The bottom is composed of moderately sorted, fine-grain sand (mean diameter 0.15-0.2 mm). The waves break as spilling or mixed spilling-plunging. A wide variety of wave and weather conditions were encountered during the experiment, from small to large (2 m) waves, from very narrow-band swell to wide-band sea, from calm to windy days (> 10 m/s). A total of 42 sensors were deployed over an area 520 m long parallel to the shore and up to 500 m offshore. Surface elevation and horizontal, orthogonal velocity components were measured along a shore-normal transect from offshore at the 10 m depth contour to the shore.

Leadbetter Beach, Santa Barbara (S.B.), California was the second NSTS experimental site (February, 1980). Leadbetter Beach has relatively straight and parallel nearshore depth contours with well-sorted fine to medium size sand. The mean nearshore slope varied between 0.017 and 0.05 during the experiment, depending on the wave climate. Well-developed cusps occurred during the beginning of the experiment.

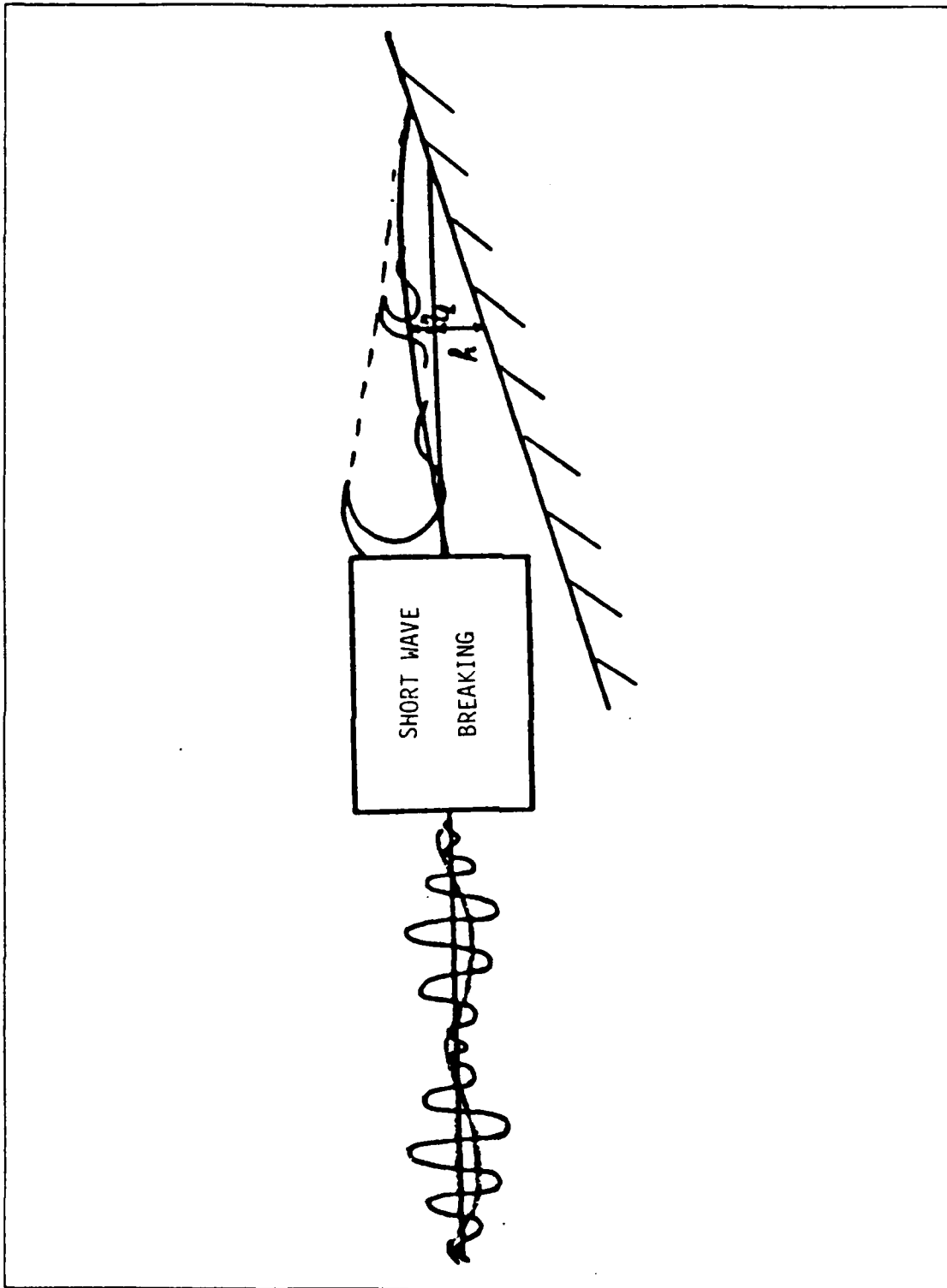


Figure 4.1 Schematic diagram of short and long wave models outside and inside the surf zone.

No major offshore bar system was apparent. The shoreline has an unusual east-west orientation along a predominantly north-south coast. The open ocean waves are limited to a narrow window of approach ($\pm 9^\circ$ centered on 249°) because of protection from Point Conception to the north and the Channel Islands to the south. The generally highly filtered ocean swell type waves from almost due west must make a right angle turn to approach the beach normally. The result is often a narrow band (in frequency and direction) spectrum of waves approaching at large oblique angles to the bottom contours in the surf zone and driving a strong longshore current. Rod and level surveys of the beach profile were obtained daily. An array of current meters and pressure sensors were deployed extensively in a similar manner as at T.P. Severe storms occurred during the experiment, causing significant changes in the shoreline configuration and beach profile. Despite the destruction of most of the instruments during the storm, a very substantial and valuable data was recorded (Gable, 1980).

Data were acquired at a sample rate of 64 Hz for several hours each day, then low-pass filtered and reduced to 2 Hz. The sensors, data acquisition system and experimental sites are fully described by Gable (1979, 1980).

B. DATA ANALYSIS

Data acquired from T.P. and S.B. have been extensively analyzed by different investigators. Incident wave analyses include shoaling, setup, swash oscillation, runup, velocity moments, longshore current and sediment transport. Infragravity waves were studied for runup, identifying both the cross-shore and longshore structures and type of the dominant motion, whether they are leaky and/or edge waves (Guza and Thornton, 1982, 1985a,b; Oltman-Shay and Guza, 1986). As mentioned before, the dynamics of the infragravity waves were not previously studied. Furthermore, their effect on the incident waves, especially inside the surf zone, is of interest to understand the nearshore processes. It is hypothesized in this study that the interaction between the short and infragravity waves generates other waves (side bands) at the sum and difference frequencies. These waves occur at the neighbourhood of the short wave frequency, and they are of importance in driving longshore current and sediment transport at the shoreline. The existence of both the infragravity waves and the side bands are investigated utilizing records of wave staffs, current meters and pressure sensors. Coupling between the incident waves and the infragravity waves are tested via

spectral and cross-correlation techniques, and different theories are discussed. Since the present developed model is monochromatic, only days of narrow banded waves are considered. Three days are selected from each experiment (total of 6 days): 3, 4, and 6 February 1980 at S.B. and 10, 20, and 21 November 1978 at T.P.

1. Spectral Analysis

Velocity and pressure time series of 68-minute length are used to compute spectra with 32 degrees of freedom and a resolution of 0.004 Hz. The power spectra are computed for all the available working sensors at each selected day. The spectra are plotted on linear scale to demonstrate the relative importance of each peak and normalized by the variance (area under spectra). In Fig 4.2, a well defined swell peak is seen at a frequency around $f_s = .06$ Hz in most of the instrument locations during 10 Nov., T.P., and in Figures (4.3, 4.4) at frequency $f_s \sim .07$ Hz in all the analyzed instruments in 3 and 4 Feb., S.B. A consistent valley near 0.05 Hz is present in almost all spectra, separating the incident wave band from the low frequency band. Within the infragravity band, a pronounced low frequency peak is shown in most of the spectra at $f_l = .017$ Hz for 4 Feb, S.B. and .0195 Hz in 10 Nov., T.P.

The infragravity energy has been studied extensively since the first observations by Munk (1949) and Tucker (1950). Huntley et al. (1981) identified a progressive low mode edge wave in the longshore direction that satisfies the dispersion relationship of edge waves. Oltman-Shay and Guza (1986) extended the work of Huntley et al. (1981) and were able to determine the energy contained in each edge wave mode. The low mode edge waves ($n \leq 2$) were found to dominate the longshore current energy while leaky mode or high mode edge waves dominated the cross-shore direction. They attributed the daily changes in infragravity energy levels to the variation in incident wave conditions and the resonant forcing of edge waves described by Gallagher (1971). Guza and Thornton (1985a) observed surf beat in 3 field sites including S.B. and T.P. They found a phase shift of $\pi / 2$ between the surface elevation and the horizontal velocity within low frequency motions ($f \leq .05$ Hz) which indicates the predominance of the standing wave structure of surf beat. This result agrees with Suhayda (1974). Guza and Thornton (1985a) rejected the hypothesis that surf beat is primarily generated by bore-bore capture within the surf zone (as hypothesized by Bradshaw, 1980 and others) because bore-bore capture models do not predict incoming surf beat energy outside the surf zone and do not describe the gradual increase in the infragravity band onshore.

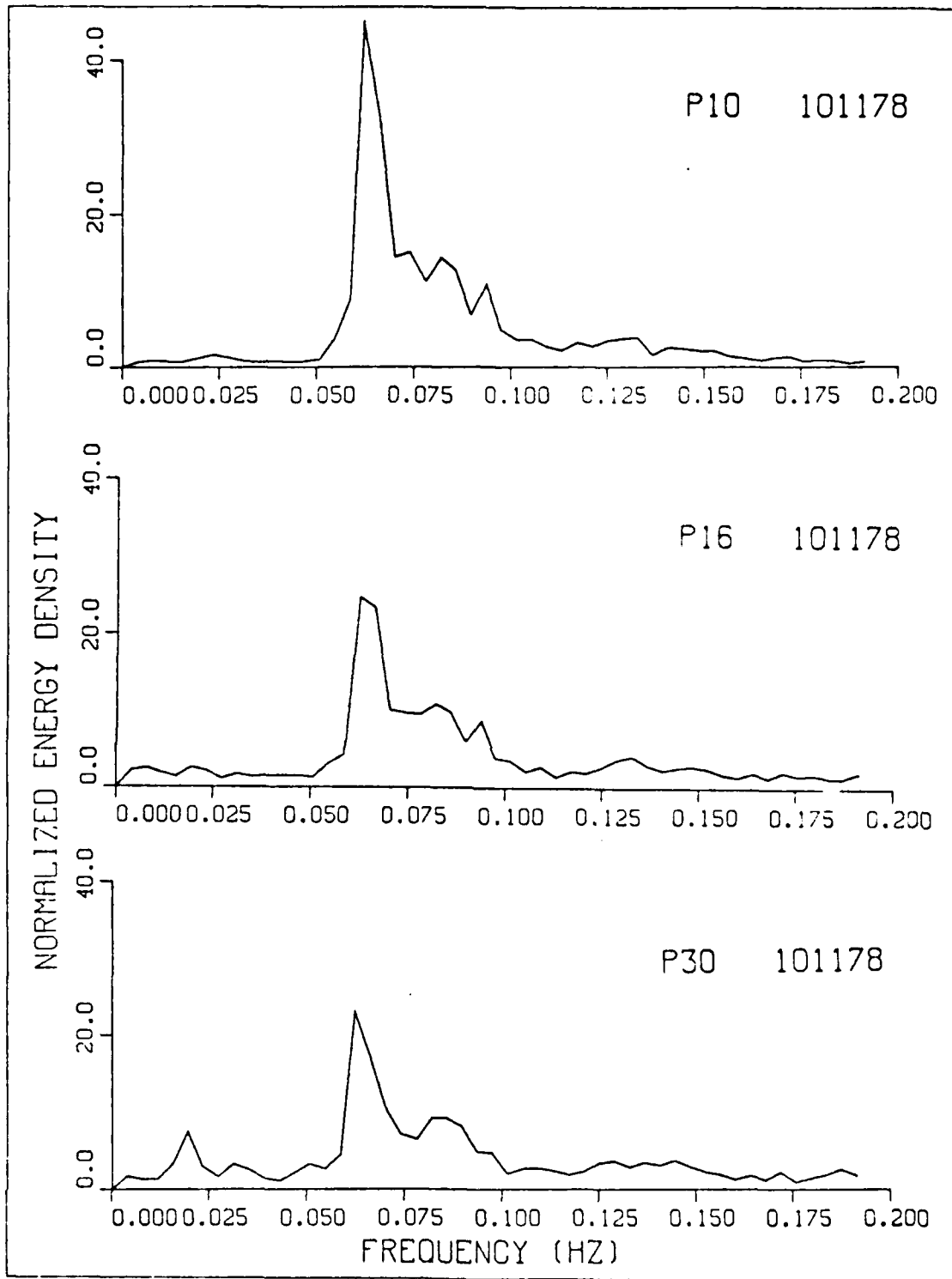


Figure 4.2. Normalized power spectra at different locations in 10 Nov., T.P., showing an onshore relative increase in the infragravity energy level.

The transformation of the incident wave spectra across the surf zone is shown in Figures 4.2 and 4.3 . A dramatic shoreward increase in the low frequency band energy is accompanied with rapid attenuation in the progressive incident wave energy due to breaking as the depth decreases. The infragravity energy can exceed the wind wave energy by a factor of 2.5 in the inner surf zone (Wright et al., 1982). In storm conditions, Holman et al. (1978) observed a considerable increase in the infragravity energy levels responding to the changes in incident wave conditions. It is clear from Figures (4.2, 4.3 and 4.4) that the spectra closer to the shoreline is dominated by the low frequency band.

The theory of wave-wave interaction presented in Chapter 3, by which side band waves are generated as a result of the non-linear interaction, can be tested using the available data. Elgar and Guza (1985), on studying the nonlinear dynamics of the shoaling waves using bispectral analysis, showed that the low frequency motion at the beach face is significantly non-linearly coupled to higher frequency modes seaward the surf zone around the peak of the power spectra. They did not resolve possible side band generation in their analysis, choosing instead to obtain higher stability (low resolution). Using higher resolution here, peaks at frequencies ($f_s \pm f_l$) are found in Fig. 4.5 which are identified as upper and lower side bands. This supports the hypothesis of the short wave modulation derived in equation 3.11 . Evidence of side bands is present for almost all the measurements on all days analyzed, but usually only the upper side band at frequency ($f_s + f_l$) is present (see Figures 4.2, 4.3 and 4.4). The side bands are not always statistically significant, however, since at least the upper side band is present for all narrow band days. Hence, it is concluded that the side bands are real. It is not clear why the lower side band is absent. The suppression of the side band may be strong lower frequency breaking or it may be caused by the seaward radiation of energy by the outgoing component of the standing long waves. Elgar (1985) showed that the low frequency reflected waves will have phase relationships relative to their incoming parts that tend to decrease bispectral level. Guza et al. (1984) show an increase in coherence between the incident wave envelope and the long standing waves when removing the reflected wave.

The time history of energy transferred between swell peak and the upper side band is demonstrated in Fig. 4.6 using almost a four-hour time series. The long record is divided into 64 segments each of 17.1 minutes with a 50% overlap to calculate the spectra. Energy appears to be transferred from the incident wave peak to higher

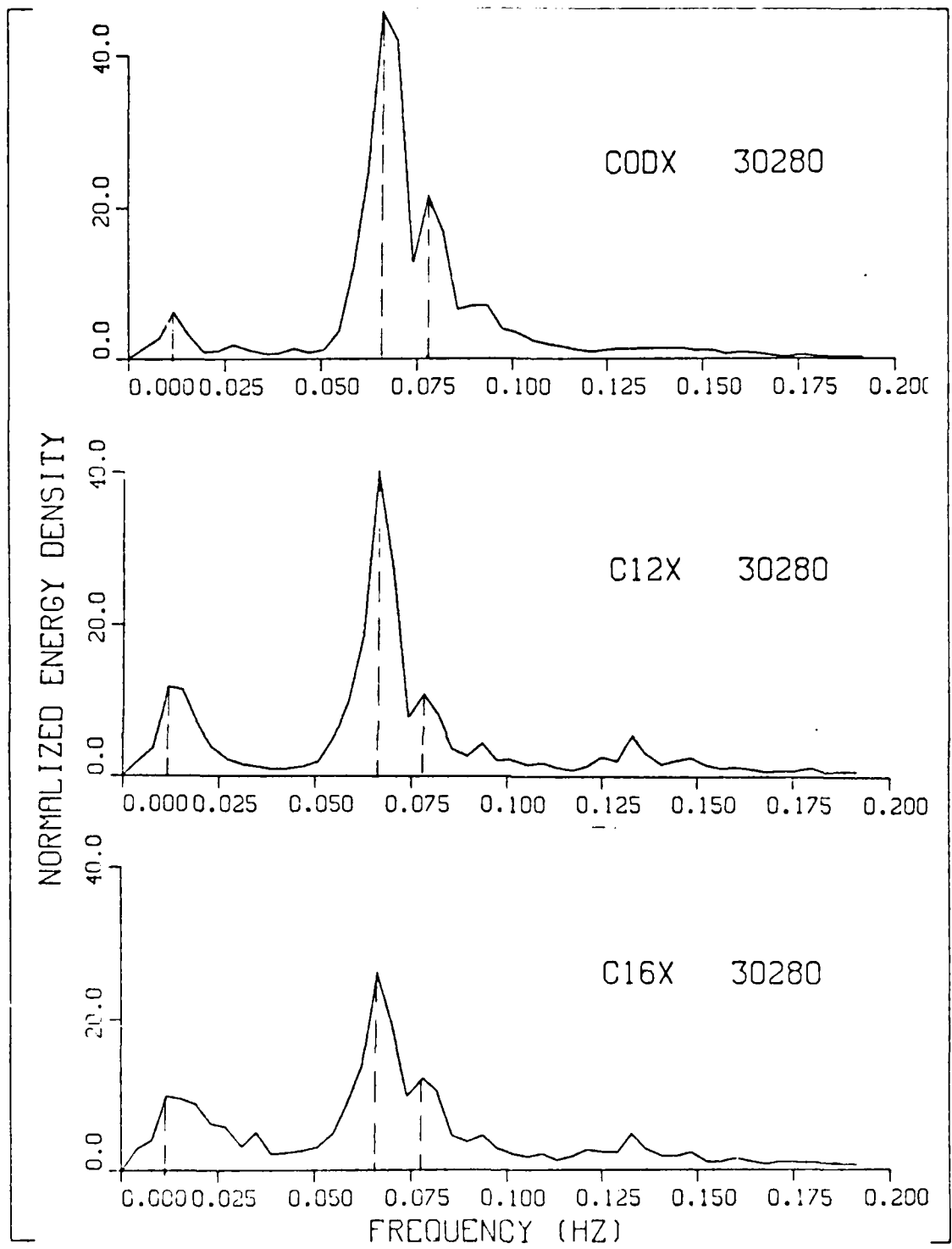


Figure 4.3 Normalized power spectra at different locations in 3 Feb., S.B.

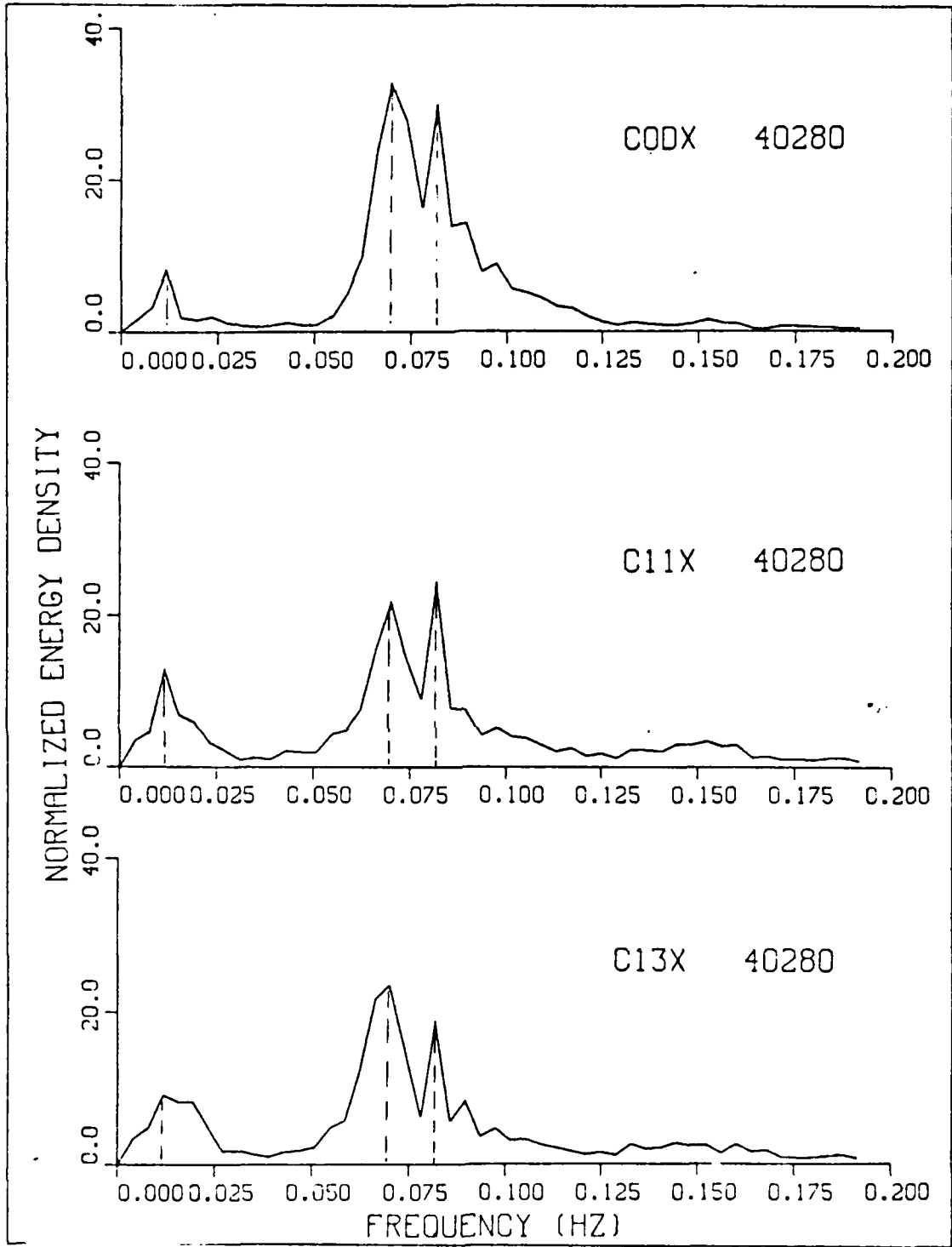


Figure 4.4 Normalized power spectra at different locations
in 4 Feb., S.B.

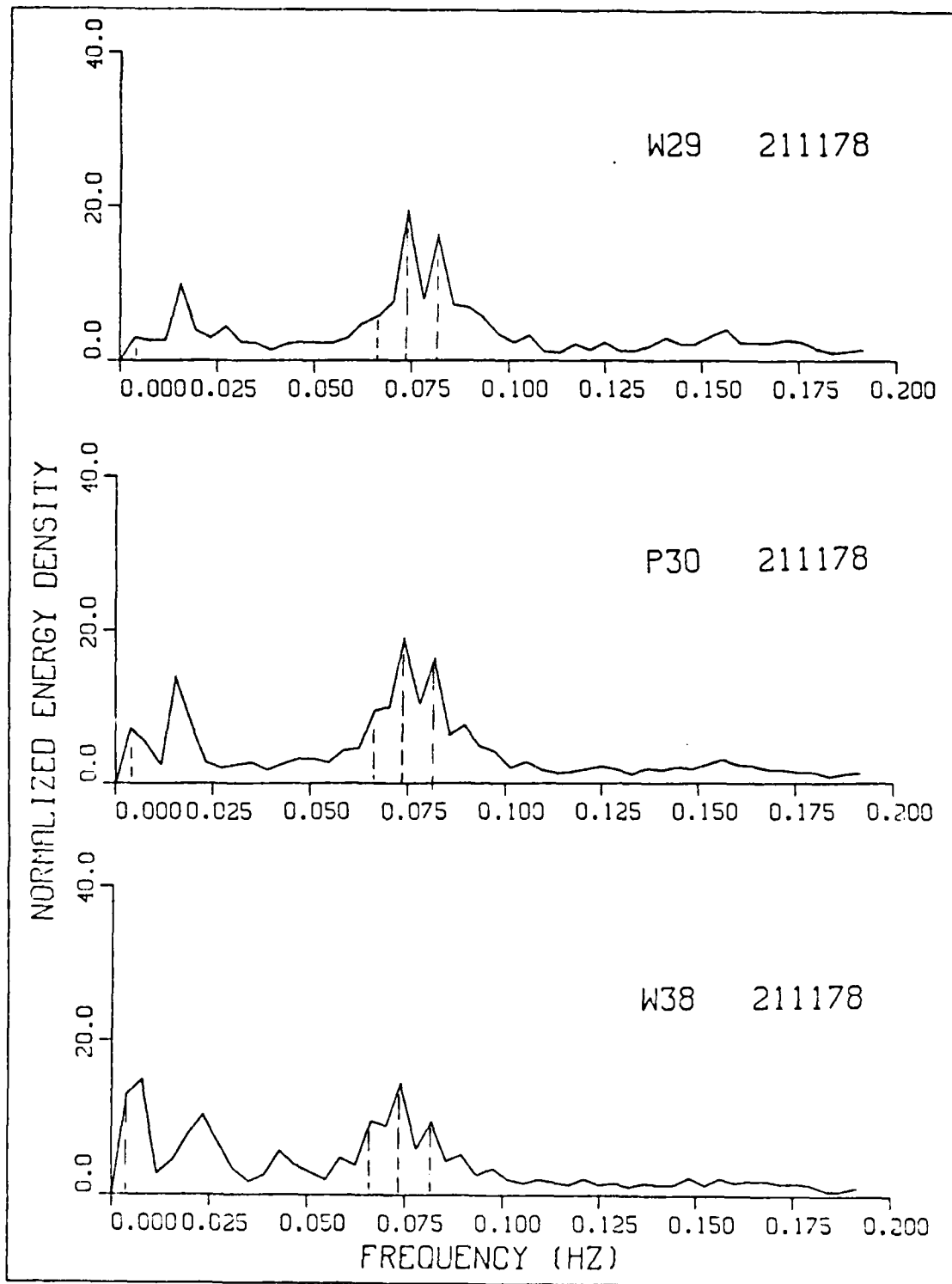


Figure 4.5. Normalized spectra showing significant peaks at frequencies of dominant long wave f_2 , short wave f_s and side bands.

frequency components. This leads to a faster growth of the upper side band than for the lower side band. The incident wave peak drops to a minimum, strengthening the upper side band. A similar mechanism could happen if lower side bands exist, which may transfer energy to low frequency components.

Using the same data set, Guza and Thornton (1985b) computed the velocity variance in 20 Nov., T. P. at each instrument location across the surf zone Fig. 4.7. Their result show no substantial differences between the observed and the predicted values when summing the potential and kinetic energy for short waves riding on long standing waves (Fig. 3.5). The decrease in short wave energy is almost balanced by the increase in low frequency energy resulting in an almost constant cross-shore velocity variance (Guza and Thornton, 1985b). Wright et al. (1982) obtained a similar variance distribution on Australian beach. Although the spectral shape of 3 Feb is similar to 4 Feb, waves in the 4 Feb are more energetic ($H_{sig} = 80$ cm). Therefore, strong non-linearities are expected.

2. Cross-Correlation Analysis

The objective of this analysis is to cross-correlate the incident wave envelope with the long waves to test the hypotheses that long waves are forced outside the surf zone and short waves modulated inside the surf zone. The cross-correlation function, C_R , is a measure of the degree of linear relationship (association) between two data sets in the time domain. Tucker (1950) correlated the incoming wave envelope and the corresponding long wave observed by a bottom mounted pressure sensor at a distance 800 m offshore. He obtained a negative maximum correlation corresponding to a 5 minute time lag. The time lag associated with the maximum correlation was approximately the time required for the incident wave group to reach the shore with velocity c_g and for the associated long wave to travel back with phase velocity \sqrt{gh} . The negative correlation was described by Longuet-Higgins and Stewart (1962) as a low frequency forced wave response due to the incident wave groupness that has a phase shift of π with the envelope of the high frequency waves. Hence, under high waves, a long wave trough is expected and vice-versa.

Huntly and Kim (1984) obtained a positive correlation between long waves and the short wave envelope at zero time lag from current meter measurements taken outside the breaker line. Their results agree with the forced wave model of Longuet-Higgins and Stewart (1962). For velocity measurements, a positive correlation is expected with the x-direction positive offshore.

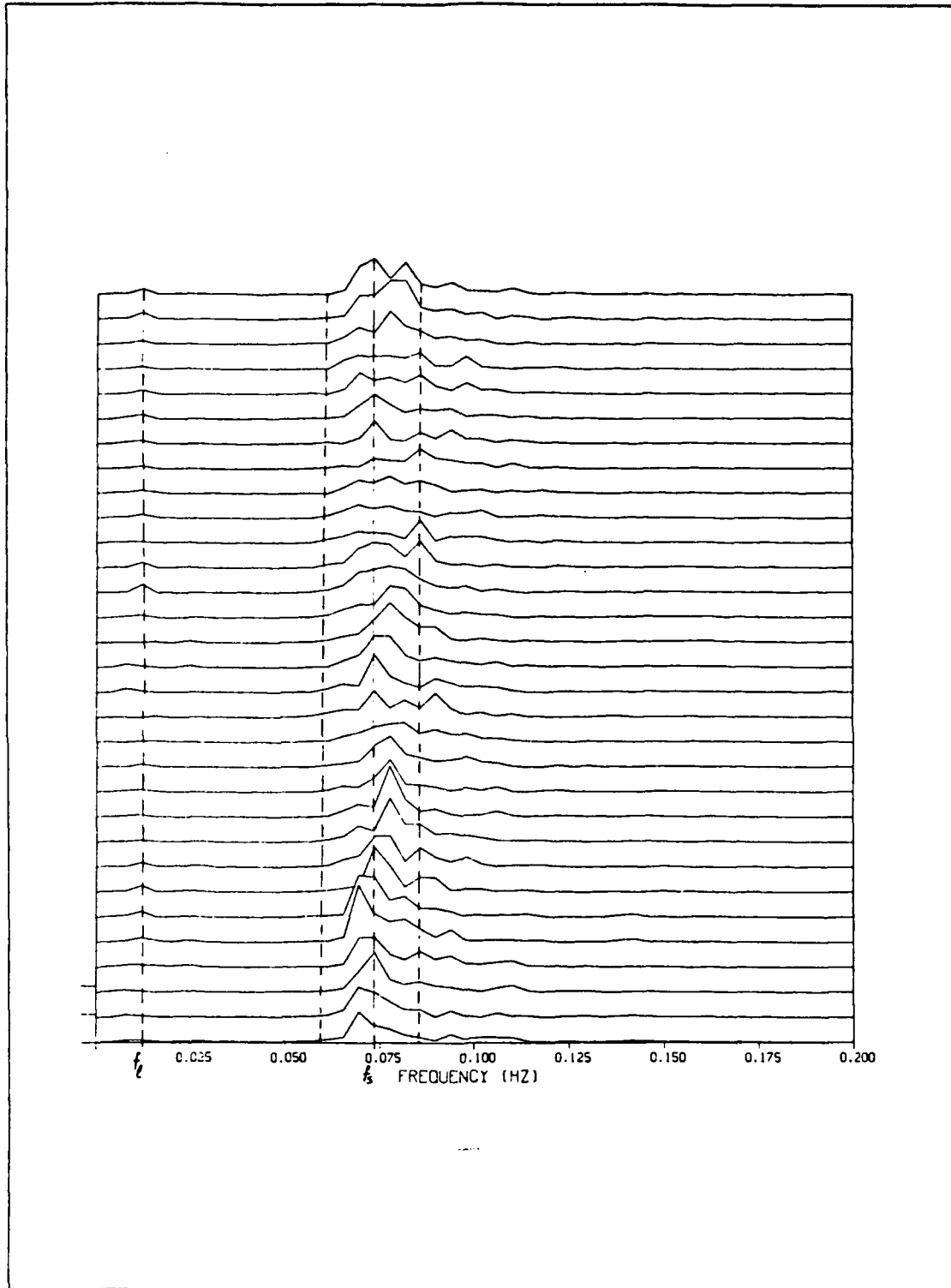


Figure 4.6 Spectral time series of current meter CODx with 50% overlapping calculated from four hour record, (4 Feb, 1980, Santa Barbara).

Guza, et al. (1984) obtained a negative correlation outside the surf zone and a positive correlation inside the surf zone when comparing the surface elevation of the short wave envelope with long waves. No explanation was given for change in signs of the correlation between outside and inside the surf zone.

Surface elevation time series are inferred from current meter data from experiments at T.P. and S.B. using the complex Fourier spectra of the horizontal velocity component, $U(f)$. Current meter records were first linearly detrended to exclude the effects of the rising and falling of the tides, then high-pass filtered using a cut-off frequency of 0.05 Hz to exclude surf beat, followed by a low-pass filter with a high frequency cutoff (0.31Hz) to exclude capillary waves. The filtering was accomplished by Fourier transforming the signals and zeroing the Fourier amplitude coefficients in the filtered frequencies. The complex surface elevation spectrum, $X(f)$, is calculated applying the linear wave theory transfer function, $H_f(f)$

$$X(f) = H_f(f)U(f) \quad (4.1)$$

Then, the complex surface elevation spectrum is inverse transformed to obtain the surface elevation time series. The entire 68-minute-record was transformed at one time to minimize the end effects, which result in spectral leakage, and to obtain maximum resolution for very sharp roll-off at the filter cut-offs. Surface elevations were also computed from pressure signals in a similar manner by transforming the pressure records using linear theory.

Using the surface elevation time series obtained in this manner, the correlation between the incident wave envelope and the corresponding low frequency motion is calculated. The low frequency motion is obtained by low-pass filtering the surface elevation time series. The high frequency wave signal is the residual after subtracting off the low frequency energy. The short wave envelope is obtained by demeaning and squaring the high frequency signal, followed by the same low-pass filter used before. Segments of the time series for the wave envelope and the associated low frequency motion suggest positive correlation for the wave sensor inside the surf zone (Fig. 4.8) and negative correlation for the current meter derived signal outside the surf zone (Fig. 4.9).

The cross correlation function is calculated using the following formula

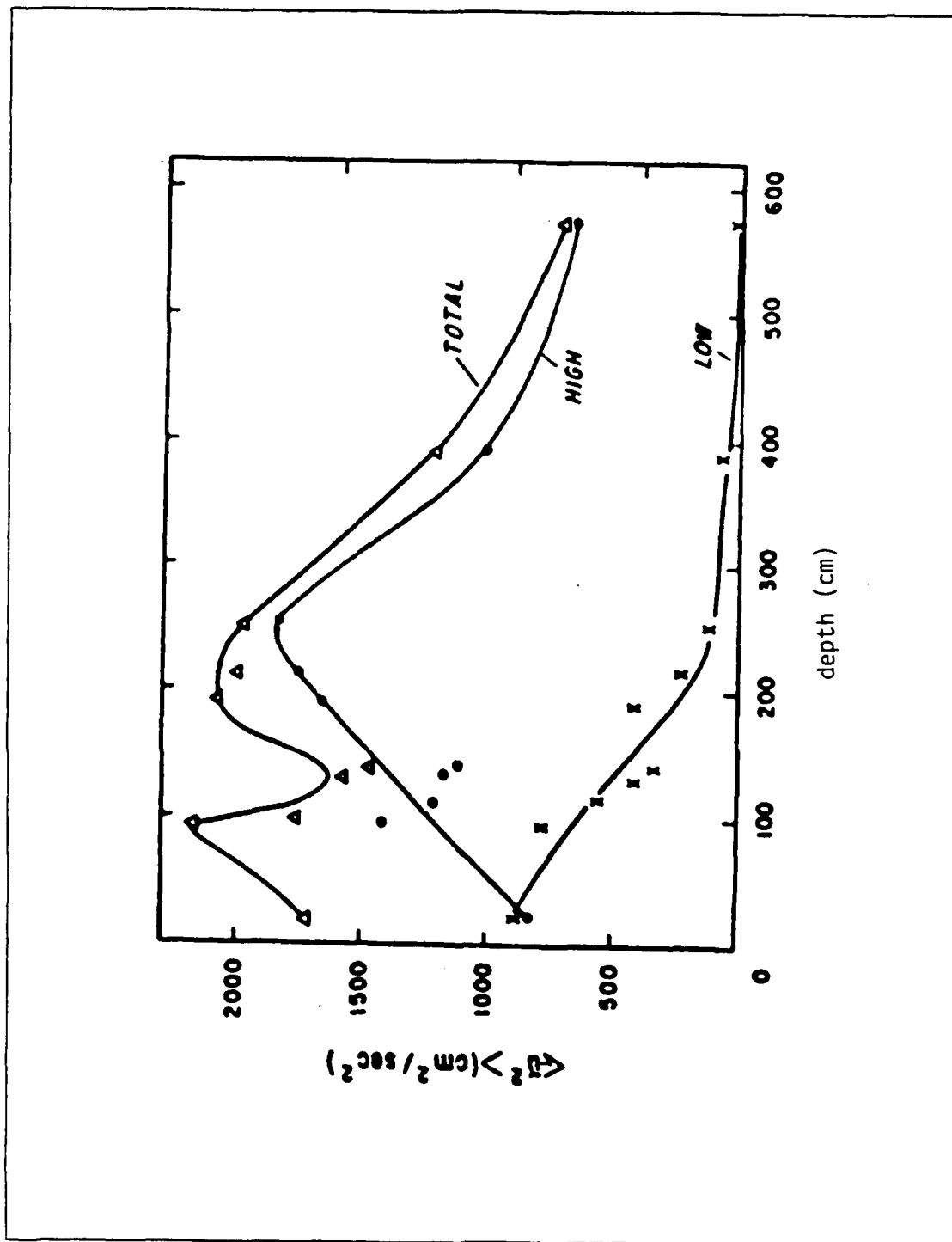


Figure 4.7 Spatial distribution of band passed velocity variance in 20 Nov., 1978.
 . Low is ($0 < f < 0.05$ Hz) and high is ($0.05 < f < .5$ Hz)
 (after Guza and Thornton, 1985b).

W38 211178

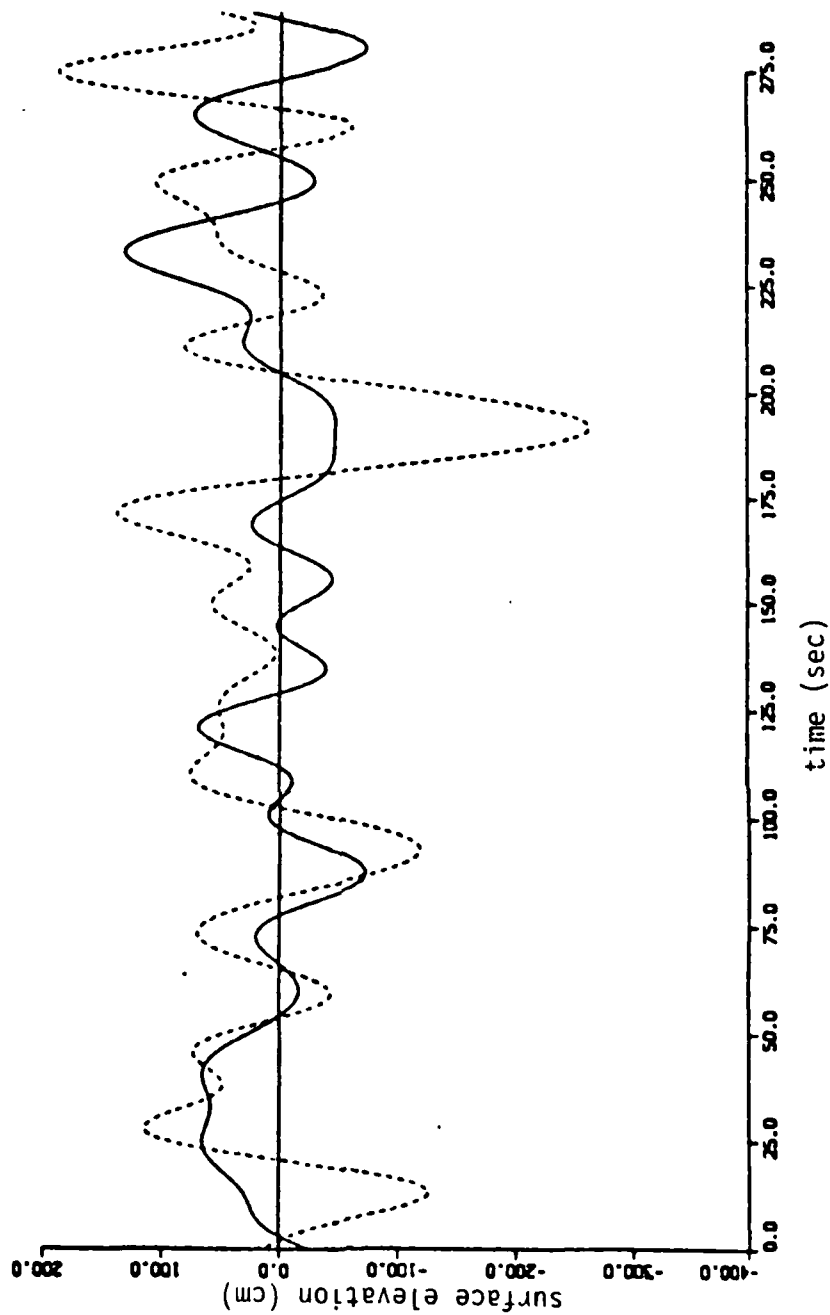


Figure 4.8 Segment of the time series for the wave envelope (solid curve) and the associated low frequency (dotted curve) for wave staff W38 (inside the surf zone) in 21 Nov., 1978, Torrey Pines.

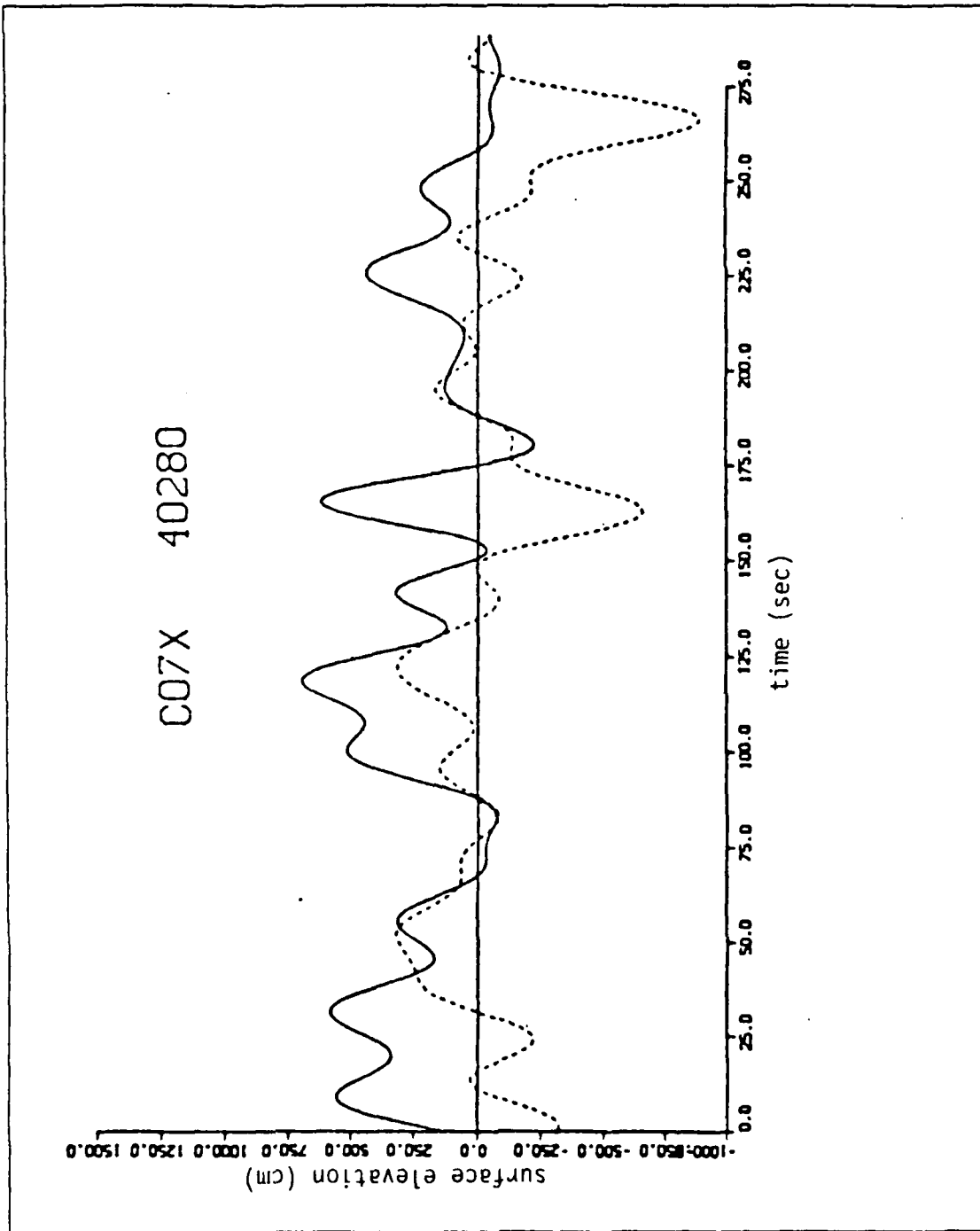


Figure 4.9 Segment of the time series for the wave envelope (solid curve) and the associated low frequency (dotted curve) for current meter C07x (outside the surf zone) in 4 Feb., 1980, Santa Barbara.

$$C_R(\tau) = \frac{1}{n\sigma_x\sigma_y} \sum_{t=1}^{n-k} (x_t - \bar{x})(y_{t+k} - \bar{y}), \quad k = 0, 1, 2, \dots \quad (4.2)$$

$$= \frac{1}{n\sigma_x\sigma_y} \sum_{t=1-k}^n (x_t - \bar{x})(y_{t+k} - \bar{y}), \quad k = -1, -2, \dots, (N-1)$$

where $\tau = k t$ is the time lag, t is the sampling time interval, n is number of data points, σ_x, σ_y are the standard deviations for the low frequency signal and the envelope, and \bar{x}, \bar{y} are the means for each of the time series. The time lag is positive when the long waves are in advance of the wave envelope, and it is negative when long waves lag the wave envelope.

A test of significance (null hypothesis) based on the "Fisher-Z Transformation" is performed with the statistic $z = \sqrt{n-3} / 2 \ln (1 + C_R / 1 - C_R)$ (Miller and Freund, 1977). At level of significance $\alpha = 0.05$, the calculated z always exceeds $z_{\alpha/2} (= 1.96)$, since the used record is long (8192 data points). Thus, the null hypothesis is rejected and the correlation is significantly different than zero.

The correlation function for the wave staff W38 (T.P.) is shown in Fig. 4.10. The maximum correlation is +0.49, corresponding to a time lag of -4.0 sec. The function shows a strong periodicity at about 40 sec. The correlation coefficient is calculated with 95% confidence to be significantly different from zero. Fig. 4.11 shows a negative correlation for C07x (S.B.), indicating the characteristics of a forced wave response outside the surf zone.

The maximum correlation coefficients and the corresponding time lags at each instrument location in 10 and 21 November, T.P. are given in Table I and II. Similarly, tables III and IV are given for 4 and 6 Feb., S.B. Lower values of C_R imply that the two random variables may be independent, that there is no linear relationship between the two signals, suggesting a free long wave (Huntly and Kim, 1984) or the possibility of some non-linear relationship. The low values of the negative C_R can be attributed to the fact that the π phase shift is only a deep water case, while the deepest instrument used is 3 m. The other reason could be the significance of the phase-locked reflected low frequency waves decreasing the coherence even for low values of reflection coefficient (Elgar, 1985). Elgar and Guza (1985) indicated that the infragravity modes do not appear to be bound with a fixed phase relationship to the high frequency wave groups, since their biphasic evolves towards lower values as waves shoal.

W38 211178

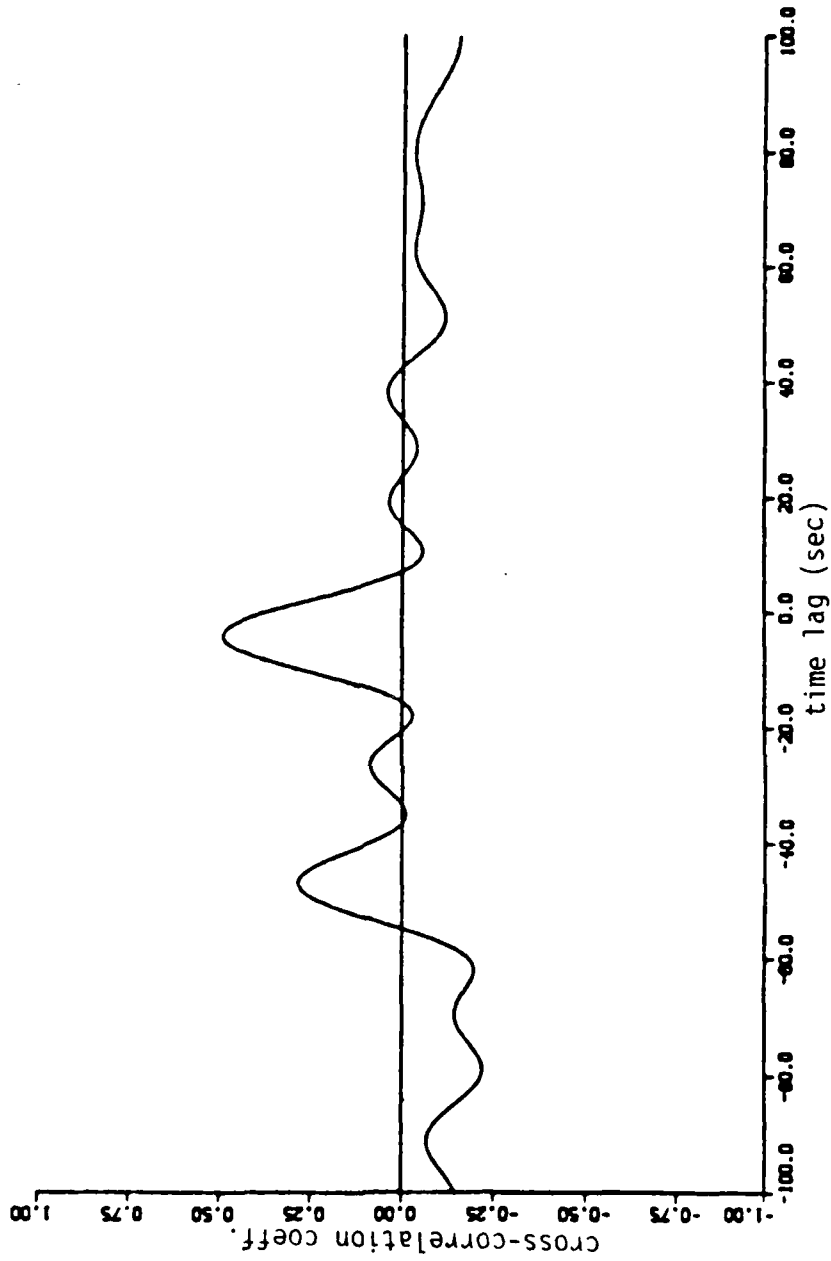


Figure 4.10 The cross-correlation function for W38, 21 Nov., 1978, Torrey Pines. A positive maximum correlation (.49) corresponds to -4.0 time lag.

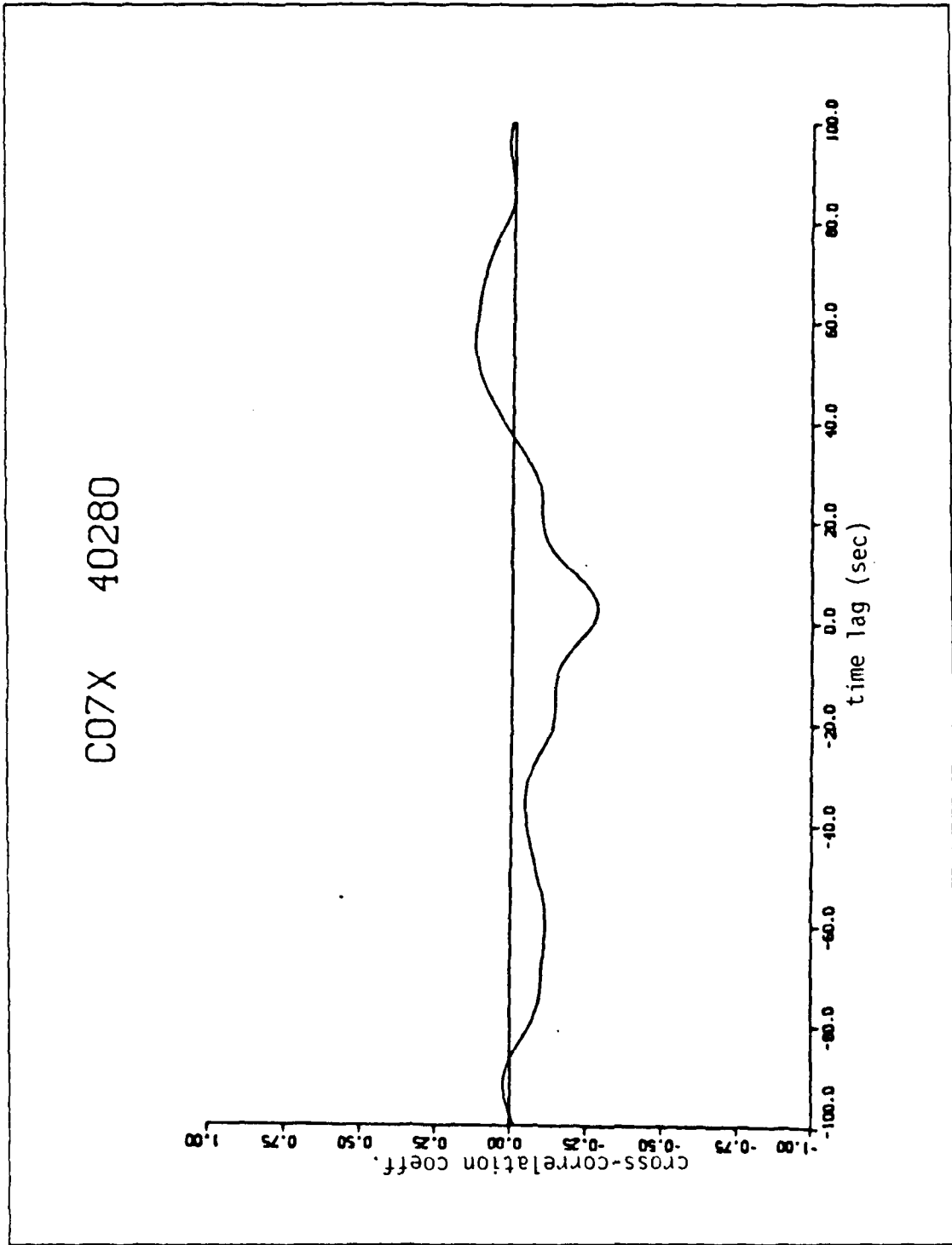


Figure 4.11 The cross-correlation function for C07x, 4 Feb., 1980, Santa Barbara. A negative maximum correlation (.29) corresponds to + 3.0 time lag.

It is of interest to observe a consistent pattern of C_R , being negative outside the surf zone and positive closer to the shoreline (Figures 4.12 and 4.13). The statistically significant values of C_R in the nearshore zone at zero time lag indicated significant coupling between the high and low frequency motions. A zero correlation in Fig. 4.12 is found to coincide with the approximate location of the breaker line. The zero correlation could be due to the two signals being non-linearity related, randomness (noise) introduced into the wave signal by the breaking wave, a possibility that the breakpoint could be at a nodal point for the long standing wave, independence of the two signals, or a transition location between forced and free long waves. Fig. 4.13 shows a consistent negative correlation outside the surf zone and a positive correlation shoreward of the midsurf zone. This could mean that the wave breaking does not destroy completely the wave groupness until some location inside the surf zone. This location might be a transition between the forced and free long waves. Elgar (1985) showed that surf beat biphases decreases as waves shoal. On some days, the correlation in Fig. 4.13 shows a rapid decrease when waves get closer to the shoreline. This might be attributed to the bore-bore capture mechanism. Mase and Iwagaki (1984) illustrated that a wave (bore) could be captured by a successive bore before the bore reaches a maximum runup height. Therefore, the number of runup waves and frequency of runup will be reduced compared to that of incident waves. The ratio of number of waves is given using the surf similarity parameter and shows a decrease in number of waves reaching a gentle slope beach.

The positive correlations obtained inside the surf zone are demonstrated by the simple model developed in chapter 3 by linear superpose the two waves. The surface elevation time series inside the surf zone is simulated using

$$\eta_T = \gamma (h + \eta_2) \cos \psi_S + \eta_2 \quad (4.3)$$

The wave envelope and low frequency motion are obtained as described above. A positive correlation is always shown at zero time lag (Fig. 4.14), which agrees with the observations.

In the following chapter, the theoretical results obtained in Chapter 3 are applied to derive wave setup, longshore currents (steady and unsteady) and sediment transport due to the combined short and long period waves.

TABLE I
 CROSS-CORRELATION BETWEEN THE WAVE ENVELOPE AND LOW FREQUENCY
 MOTION AT EACH INSTRUMENT (10 NOV., 1978, I.P.).

Instrument	P7	P7A	P10	P16	P30	C36	C37	C39	C40
Offshore Distance (m)	360	303	234	159.2	73.4	61.2	47.1	33.2	17.4
Depth (m)	7.67	7.05	5.93	3.84	1.70	1.48	1.24	1.07	0.80
C_{max}	-0.23	-0.37	+0.26	+0.13	+0.16	+0.10	+0.17	+0.13	+0.30
τ (sec) at C_{max}	0.0	-4.5	-19.0	-52.0	-41.0	+13.0	-2.5	-4.0	-6.0
C ($\tau = 0$)	0.23	-0.21	-0.18	-0.07	+0.06	+0.09	+0.15	+0.06	+0.15

TABLE II
 CROSS-CORRELATION BETWEEN THE WAVE ENVELOPE AND LOW FREQUENCY MOTION
 AT EACH INSTRUMENT (21 NOV., 1978, T. P.)

Instrument	P ₄	P ₇	P _{7A}	P ₁₀	P ₁₆	W ₂₉	P ₃₀	W ₃₈	W ₄₁
Offshore distance (m)	456	360	303	233	159	103	73	47	17
Depth (m)	10.06	7.37	6.70	5.54	3.27	1.65	1.26	1.02	0.58
C _{max}	-0.27	-0.15	-0.15	-0.18	-0.29	+0.18	+0.28	+0.49	+0.41
τ sec	+1.0	0.0	-2.0	-5.0	-3.0	+1.0	-2.0	-4.0	-2.0
C (τ = 0)	-0.27	-0.15	-0.15	-0.14	-0.27	+0.18	+0.28	+0.38	+0.40

TABLE III
 CROSS-CORRELATION BETWEEN THE WAVE ENVELOPE AND LOW FREQUENCY MOTION
 AT EACH INSTRUMENT (4 FEB., 1980, S.B.).

Instrument	P	P	C	C	C	C	C	C	C	C	C	C	C	C
	03	12	07x	11x	12x	13x	14x	15x	16x	22x	20x	21x	2Lx	
Offshore														
Distance (m)	72	60	43	38	34	31	28	25	22	19	13	10		
Depth (m)	3.0	2.4	1.7	1.6	1.4	1.3	1.2	1.2	1.0	0.9	0.7	0.5		
C_{max}	-0.3	-0.3	-0.3	-0.2	-0.2	-0.2	-0.2	-0.2	-0.1	+0.3	+0.3	+0.2		
τ (sec) at C_{max}	-3.	-2.	-3.	-13.	-2.	+2.	+3.	-14.	-15.	-6.	-6.	-6.		
$C (\tau = 0)$	-0.3	-0.3	-0.3	-0.2	-0.2	-0.2	-0.2	-0.1	+0.0	+0.1	+0.1	+0.0		

TABLE IV
 CROSS-CORRELATION BETWEEN THE WAVE ENVELOPE AND LOW FREQUENCY MOTION
 AT EACH INSTRUMENT (6 FEB., 1980, S. B.).

Instrument	COD	P03	007	C12	C13	C14	C17	C22	C20
Offshore Distance (m)	126	66	37	28	25	22	13	13	7
Depth (m)	6.16	2.79	1.38	1.03	0.95	0.90	0.71	0.70	0.50
C_{\max}	+0.21	+0.17	-0.18	-0.19	-0.16	+0.13	+0.52	-0.14	-0.24
τ (sec) at C_{\max}	-70.0	-36.0	-1.0	-1.50	+1.0	-27.0	0.0	-15.0	+8.0
$C(\tau = 0)$	-0.08	-0.02	-0.18	-0.19	-0.16	+0.03	+0.52	+0.08	+0.03

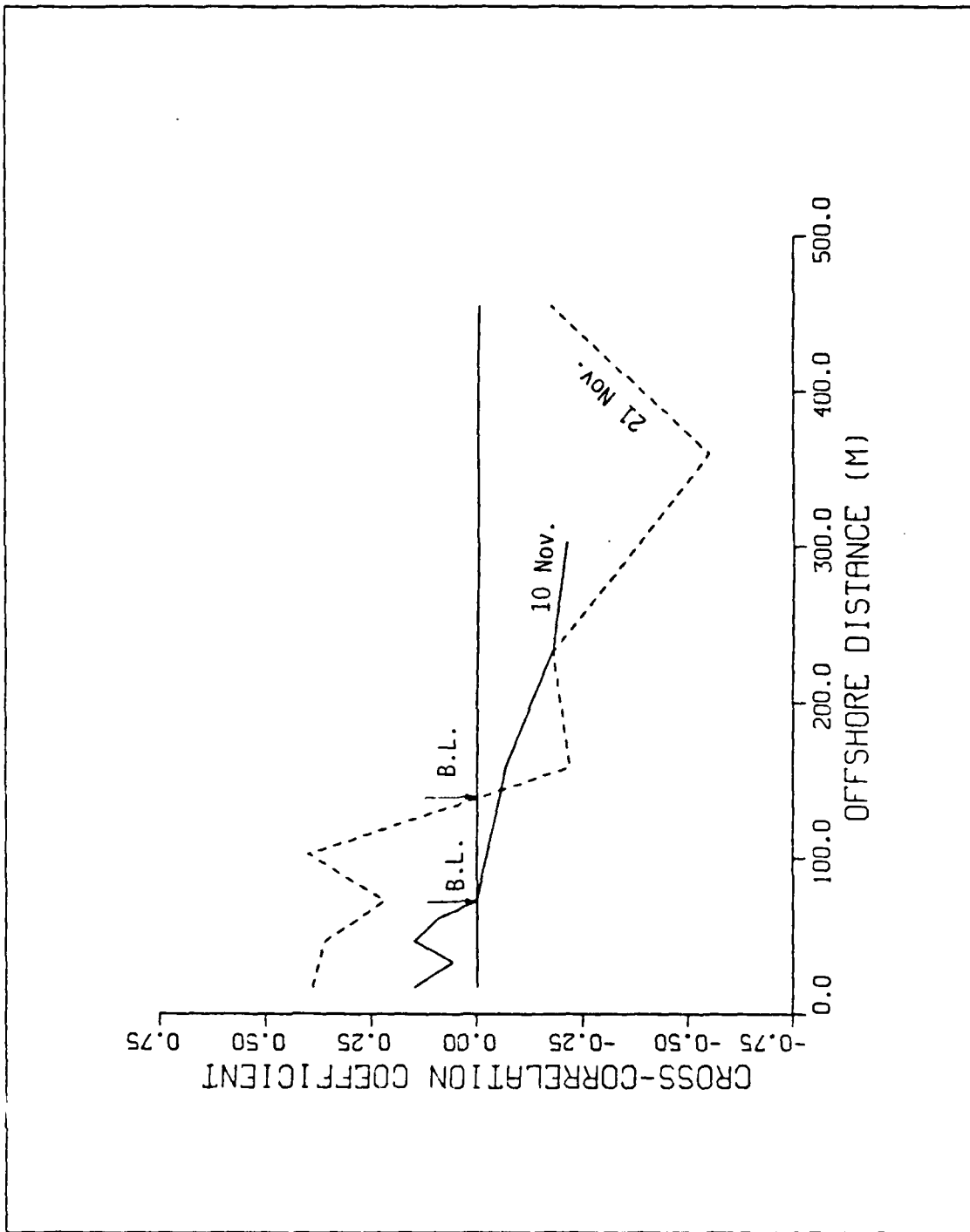


Figure 4.12 Spatial distribution of cross-correlation coefficients showing a dominant negative correlation outside the surf zone and a positive correlation inside the surf zone. B. L. is the breakerline.

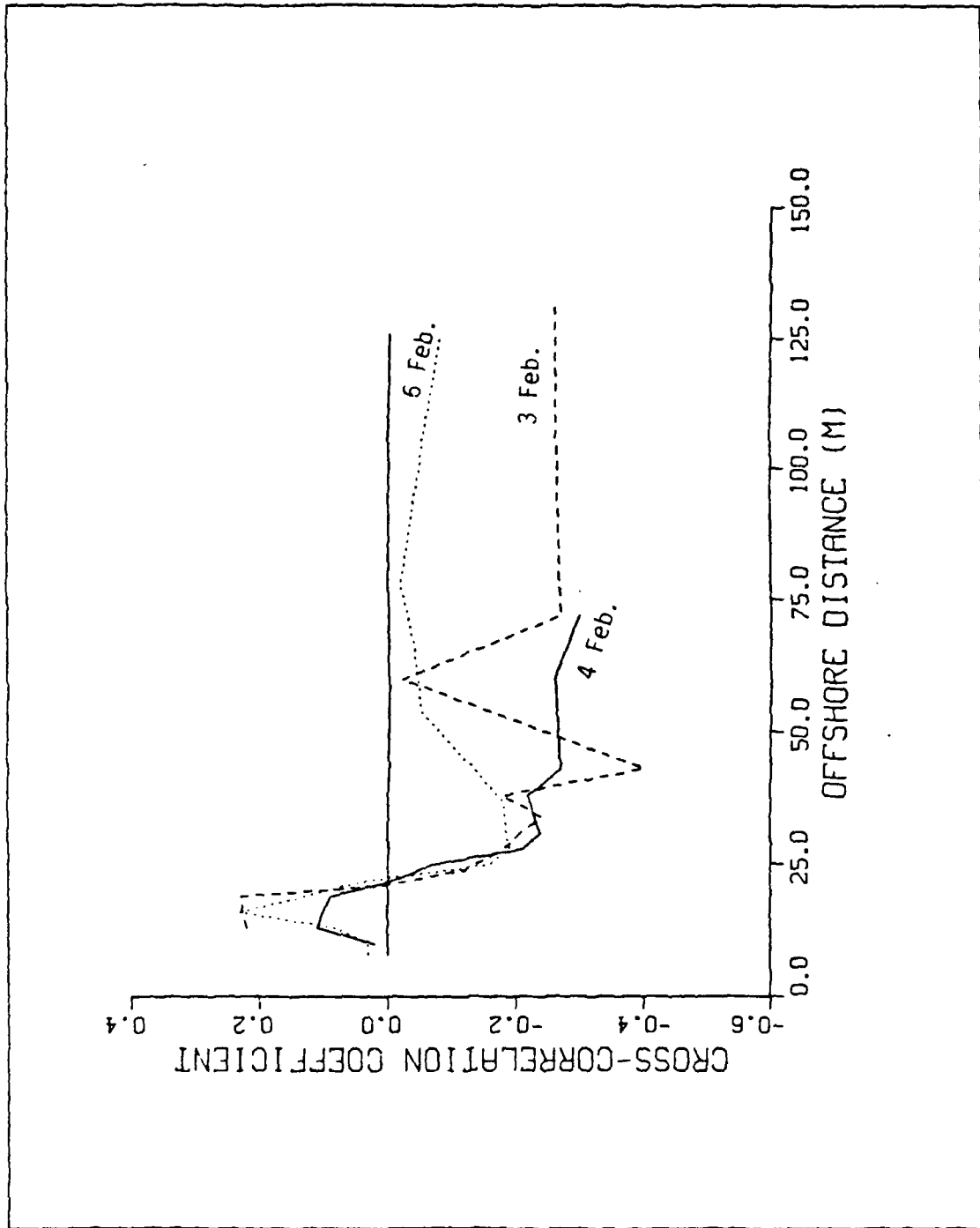


Figure 4.13 Spatial distribution of cross-correlation coefficients showing a dominant negative correlation outside the surf zone and a positive correlation after midsurf zone.

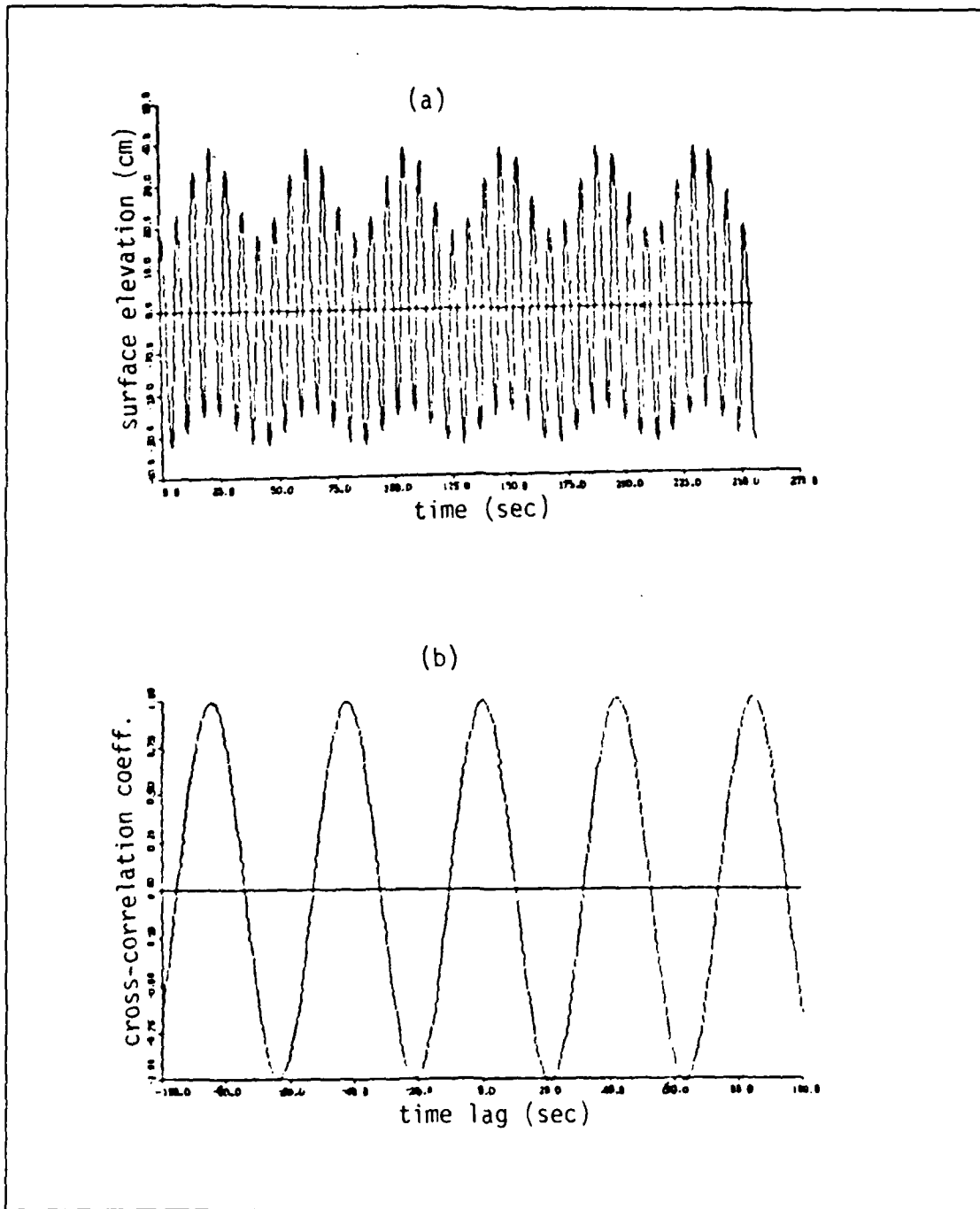


Figure 4.14 Theoretical model to examine the positive correlation between the wave envelope and the associated low frequency motion within the surf zone, (a) segment of time series (b) cross-correlation function.

V. APPLICATIONS

A. WAVE SETUP AND SETDOWN

1. Background

In the nearshore zone, it is observed that waves during shoaling and breaking produce a variation in the mean water level (MWL). This variation in MWL is considered a primary cause of nearshore circulation, such as rip currents. The change in MWL, $\bar{\eta}$, is characterized by two regions (a) a gradual depression of the sea water level starting from offshore, and reaching a maximum at the breakerline, and (b) an increase in the MWL shoreward of the breaker line. The depression is termed "setdown" and the upward slope is called "setup."

To study the wave setdown and setup, the X-component of the horizontal momentum flux equation is considered where the waves are assumed to be steady state and propagating normal to the shoreline over straight and parallel depth contours,

$$\frac{\partial S_{xx}}{\partial x} = -\rho g (h + \bar{\eta}) \frac{\partial \bar{\eta}}{\partial x} \quad (5.1)$$

Equation 5.1 indicates that the change of the excess momentum flux due to wave motion in the cross-shore direction is mainly balanced by the mean water slope $d\bar{\eta}/dx$, assuming no gradients in the Y-direction and neglecting the frictional forces.

It is common to separate the nearshore zone into two dynamical regions of "outside" and "inside" the surfzone.

(1) Outside the Surf Zone :

If waves are assumed to propagate onshore without any energy loss, then the onshore component of the radiation stress is expected to increase steadily as the depth decreases. Therefore, the mean water level is lowered (set down) by the presence of the unbroken waves. Longuet-Higgins and Stewart (1962) integrated equation 5.1 by assuming that $\bar{\eta} \ll h$ to obtain

$$\bar{\eta} = -\frac{1}{2} \frac{a^2 k}{\sinh 2kh} \quad (5.2)$$

This equation is second order in local wave amplitude. The setdown increases steadily until the breaking zone. Without referring to the radiation stress, Longuet-Higgins (1967) also derived the above solution using Bernoulli's integral equation. This simple technique will be illustrated and applied below.

(2) Inside the Surf Zone

As waves break, the wave amplitude inside the surf zone is assumed to be controlled by the total local water depth including the wave setup $\bar{\eta}$, simulating a spilling breaker type, i.e.

$$a = \gamma (h + \bar{\eta}) \quad (5.3)$$

The cross-shore component of the radiation stress, S_{xx} , is a function of the energy density which decreases inside the surf zone and reduces to $3/2 E$ in shallow waters such that

$$S_{xx} = \frac{3}{4} \rho g \gamma^2 (h + \bar{\eta})^2 \quad (5.4)$$

Both the gradients of S_{xx} and the forcing in equation 5.1 have a negative slope. Therefore, the change in the MWL inside the surf zone is expected to be positive, representing a wave setup. Integrating equation 5.1 gives

$$\bar{\eta} = N (h_b - h) + \bar{\eta}_b \quad (5.5)$$

where $N = (1 + 2/(3 \gamma^2))^{-1}$. The subscript b indicates the value at the breakerline where $\bar{\eta}_b = - \gamma H_b / 8$ is determined from equation 5.2. Equation 5.5 shows an increase in the mean water level with decreasing depth, balancing the decreasing radiation stress due to wave dissipation inside the surf zone. It should be noted that

Bernoulli's integral outside the surf zone is not applicable inside the surf zone since the motion is no longer irrotational.

Bowen et al. (1968) demonstrated the above theoretical results by careful measurements in the laboratory. Experimental results agreed well with the theory. However, just outside the breaking point, their experimental values were less than the theoretical predicted since the theory does not consider energy dissipation. Also, very close to the shoreline, Bowen et al. (1968) found a residual wave height (possibly due to a standing wave) to persist and corrected the above equation by letting the setup slope be tangential to the beach slope, i.e. $d\eta/dx \rightarrow -dh/dx$ as $(h + \eta) \rightarrow 0$. Van Dorn (1976) found that the setup gradient at the shoreline is actually steeper than predicted by equation 5.5, which agrees with Bowen et al. (1968). Battjes (1974) and Battjes and Janssen (1978) used a random wave model, which predicts smaller setup values.

In addition to the wave setup laboratory investigations, a few field measurements have been reported. Dorrestein (1961) measured the change in mean water level across the surf zone during times when the significant offshore wave height ranged from 0.8 to 1.6 m. He measured a maximum setup of 0.15 m. Guza and Thornton (1981) measured the setup at the shoreline when the significant offshore wave height varied from 0.6-1.6 m. The maximum setup at the shoreline was found to be about $0.17 H_0$, where H_0 is the deep water significant wave height. Holman and Sallenger (1985) measured the setup under conditions of incident significant wave height varying from 0.4- 4.0 m. They found the setup to vary linearly with the surf similarity parameter $\zeta_0 = \beta (H_0/L_0)^{-1/2}$.

2. Changes in Setup and Setdown Due to the Presence of Long Waves

Changes in the wave setup and setdown due to the presence of long waves can be demonstrated by considering the same wave field used before, i.e. oblique short waves riding on a normally incident long period standing wave. The wave setdown is evaluated applying Bernoulli's integral equation (Longuet-Higgins, 1967). First, the vertical momentum equation is integrated over depth and averaged over time.

$$\left. (\bar{p} + \rho \bar{w}^2) \right|_z - \rho g \bar{\eta} = 0 \quad (5.6)$$

where p is the pressure and the overbar denotes mean quantities. Next, the time averaged Bernoulli's integral equation is evaluated at $z = 0$, assuming the flow is irrotational,

$$p \Big|_{z=0} + \frac{1}{2} \rho (\bar{u}^2 + \bar{v}^2 + \bar{w}^2) \Big|_{z=0} + \text{Constant} = 0 \quad (5.7)$$

The pressure term is eliminated by combining equations 5.6 and 5.7 to obtain

$$\bar{\eta} = - \frac{1}{2g} (\bar{u}^2 + \bar{v}^2 - \bar{w}^2) \Big|_{z=0} + \text{Constant} \quad (5.8)$$

The difference in mean sea level $\delta \bar{\eta}$ is obtained by applying equation 5.8 at two different locations $(x_1, y_1, 0)$ and $(x_2, y_2, 0)$, which avoids evaluating the constant.

$$\delta \bar{\eta} = - \frac{1}{2g} (\bar{u}^2 + \bar{v}^2 - \bar{w}^2) \Big|_{z=0} \Big|_2^1 \quad (5.9)$$

For the combined short and long standing waves, equation 5.9 is used to evaluate the setdown as follows. Each velocity component is expressed as the sum of the short and long standing wave velocities as given before in chapter 2. Let location 2 be in deep water ($h \rightarrow \infty$) where the setdown is zero. Substituting into equation 5.9 and averaging over the long wave period gives

$$\bar{\eta} = - \frac{a_s^2 k}{2 \sinh 2kh} - \frac{1}{2g} (\bar{u}_l^2 - \bar{w}_l^2) \quad (5.10)$$

where subscripts s and l refer to short and long waves. The first term in equation 5.10 is identified as the the setdown solution (equation 5.2) when considering the short wave only. At the breakerline, the depth controlled breaking model is utilized and setdown reaches a maximum to give

$$\bar{\eta}_b = - \frac{\gamma^2 (h_b + \eta_{\lambda b})^2}{4 h_b} - \frac{1}{2g} (\overline{u_{\lambda}^2} - \overline{w_{\lambda}^2}) \quad (5.11)$$

where the subscript b refers to conditions at the breakerline.

Wave setup can be evaluated by spatially integrating the X-momentum flux equation, where the radiation stress component S_{xx} for the combined wave fields is given by equation 3.74 . The constant of integration is evaluated by applying the obtained setup equation at the breakerline where the change of the mean sea level is known from equation 5.11 . The resulting equation is quadratic in $\bar{\eta}$ and has two roots. One root is disregarded since it unreasonably predicts setdown at the shoreline. The second root gives

$$\bar{\eta} = -(h + \sqrt{h^2 - Q}) \quad (5.12)$$

where

$$\begin{aligned} Q = & -[\bar{\eta}_b^2 + 2 h_b \bar{\eta}_b + \frac{1}{2}\{3\gamma^2 (h_b^2 - h^2) \\ & + a_{\lambda}^2 (\frac{3\gamma^2}{2} - 1) (J_{0_b}^2(x) - J_0^2(x)) \\ & + 2a_{\lambda}^2 (J_{1_b}^2(x) - J_1^2(x))\}] \end{aligned} \quad (5.13)$$

Using Longuet-Higgins' setup model for short waves as a reference, the setup is relatively increased closer to the shoreline due to the presence of the long standing wave (Fig 5.1). However, the setdown is also increased at the breakerline compared with the reference model. The relative increase in setup appears to be over-predicted and suggests the importance of including damping terms, such as frictional dissipation and/or percolation, in the swash zone.

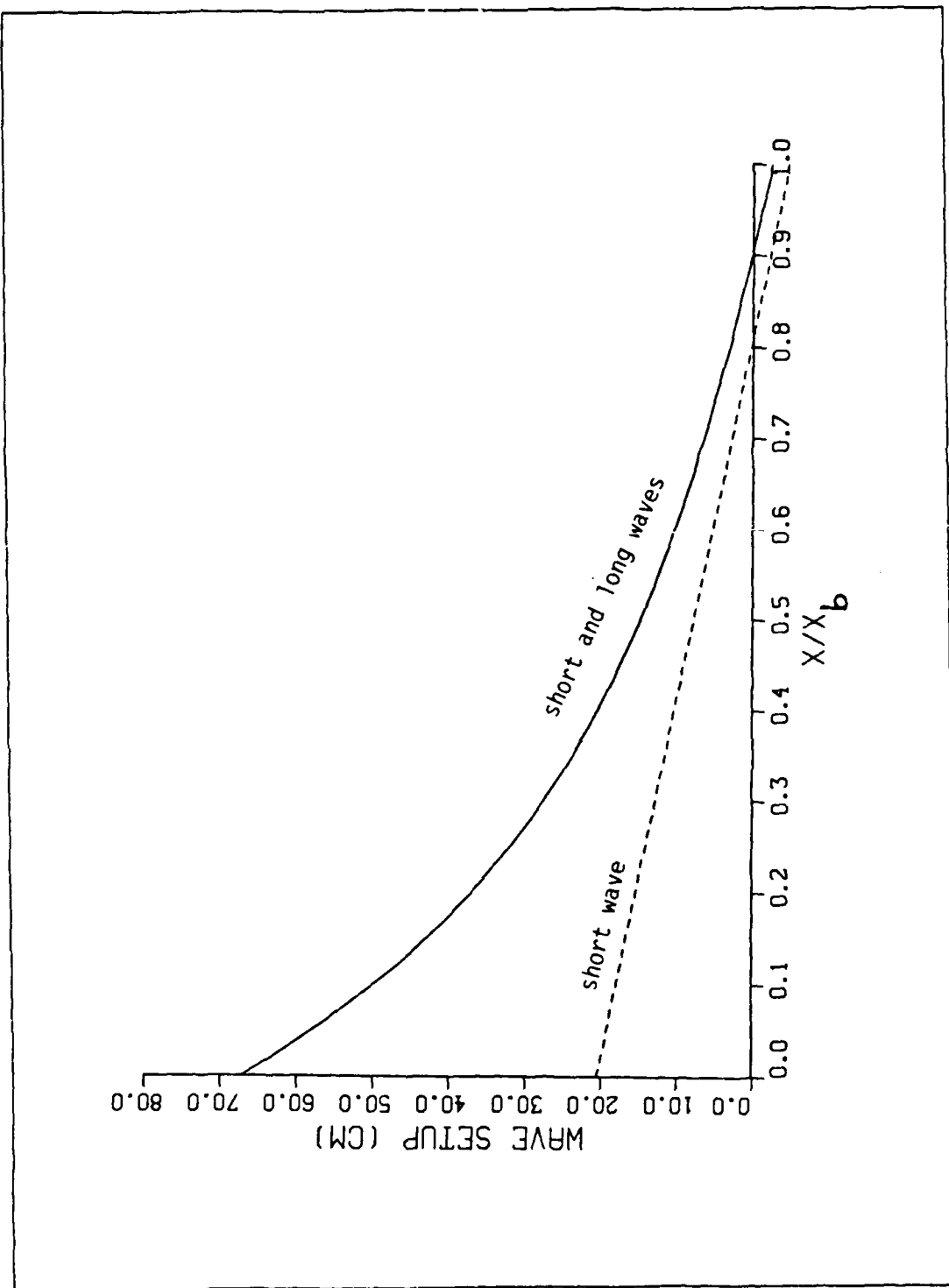


Figure 5.1 Wave setup due to both incident and infragravity waves compared with Longuet-Higgins and Stewart model (1962).

B. LONGSHORE CURRENT

1. Background

When waves obliquely approach the surf zone, a mean current parallel to the shoreline is generated, which is important in transporting sediment alongshore. In the simplest formulations, the longshore current is assumed steady and two dimensional, being independent of the longshore topographic changes. The linear Y-momentum flux equation is simplified such that the gradient of the radiation stress component $\partial S_{yx} / \partial x$ is balanced by the bottom shear stress,

$$\frac{\partial S_{yx}}{\partial x} = -\tau_y \quad (5.14)$$

Outside the surf zone, the wave energy is assumed non-dissipative and the excess momentum flux in the Y-direction is a conservative quantity. Therefore, no driving force is expected outside the surf zone for generating a longshore current (Bowen, 1969). Inside the surf zone, energy is dissipated due to wave breaking, causing a change in the momentum flux. The onshore changes in momentum flux drive a longshore current primarily confined to the surf zone.

Numerous models of longshore current on a long straight beach have been done since the introduction of the radiation stress concept. For obliquely incident waves on plane beaches, analytical solutions were derived for monochromatic waves by Bowen (1969) and Longuet-Higgins (1970 a,b) and for random waves by Thornton and Guza (1986). Numerical treatments (e.g. Thornton, 1970; Jonsson et al., 1974; Madsen et al., 1978); Wu and Liu, 1984, and others) have employed arbitrary beach profile and/or including setup and/or non-linear inertial terms. In monochromatic wave models, lateral mixing is introduced to smooth out the discontinuity in the longshore distribution due to the intensive current shear at the breakerline (Bowen, 1969; Thornton, 1970; Longuet-Higgins, 1970a). For random waves models, there is no need to include the lateral mixing (Collins, 1970; Battjes, 1972) since the waves transform and break over a considerable horizontal distance resulting in a smooth change in the rate of energy dissipation and S_{yx} .

Periodic variation and unsteadiness in the longshore current measurements have been reported by Wood and Meadows (1975) and Meadows (1976), but neither

analytical nor numerical solutions have been attempted. Meadows (1976) suggested three distinct longshore velocity components, a steady component and two fluctuating components, with one at a short wave frequency and the other at low frequency. Guza and Thornton (1978) and Holman and Bowen (1984) observed low frequency components in the longshore velocity spectra. Since the longshore current is a time-averaged velocity, Guza and Thornton (1978) stated that an appropriate temporal averaging time for mean longshore current is unknown. The above studies suggest that the low frequency wave motion can be important inside the surf zone.

Infragravity waves are included in the following wave description inside the surf zone, allowing a more complete description of the wave field. The changes in S_{yx} due to obliqueness of the short wave and the total bed shear stress are derived. Then, the steady and unsteady longshore current formulations are considered on plane sloping beaches.

2. Wave Refraction and Radiation Stress

The depth contours are assumed to be straight and parallel, and obliquely incident waves are therefore refracted according to Snell's law,

$$\frac{\sin \alpha}{c} = \frac{\sin \alpha_b}{c_b} = \text{Constant} \quad (5.15)$$

where c is the phase speed. The S_{yx} component for the combined short and long waves is given by equation 3.77. Assuming a small angle of wave incidence ($\cos \alpha \sim 1$), Snell's constant ($\sin \alpha / c$), which contains all the wave angle information, can be introduced into equation 3.77 to yield

$$S_{yx} = \frac{1}{2} \rho g \left(\frac{\sin \alpha}{c} \right) \sqrt{gh} \gamma^2 (h + \eta_l)^2 \quad (5.16)$$

Another approach for deriving equation 5.16 can be shown by using equation 3.67, where

$$S_{yx} = \frac{EC_g}{c} \sin \alpha \cos \alpha \quad (5.17)$$

By assuming a small angle of wave incidence, 5.17 is reduced to $E c_g (\sin \alpha / c)$ where E is given by $1/2 \rho g \gamma^2 (h + \eta_1)^2$. This will give the same solution as equation 5.16. This result can be attributed to the fact that standing waves by themselves do not contribute directly to the longshore momentum flux since they are oriented in the cross-shore direction, and no S_{yx} forcing is expected for a normal standing wave. The contribution of the infragravity waves manifests itself by the generation of momentum at the side bands. Averaging equation 5.16 over the long wave period gives

$$S_{yx} = \frac{1}{2} \rho g \left(\frac{\sin \alpha}{c} \right) \sqrt{gh} \gamma^2 (h^2 + \frac{1}{2} a_k^2 J_0^2(x)) \quad (5.18)$$

That is to say, the S_{yx} forcing is increased by the formation of the side bands (second term in bracket). The longshore current forcing term $\partial S_{yx} / \partial x$ for both steady and unsteady cases is compared in Fig. 5.2 with the Longuet-Higgins (1970a) model where only short waves are considered. In general, the combined forcing by short and long waves increases in the vicinity of the shoreline due to the relative growth of the side bands.

3. Bottom Shear Stress

Inside the surf zone the bottom stress can no longer be neglected, especially when considering the change of momentum flux in the Y-direction. Assuming the quadratic shear stress formula, the averaged alongshore bottom shear stress, exerted by the oscillating wave motion is given by

$$\tau = \rho c_f \overline{|\vec{u}_T| u_T} \quad (5.19)$$

where c_f is the friction coefficient and u_T is the vector sum of the current and the inviscid orbital velocities for both short and long waves measured just above the

AD-A174 634

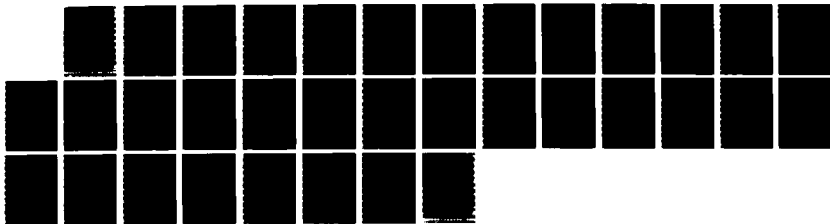
SHORE WAVE MODULATION DUE TO INFRAGRAVITY WAVES IN THE
NEARSHORE ZONE WITH APPLICATIONS(U) NAVAL POSTGRADUATE
SCHOOL MONTEREY CA S M ABDELRAHMAN SEP 86

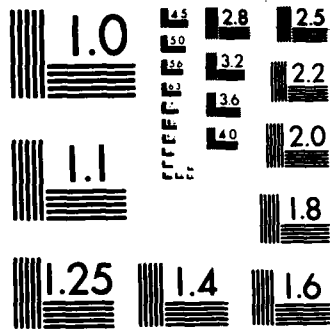
2/2

UNCLASSIFIED

F/G 8/3

NL





MICROCOPY RESOLUTION TEST CHART
NATIONAL BUREAU OF STANDARDS 1963 A

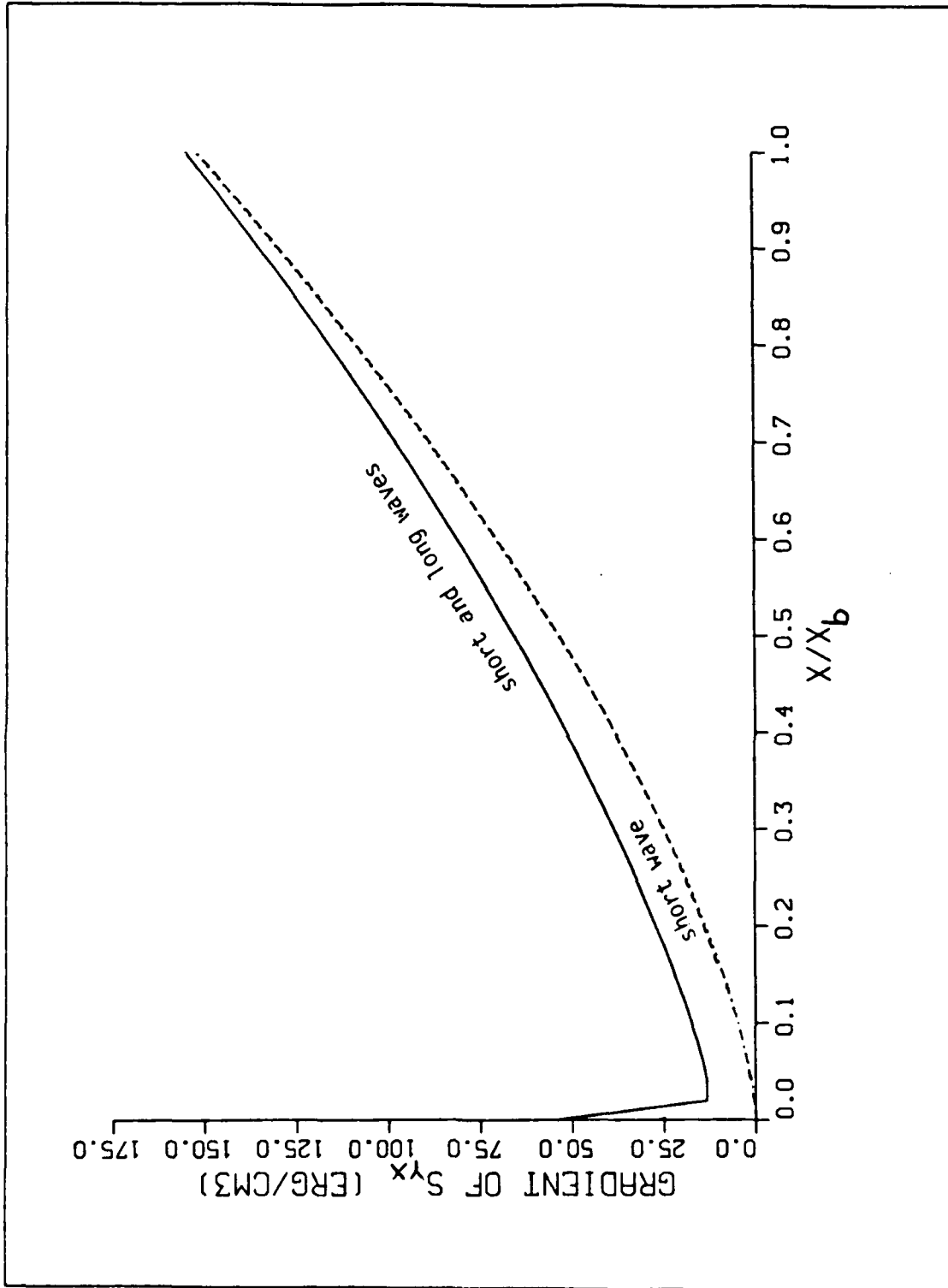


Figure 5.2 Gradient of the longshore current forcing across the surf zone.

bottom boundary layer. The absolute value is necessary to insure that the stress reverses with velocity reversals. Longuet-Higgins (1970a) assumed a small angle of wave incidence and a weak current compared to the water particle motion of the waves, and he was able to simplify 5.19 to

$$\tau_y = \rho c_f \overline{|\vec{u}_T|} V \quad (5.20)$$

where V is the mean motion in the longshore direction which is assumed uniform over depth. The weak current assumption has been shown to be a reasonable approximation for many field applications (Liu and Dalrymple, 1978). The total velocity vector u_T can be resolved into its components in the cross-shore and alongshore directions:

$$\vec{u}_T = \{(u_s + u_l) + U\}\vec{i} + \{(v_s + v_l) + V\}\vec{j} \quad (5.21)$$

where u_s and u_l are the X-component of the orbital velocities and i, j are the unit vectors in the x and y directions respectively. U and V are mean velocities. Assuming uniform currents alongshore, the mean cross-shore velocity U is zero according to the conservation of mass, since the beach forms a boundary in the X-direction. Considering an oblique short wave riding on a cross-shore long standing wave, i.e. $v_l = 0$, equation 5.21 can be rewritten

$$\vec{u}_T = \{(u_s \cos \alpha + u_l)\}\vec{i} + \{(u_s \sin \alpha) + V\}\vec{j} \quad (5.22)$$

The absolute value of the total velocity vector is

$$|\vec{u}_T| = \sqrt{(u_s \cos \alpha + u_l)^2 + (u_s \sin \alpha + V)^2} \quad (5.23)$$

Assuming a small angle of wave incidence ($\alpha < 10^\circ$), $\cos \alpha$ can be approximated to be unity, which simplifies 5.23 to

$$|\vec{u}_T| = \sqrt{(u_s + u_\ell)^2 + v^2 + 2u_s v \sin \alpha} \quad (5.24)$$

It follows that $u_s \sin \alpha$ is small and can be neglected, then

$$|\vec{u}_T| = \sqrt{(u_s + u_\ell)^2 + v^2} \quad (5.25)$$

which can be rearranged into

$$|\vec{u}_T| = |u_s + u_\ell| \sqrt{1 + \left(\frac{v}{u_s + u_\ell}\right)^2} \quad (5.26)$$

Note that $u_s + u_\ell = u_T$ according to equation 3.56. Then, using the weak current assumption, $v/u_T \ll 1$, to simplify the analysis gives

$$|\vec{u}_T| = |u_s + u_\ell| \quad (5.27)$$

Since the two velocities u_s and u_ℓ are almost collinear (both acting almost in the X-direction), equation 5.27 gives the basic relationship

$$|\vec{u}_T| \approx |u_s| + |u_\ell| \quad (5.28)$$

Equation 5.28 can be evaluated using 3.57 and 2.17 and averaged over the short wave period to give

$$|\vec{u}_T| = \sqrt{g/h} \left\{ \frac{2\gamma}{\pi} |h + a_2 J_0(\chi)| + a_\ell |J_1(\chi) \sin \omega_2 t| \right\} \quad (5.29)$$

The alongshore bottom shear stress averaged over the short wave period is then given by the use of 5.20 ,

$$\tau_y = \rho c_f \sqrt{g/h} \left\{ \frac{2\gamma}{\pi} (|h + a_2 J_0(\chi)| + a_2 |J_1(\chi) \sin \omega_\ell t|) \right\} V \quad (5.30)$$

Since 5.29 is still time dependent, the expression is averaged over the long wave period to fit the steady formulation

$$|u_T| = 2/\pi \sqrt{g/h} \{ |\gamma h + a_1 (\gamma J_0(\chi) + J_1(\chi))| \} , \quad (5.31)$$

The corresponding longshore bottom stress is given as

$$\tau_y = \frac{2}{\pi} \rho c_f \sqrt{g/h} \{ |\gamma h + a_2 (\gamma J_0(\chi) + |J_1(\chi)|) \} V \quad (5.32)$$

4. Longshore Current Models

Obliquely incident short waves riding on a normally incident long standing wave are considered to develop steady and unsteady longshore models.

a. Unsteady Model

Neglecting the nonlinear mean advective terms, the linearized Y-momentum flux equation has the form

$$\frac{\partial M_y}{\partial t} + \frac{\partial S_{yx}}{\partial x} = - \tau_y \quad (5.33)$$

where $M_y = V \rho h$ is the mean longshore mass transport averaged over the short wave period. No variation in the longshore direction is allowed in equation 5.33, and the

lateral mixing is ignored for simplicity. Assuming an unsteady longshore current appears to be more general, especially with the presence of irregular oscillatory waves (Wood and Meadows, 1975). Thus, equation 5.33 can be written in terms of the longshore current V :

$$\rho h \frac{\partial V}{\partial t} + \rho c_f \overline{|\vec{u}_T|} V = - \frac{\partial S_{yx}}{\partial x} \quad (5.34)$$

The onshore divergence of the radiation stress S_{yx} is considered the significant forcing for generating longshore currents and is given by differentiating 3.77 ,

$$\frac{\partial S_{yx}}{\partial x}(x, t) = N^* \{ B^*(x) + C^*(x) \cos \omega_\ell t + D^*(x) \cos \omega_\ell t \} \quad (5.35)$$

where N^* is a constant and B^* , C^* and D^* are functions of space only. N^* is given as

$$\begin{aligned} N^* &= \rho \frac{\sqrt{g^3}}{2} \left(\frac{\sin \alpha}{c} \right) \gamma^2 \\ B^* &= \frac{5}{2} \tan \beta h^{5/2} \end{aligned} \quad (5.36)$$

and

$$\begin{aligned} C^* &= a_\ell \left[\frac{3h\sqrt{g}J_0(x) - 2h^{3/2}\omega_\ell J_1(x)}{\sqrt{gh}} \right] \\ D^* &= \frac{a_\ell^2}{4} \left[\frac{\sqrt{g} \tan \beta J_0(x) - 4\omega_\ell \sqrt{h} J_1(x)}{\sqrt{gh}} \right] \end{aligned}$$

The longshore current forcing, $\partial S_{yx} / \partial x$ decreases onshore, then increases closer to the shoreline, having a singular point at $x = 0$ (see Fig 5.2); the computed values stop at $x = 2$ cm. The forcing term is shown to oscillate at the long wave frequency (Fig 5.2). Dividing equation 5.34 by ρh and calling the resulting forcing term $q^*(x, t)$, equation 5.34 can be simplified to

$$\frac{\partial V}{\partial t} + P^*(x, t) V = q^*(x, t) \quad (5.37)$$

where p^* is given by

$$p^*(x, t) = c_f \sqrt{g/h^3} \left\{ \frac{2\gamma}{\pi} |h + a_\ell J_0(x)| + a_\ell J_1(x) \sin \omega_\ell t \right\} \quad (5.38)$$

It can be shown that the time dependent term (second term between brackets) is small compared with the short wave contribution in the swash zone, since $u_1 / |u_s| \rightarrow 0$ at the shoreline. Equation 5.38 then reduces to

$$p^*(x, t) = c_f \sqrt{g/h^3} \left\{ \frac{2\gamma}{\pi} |h + a_\ell J_0(x)| \right\} \quad (5.39)$$

Equation 5.37 is completed by specifying the initial condition $V(x, 0) = 0$. An analytical solution to the unsteady longshore current is obtained using an integrating factor. Despite the fact that both the forcing term and the bed shear stress have a singular point at the shoreline, the resulting longshore current is well behaved and has a finite value at the shoreline. The general solution can be expressed in four terms as

$$V(x, t) = V_{\text{steady}} + V_{\text{unsteady 1}} + V_{\text{unsteady 2}} + V_{\text{transient}} \quad (5.40)$$

The first term is a steady term and is given by

$$\begin{aligned} V_{\text{steady}} = & \frac{5\pi}{8} \left(\frac{\sin \alpha}{c} \right) \frac{\gamma^2 \tan \beta}{c_f A^*} gh^2 \\ & + \frac{\pi}{16} \left(\frac{\sin \alpha}{c} \right) \frac{\gamma^2 a_\ell^2}{c_f A^*} [g \tan \beta J_0^2(x) \\ & - 4\omega_\ell J_0(x) J_1(x) \sqrt{gh}] \end{aligned} \quad (5.41)$$

where $A^* = \gamma (h + a_1 J_0(\chi))$. The steady term is similar to the steady solution given by Longuet-Higgins (1970a) differing only by the second term in the A^* expression. The second term in 5.41 is an additional steady component as a result of the side band formation. The two unsteady terms are functions of the frequency of the long wave and its first harmonic and are given by

$$V_{\text{unsteady 1}} = \frac{\gamma^2 \pi^2 g a_\ell}{2 [4 c_f^2 g A^{*2} + \pi^2 \omega_\ell^2 h^3]} \left(\frac{\sin \alpha}{c} \right) \times [3 \tan \beta J_0(\chi) h^2 \sqrt{gh} - 2 \omega_\ell J_1(\chi) h^3] \quad (5.42)$$

$$V_{\text{unsteady 2}} = \frac{\pi^2 \gamma^2 a_\ell^2 g}{32 [c_f^2 g A^{*2} + \pi^2 \omega_\ell^2 h^2]} \left(\frac{\sin \alpha}{c} \right) \times (P^* \cos \omega_\ell t + \omega_\ell \sin \omega_\ell t) \times [\tan \beta J_0^2(\chi) \sqrt{gh^3} - 4 \omega_\ell J_0(\chi) J_1(\chi) h^2] \quad (5.43)$$

$$(P^* \cos 2\omega_\ell t + 2\omega_\ell \sin 2\omega_\ell t)$$

The fourth term in equation 5.40 is the constant of integration and is evaluated by applying the initial condition at time zero. This term is identified as a transient term which grows very rapidly to a steady state within a few long wave periods.

$$V_{\text{transient}} = -[(V_{\text{steady}} + V_{\text{unsteady 1}} + V_{\text{unsteady 2}}) \Big|_{t=0}] e^{-P^* t} \quad (5.44)$$

In the vicinity of the shoreline, the longshore current is found to be finite and steady and is given by

$$v \Big|_{x=0} = \frac{\pi}{16} \frac{\gamma \tan \beta}{c_f} a_\ell g \left(\frac{\sin \alpha}{c} \right) \quad (5.45)$$

The spatial distribution of the longshore current is shown in Fig 5.3 . The dominance of the side bands and the oscillating components starts at the most shoreward 1/5 of the surf zone width. At the breakerline, intensive shear occurs as expected in monochromatic models. Lateral mixing, if added, will diffuse the shear and smooth the longshore distribution as described before. Comparison with Longuet-Higgins' (1970a) model shows an onshore increase of the longshore current and a relative decrease closer to the breakerline. The decrease is due to the the increase in the bottom shear stress.

The time variability of the longshore current is evident in Fig 5.4 , where the current is shown to oscillate at the infragravity wave frequency. In the vicinity of the shoreline, the first harmonic ($V_{unsteady2}$) dominates the fundamental frequency component. The transient term is just an initial response to the wave system that becomes negligible within a few infragravity wave periods.

b. Steady Model

For steady flow, equation 5.14 is used in which the cross-shore gradient of S_{yx} is balanced by the bottom stress. As in the analysis of the unsteady model, wave setup is not included. Steady solutions with and without considering lateral mixing are developed. Averaging over long wave periods is required to eliminate the time dependency in the equations describing the unsteady models. The bed shear stress is given by equation 5.32 , and the transverse radiation stress component is obtained by averaging equation 5.35 over the long wave period. Substituting in equation 5.14 , the steady longshore current is given by

$$\begin{aligned}
 V_{steady} = & \frac{5\pi}{8} \left(\frac{\sin \alpha}{c} \right) \frac{\gamma^2 \tan \beta}{c_f \Lambda^{**}} g h^2 \\
 & + \frac{\pi}{16} \left(\frac{\sin \alpha}{c} \right) \frac{\gamma^2 a^2}{c_f \Lambda^{**}} [g \tan \beta J_0^2(\chi) \\
 & - 4\omega_{\chi} J_0(\chi) J_1(\chi) \sqrt{gh}]
 \end{aligned}
 \tag{5.46}$$

where $\Lambda^{**} = \gamma h + a_1 (\gamma J_0(\chi) + J_1(\chi))$. The first term of 5.46 is similar to the steady term in the unsteady case except for Λ^{**} . At the shoreline, the growing side

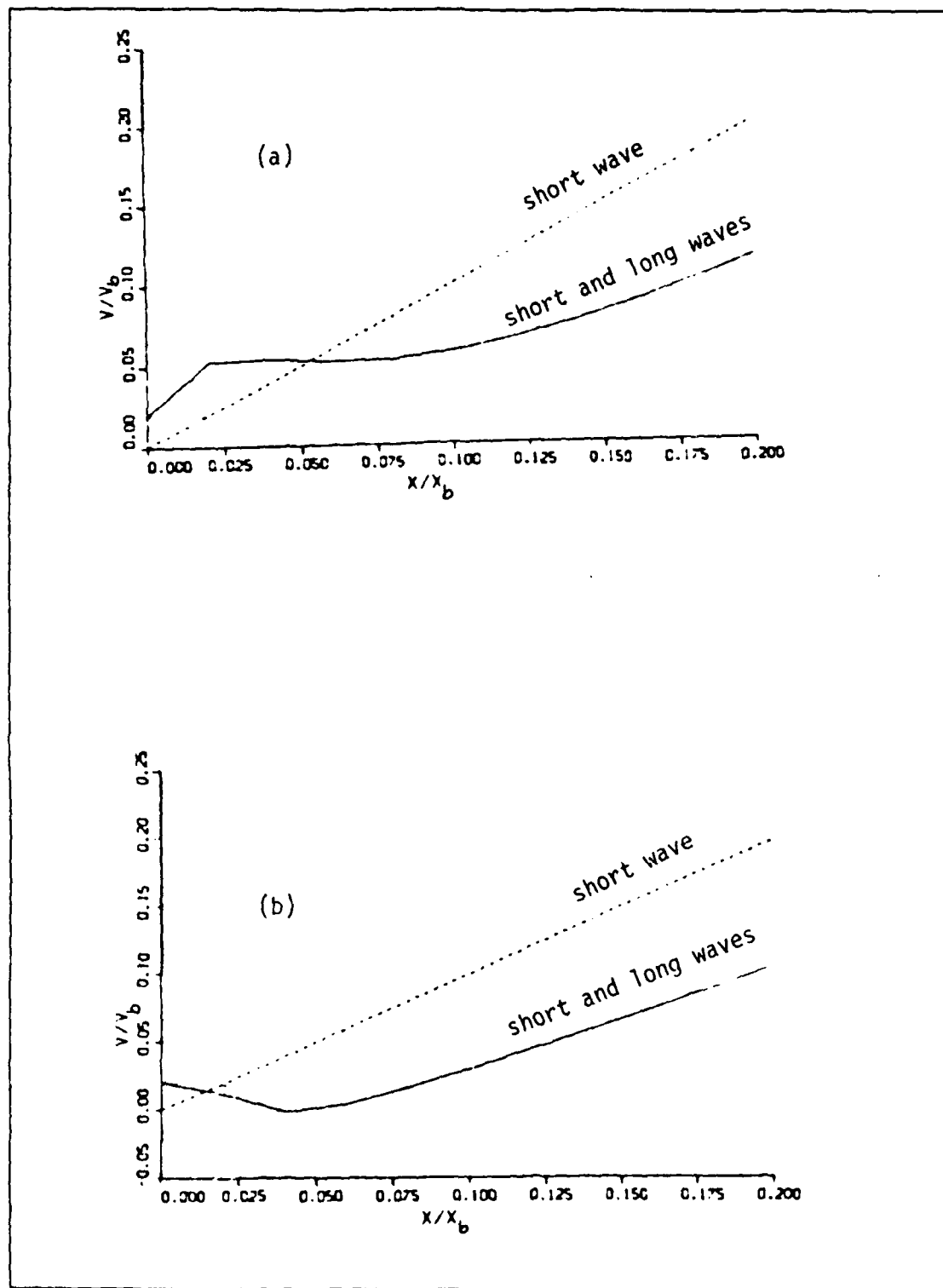


Figure 5.3 Unsteady longshore current distribution, at time (a) $t = \text{long wave period}$ (b) $t = 1/2 \text{ long wave period}$.

bands will have a steady and finite contribution to the longshore current given by equation 5.45, i.e. for both steady and unsteady models the magnitude of the current is the same at the shoreline.

Ignoring the exchange of momentum due to horizontal turbulent eddy transport increases the current shear at the breakerline and results in a sharp discontinuity in the velocity distribution. The presence of any horizontal mixing couples the adjacent water elements together and diffuses the momentum in the cross-shore direction. Adopting the concept of eddy viscosity, Longuet-Iiggins (1970b) expressed the mixing term to be proportional to the mean current V such that

$$\tau_{yx} = \frac{\partial}{\partial x} (\nu D \frac{\partial V}{\partial x}) \quad (5.47)$$

where $\nu = N\rho x \sqrt{gD}$ is the horizontal eddy viscosity, D is the total water depth and N is non-dimensional coefficient, ($0 < N < 0.16$). Thus, the steady Y-momentum flux equation becomes

$$\frac{\partial S_{yx}}{\partial x} = -\tau_y + \frac{\partial}{\partial x} (\nu D \frac{\partial V}{\partial x}) \quad (5.48)$$

Equation 5.48 can be rewritten as a second order differential equation in V such that

$$\partial S_{yx} / \partial x = m_1(x) \partial^2 V / \partial x^2 + m_2(x) \partial V / \partial x + m_3(x) V \quad (5.49)$$

where

$$m_1 = N x h \sqrt{gh}$$

$$m_2 = 5/2 N h \sqrt{gh}$$

$$m_3 = -\rho c_f |\vec{u}_1|$$

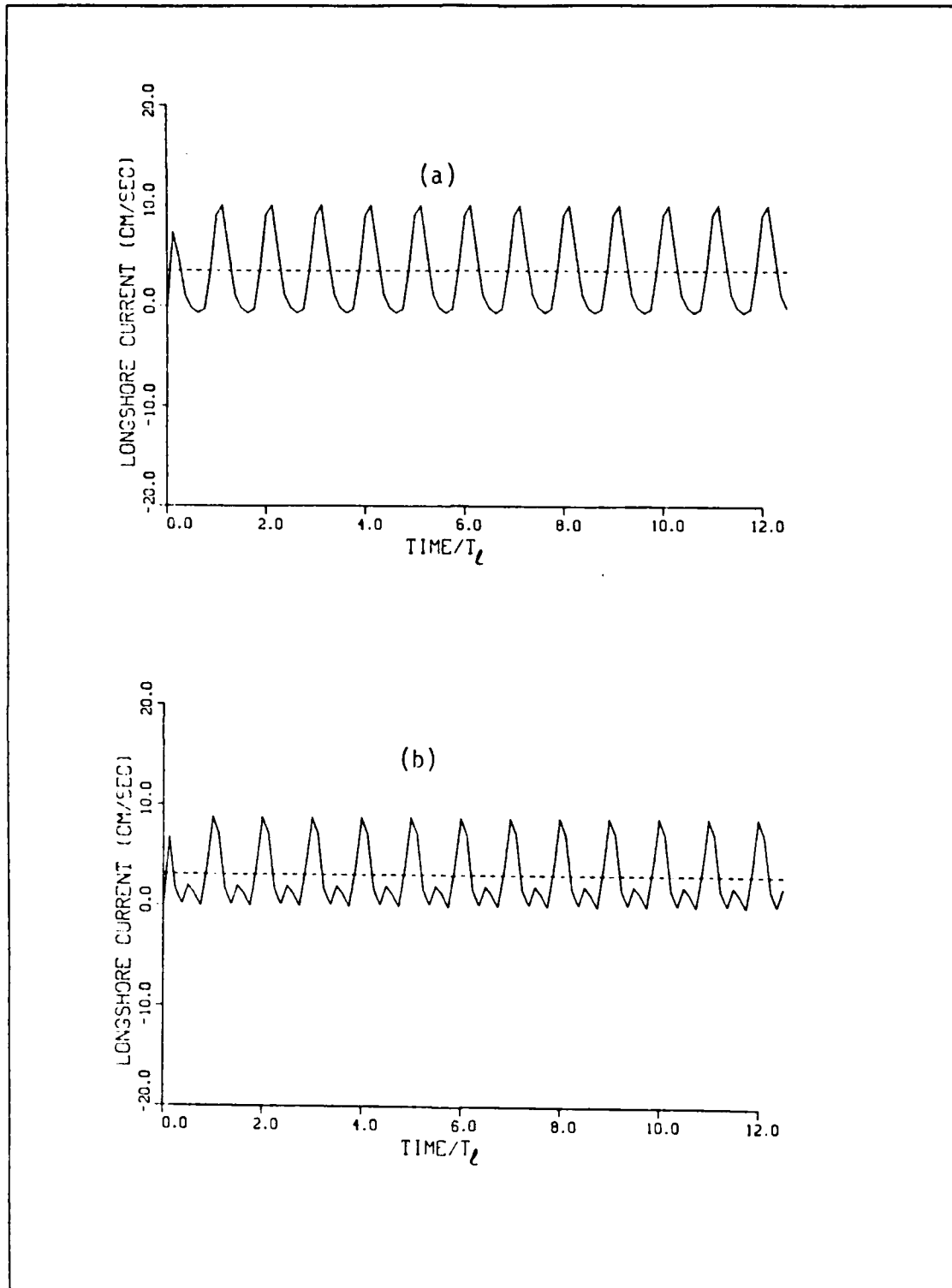


Figure 5.4 Time variability of the longshore current
 (a) $x = 2.0$ m (b) $x = 1.0$ m.

and $|u_T|$ is defined by equation 5.31 . Equation 5.49 is solved numerically using a finite difference scheme. The coefficients m_1 , m_2 and m_3 are evaluated at mid-points. A tri-diagonal matrix is generated over a domain equal to twice the surf zone width. Two boundary conditions are specified at the shoreline and away from the breakerline. At the shoreline, the eddy viscosity term goes to zero, i.e. the mixing length goes to zero at a boundary, and equation 5.48 reduces to 5.14 . Therefore, the steady solution without considering eddy viscosity, equation 5.45, is used to specify the boundary condition at the shoreline. This approach is necessary because equation 5.49 is singular at $x = 0$, and care must be exerted during the numerical formulation to avoid mathematical inconsistency. The longshore current is assumed to vanish at a distance of one surf zone width seaward the breakerline.

Steady longshore current models induced by short and long waves are shown in Fig. 5.5 compared with Longuet-Higgins (1970a) model. A comparison with Longuet-Higgins (1970a) model shows a relative decrease in the current seaward the inner surf zone. This can be attributed to the increase in the total horizontal velocity associated with the bottom shear stress. It can be seen that including the lateral mixing smooths the longshore current profile at the breakerline and shifts the maximum velocity onshore. The longshore current distribution is similar to the results obtained from the EOF analysis by Guza et al. (1986) showing a non-vanishing current at the shoreline (Fig. 1.4).

C. LONGSHORE SEDIMENT TRANSPORT

Incident waves arriving obliquely to the breaking zone, releasing their energy and momentum, generate a longshore current which in turn drives the longshore sediment transport along the beach. Knowledge of sediment transport rate is essential to the understanding of various coastal engineering problems, such as topographic changes in beach profiles and the associated marine protective works. For estimating the longshore sediment transport, there are three general approaches: the wave power model, the traction approach and Bagnold's energetics model. In the wave power model, the rate of total longshore transport Q_ℓ is simply assumed to be proportional to the longshore component of wave power P_ℓ at the breakerline to some power n (Watts, 1953),

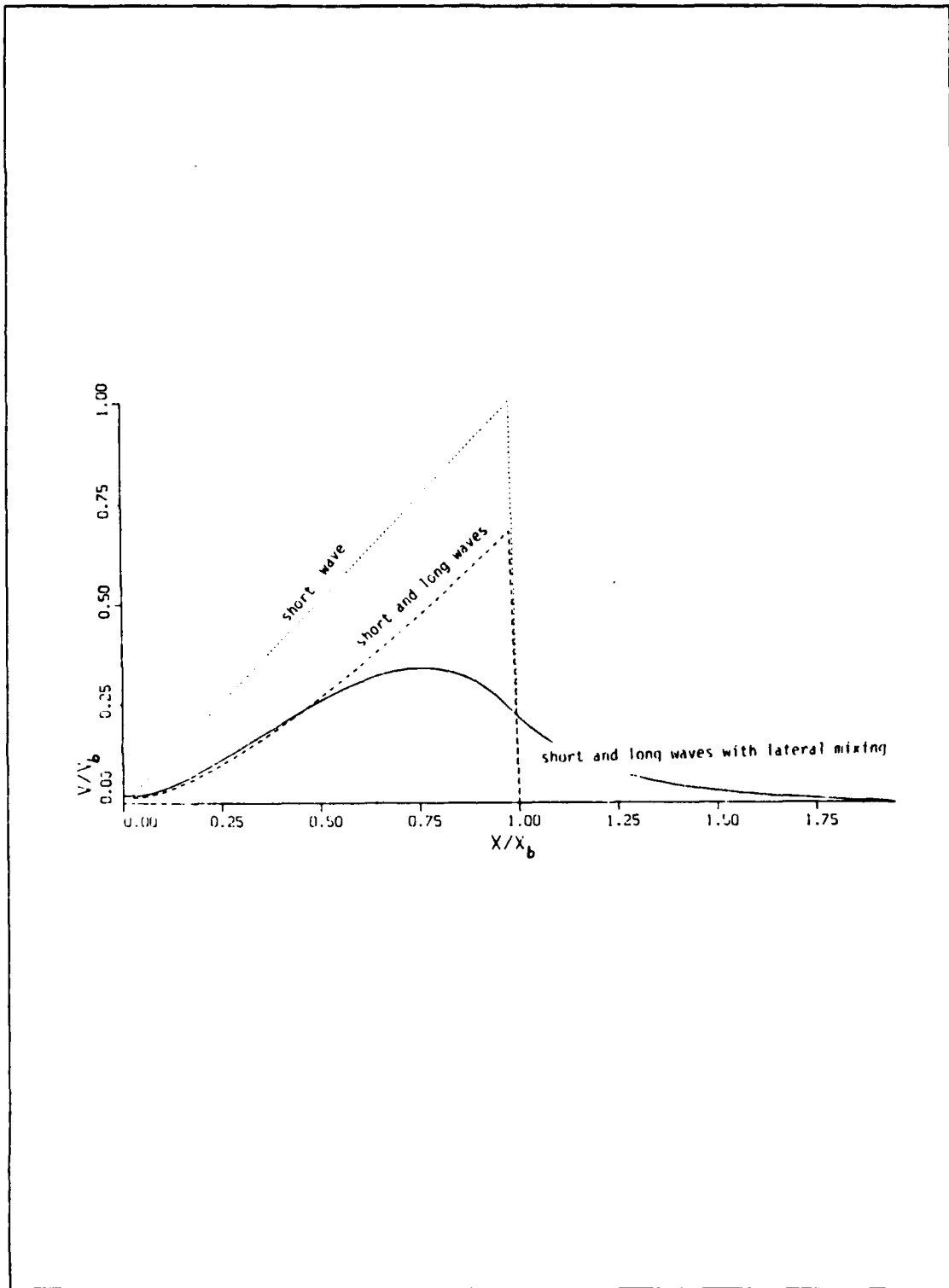


Figure 5.5 Steady longshore Current models, with and without adding lateral mixing, compared with Longuet-Higgins model (1970a).

$$Q_{\lambda} = K P_{\ell}^n \quad (5.50)$$

where K and n are empirical coefficients. P_{ℓ} is given by

$$P_{\ell} = (EC_g)_b \cos \alpha_b \sin \alpha_b \quad (5.51)$$

which can be expressed in terms of the radiation stress (Longuet-Higgins, 1972)

$$P_{\ell} = S_{yx} C \quad (5.52)$$

Inman and Bagnold (1963) found n in equation 5.50 to be unity and suggested the use of the immersed weight sand transport rate

$$I_{\lambda} = (\rho_s - \rho_w) g a' Q_{\ell} \quad (5.53)$$

where ρ_s , ρ_w are the density of sand and water and a' is the sand porosity (roughly 0.60). Komar and Inman (1970) measured longshore sand transport rate, combined their data with other data to seek a general formula. Most of the data falls onto a single trend satisfying the simple relation

$$I_{\lambda} = 0.77 P_{\ell} \quad (5.54)$$

where P_{ℓ} is in watts/m when specifying wave height in terms of H_{rms} and Q_{ℓ} is in m^3 /day. However, Equation 5.54 is empirical with no real consideration to sand transport mechanisms. In addition, the coefficient .77 has a high degree of uncertainty.

The traction approach includes work done by Bijker (1971), Swart (1976), Madsen and Grant (1976) and others. For instance, Madsen and Grant (1976) adapted the Einstein-Brown sediment transport equations to time-varying sand movements under combined waves and unidirectional currents. The bottom stress and resulting sand transport vary with time. Their model is relatively complicated and requires parameters for which no data are available.

Bagnold's energetic model assumes that the total sediment transport is the sum of the bed load and the suspended load transport. Bed load is maintained by grain-to-grain contact within 10 cm of the bottom while the suspended mode, containing generally finer grains, is lifted from the bed by the turbulent action of the wave-induced vertical motion. The suspended sediment grains are supported via turbulent diffusion. They move with nearly the local water velocity. However, they are also falling vertically relative to the local supporting fluid with a fall velocity, W . Thus, part of the available energy is extracted to maintain the particles in the water column. Bagnold (1963) developed the total load sediment equation for steady, two-dimensional stream flow,

$$\begin{aligned}
 i &= i_B + i_S \\
 &= \left\{ \frac{\epsilon_B}{\tan \phi - \tan \beta} + \frac{\epsilon_S}{\frac{W}{u} - \tan \beta} \right\} \Omega
 \end{aligned}
 \tag{5.55}$$

where

i = total immersed weight sediment transport (bed and suspended)

ϵ_B = bed load efficiency

ϵ_S = suspended load efficiency

ϕ = internal angle of repose of the sediment

$\tan \beta$ = slope of the stream bed

u = mean velocity of the stream

W = fall velocity of the sediment

Ω = rate of energy production of the stream

Inside the surf zone (oscillatory flow), Bagnold (1963) relates the rate of immersed weight transport to the work done by waves and current on the bed surface. The mechanics of sand particle movement are described as a back-and-forth motion by the oscillatory wave motion close to the bed with essentially no net transport. Wave

energy is expended in supporting and suspending the moving sand above the bed. Once the sediments are suspended, the presence of any unidirectional current superimposed on the to-and-fro motion can then produce a net drift of sediment. Bagnold (1963) derived the following relationship

$$i_{\theta} = K' \Omega \frac{u_{\theta}}{u_m} \quad (5.56)$$

where i_{θ} is the time averaged immersed weight transport rate per unit width in the direction θ determined by the unidirectional current u_{θ} , Ω here is the available wave power due to energy losses by the fluid drag at the bed surface, u_m is the magnitude of the orbital velocity of wave motion, and K' is a dimensionless coefficient. The success of the wave power and Bagnold's energetics approaches is due to their relative simplicity, requiring only one or two parameters specified from the data.

Equation 5.56 has been used as a basis for the development of a number of longshore transport models. Inman and Bagnold (1963) specified the various parameters of waves at the breakerline to calculate the longshore immersed weight transport rate,

$$I_{\ell} = K' (EC_g)_b \cos \alpha_b \frac{v_b}{u_m} \quad (5.57)$$

Equation 5.57 can be viewed as a general relationship because it does not specify the forcing for the longshore current. It could be due to a tidal current, a nearshore cell circulation, wind or to oblique wave approach. Komar and Inman (1970) required K' to be equal to 0.28 to agree with their data.

Bowen (1980) applied Bagnold's model to the problem of on-offshore sediment transport on beaches with normally incident waves and onshore steady current (no longshore currents). Bowen used Stokes second order wave theory to predict the equilibrium beach profile as a function of incident wave characteristics. Using a similar approach, Bailard and Inman (1981) derived a general bed load equation in the longshore and cross-shore directions by considering time-varying flow over a sloping

bottom. Their solution reduces to equation 5.56 for steady, two-dimensional flow and assuming a weak current and a small angle of incidence. Bailard (1981) extended the work of Bailard and Inman (1981) to include the suspended sediment load to give a more general expression. The total longshore sediment transport of Bailard (1981) solution is given by

$$i_{\ell} = \rho c_f \frac{\epsilon_B}{\tan \beta} (\overline{u^2}) v \quad (5.58)$$

$$+ \rho c_f \frac{\epsilon_S}{W} \overline{|u|^3} v$$

where the first term on the R.H.S. represents the bed load and the second term is the suspended load. The total average sediment transport can be obtained by integrating equation 5.58 across the surf zone from zero to the breakerline (x_b).

$$I_{\ell} = \int_0^{x_b} i_{\ell} dx \quad (5.59)$$

Calibration of the model can be done using the wave power model.

There is considerable uncertainty concerning the relative importance of bed load versus suspended load within the surf zone. According to field measurements, Komar(1978) suggested that the suspended sediment transport rate accounts for less than 20% of the total transport. However, Downing (1984) estimated the suspended load on a dissipative beach to account for as much as 45% of the littoral drift. Sternberg et al. (1984) measured the suspended sediment rate at Leadbetter Beach, Santa Barbara and found that the measured suspended sediment longshore transport rate is equal to the total longshore transport rate as predicted by equation 5.57. This result agrees with the data acquired by Kana and Ward (1981) during a storm. Sternberg et al. (1984) found maximum suspended sediment occurred at the midsurf zone region, and pointed out that the suspended sediment appears to be high in the swash-backwash region.

Kraus et al. (1981) measured the longshore sand transport distribution using multicolor fluorescent sand tracer; a distinct bimodal distribution was obtained.

Maxima in transport occurred in the swash and/or within the breaker zone, where suspended load transport is expected to be relatively high due to the turbulence. White and Inman (1986) measured the longshore sediment rate in Santa Barbara and also found a bimodal distribution across the surf zone with maxima near the break point and in the swash zone (Fig 5.6). They estimated the longshore suspended load to be roughly 10-30% of the total longshore transport rate.

The above results show a large volume of sediment in the swash zone which is not predicted by any available model. Waddell (1973) found a low-amplitude migration of bed forms which migrated consistently downslope suggesting that uprush sediment transport was primarily through suspension sediment. Bradshaw (1980) pointed out that the swash-backwash collision process (low frequency waves) is significant and results in temporary suspension of a large volume of sediment in the roll wave. Wright et al. (1982) demonstrated the dominance of the suspended sediment in the inner and swash zone using a turbidimeter situated 10 cm above the bed. The time series shows pronounced turbidity maxima at infragravity intervals. In general, the predictions of littoral drift have a high degree of uncertainty, which results partly from our basic inability to make accurate measurements of sand transport on beaches.

1. Longshore Sediment Transport due to short and long waves

The incident waves are assumed to approach obliquely the surf zone at a small angle riding on a cross-shore long standing wave. Following Bailard (1981), equation 5.58 is used to calculate the total longshore sediment transport distribution. Based on laboratory and field data, Bailard (1981) estimated the efficiency coefficients to be $\epsilon_B = 0.13$ and $\epsilon_S = 0.025$ and $W = 0.04$ m/sec . The total horizontal velocity squared averaged over long wave period is used in evaluating the bed load term in equation 5.58

$$\overline{u_T^2} = \frac{1}{2} \gamma^2 gh + a^2 \left(\frac{g}{h}\right) \left\{ \gamma^2 J_0^2(x) + \frac{J_1^2(x)}{2} \right\} \quad (5.60)$$

Similarly, the averaged cubic total horizontal velocity is evaluated to calculate the suspended load term,

$$\begin{aligned}
\overline{|u_T|^3} = & \frac{1}{\pi} (2\gamma^3 (gh)^{3/2} + 3\gamma^2 a_x g \sqrt{gh} [2\gamma J_0(\lambda) + J_1(\lambda)]) \\
& + 3\gamma^2 a_x^2 J_0(\lambda) g \sqrt{g/h} [J_1(\lambda) + 2J_0(\lambda)] \\
& + a_x^3 \left(\frac{g}{h}\right)^{3/2} [2\gamma^3 J_0^3(\lambda) + J_1^3(\lambda) + \frac{3}{2}\gamma^2 J_0^2(\lambda) J_1(\lambda)]
\end{aligned} \tag{5.61}$$

The steady longshore current, with lateral mixing added, is utilized to derive the sediment alongshore. The longshore sediment transport distribution due to the combined waves is shown in Fig 5.7. Note that including the lateral mixing smooths the distributions of both the longshore current and sediment transport at the breakerline. The resulting distribution qualitatively simulates the bimodal distribution given by White and Inman (1986), since it describes the maximum sediments near both the shoreline and the breakerline.

Unlike previous models, the wave energy has been shown to exist at the shore (in the swash zone), and hence observable dynamical processes can be described analytically. None of the available models for predicting the longshore sediment transport explain the increase in longshore sediment transport in the swash zone. All the previous models predict no transport at the shoreline which has been shown to be unrealistic. It is shown that the longshore sediment transport model presented here estimates correctly the bimodal distribution and shows the dominance of the suspended load, which agrees with some of the above results. The main improvements of the presented model are the inclusion of the infragravity waves and, therefore, describing the swash dynamics and the increase of sediment transport at the shoreline.

D. MODEL VALIDATION

The wave-wave interaction approach within the inner surf zone suffers from our inability to model the breaking process accurately. Nonetheless it can lead to greater insight into the inner surf zone dynamics. Several assumptions are necessary for simplifying the analysis due to the complexity of real surf zone processes, but it is believed that they have some physical basis. It is assumed that the linear theory describes the waves adequately for the order of the analysis, and inside the surf zone spilling breakers are assumed, where wave height is strongly controlled by the local depth. Non-breaking long period waves on a plane sloping bottom are assumed to be either leaky mode or edge waves with a frequency $\omega_1 \ll \omega_s$. Basic assumptions of straight and parallel beach contours have been used for simplicity where no longshore depth variation is allowed. Plane sloping bottom is assumed for simplicity. The

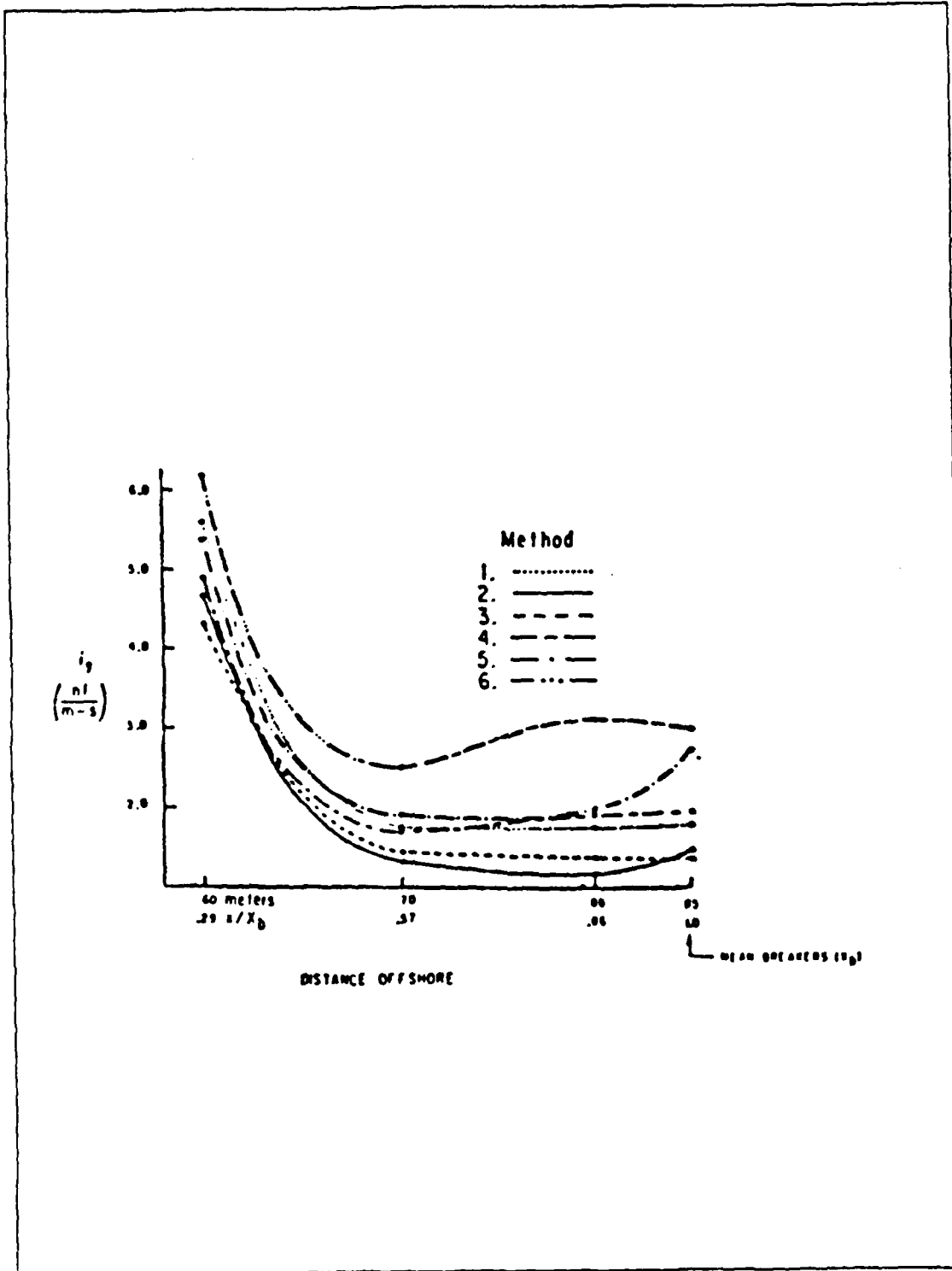


Figure 5.6 Measured longshore sediment transport rate i_s distribution, Santa Barbara (after White and Inman, 1986).

sensitivity of the model to the change in beach slope is clear since infragravity waves modify the local water depth and, therefore modulate the total energy. Limitation to narrow banded incident and infragravity waves is required for the model input. It must be noted that using a monochromatic description of both incident and infragravity waves may raise questions about quantitative predictions since the processes in nature are stochastic. However, the developed model gives a number of qualitative results which may be useful in understanding the inner surf zone dynamics. Application of the model to different nearshore processes leads to a simple physical picture of the nature of the wave-wave interactions in the inner surf zone. The validity of this model is confirmed by comparison with field data, where the resulting distributions at least qualitatively simulate actual distributions.

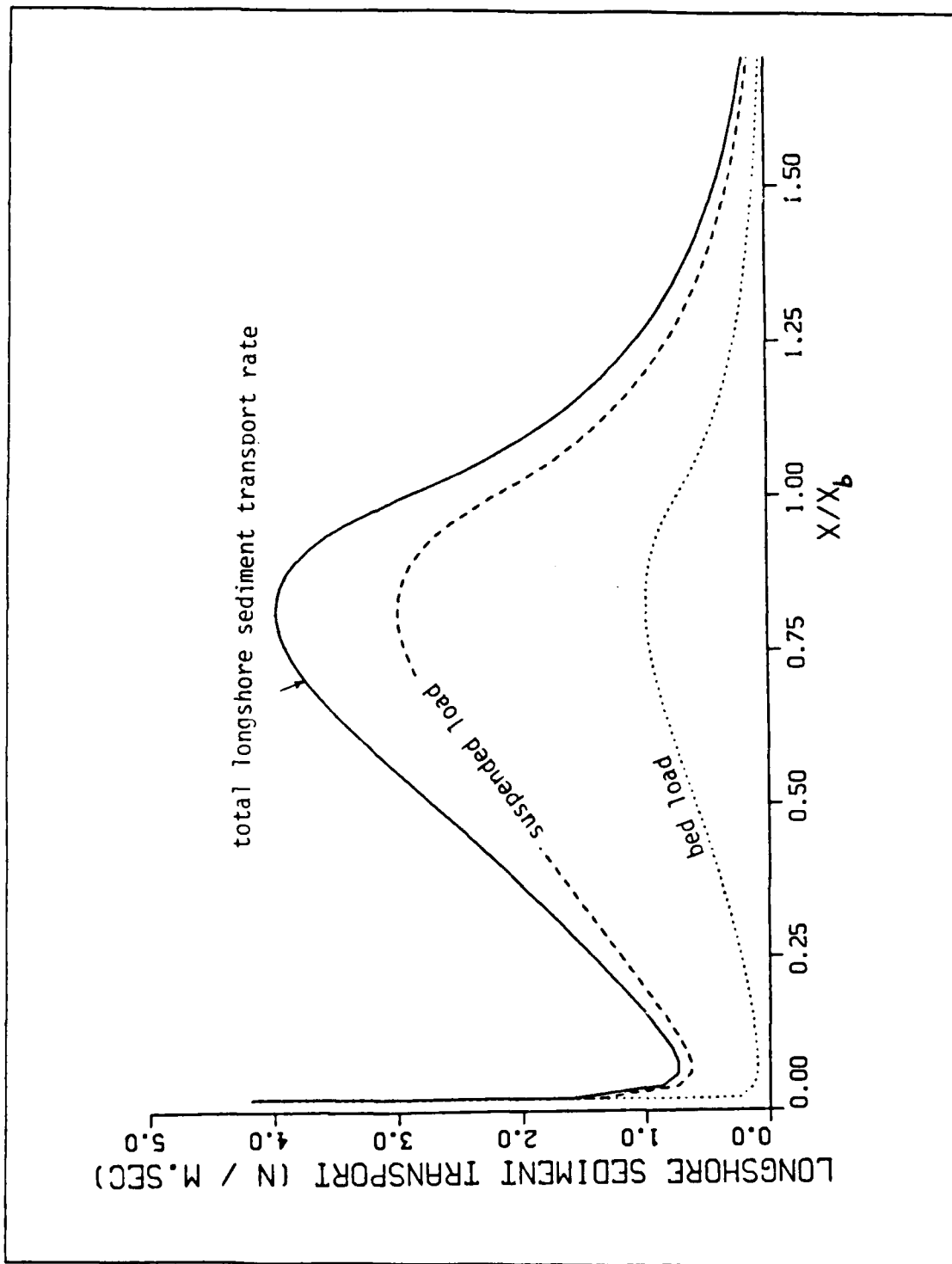


Figure 5.7 Longshore sediment transport distribution model due to both short and long waves showing a bimodal structure.

VI. SUMMARY AND CONCLUSIONS

The modulation of incident short period wind waves superposed on infragravity waves are investigated. Modeling the short waves as depth limited breakers, the short waves are shown to be modulated in amplitude, wavenumber and direction due to the slowly varying depth caused by the long standing waves. Furthermore, modulation results in additional energy at the side band frequencies near the incident wave peak. The energy calculations show a gradual growth of the side bands onshore with non-vanishing energy at the shoreline (order of 15%). An analytical expression is developed to describe the surface elevation of the modulated short waves as an infinite sum of spectral components at the incident and side bands frequencies. It is shown that the modulated short wave transfers energy to the side bands as the depth decreases. Therefore, it is suggested that the spectral components of the lower side bands may strengthen the infragravity wave band as the depth decreases resulting in the infragravity waves dominating the power spectra.

The changes in the wavenumber and direction of the short wave due to the presence of a long wave are calculated by using a moving frame of reference that reduces the non-breaking long wave to a slowly varying current. On a plane sloping beach, the wavenumber modulation is shown to increase with increase angle of wave approach. The excess momentum flux components and bed shear stress due to the combined waves are rederived analytically and show periodicity at the frequency of the long waves.

Spectral analysis shows the dominance of the infragravity waves closer to the shoreline. Using narrow band data with high resolution ($df = .004$ Hz), side band peaks can be identified at frequencies ($f_s \pm f_l$). On almost all days and for all the instruments, the upper side band is well defined in the power spectra, but the lower side band is suppressed. The reason for the lack of the lower side bands on most days is not known. However, breaking of the low frequency waves and/or radiation of energy by outgoing component of the standing wave may cause suppression of the lower side bands.

Most days show a positive correlation between the incident wave envelope and low frequency motion inside the surf zone, while a negative correlation is observed in

deeper water in agreement with Longuet-Higgins and Stewart's (1962) explanation of forced waves. The positive correlation is explained by the short wave modulation due to the presence of long waves. However, the values of the measured cross correlation coefficients are found to be low (although statistically significant), partly due to the reflected wave field, that decreases the coherence (Elgar, 1985). On some days, the observed zero cross-correlation was found at approximately the breakerline and other days in the inner surf zone. This may suggest a nodal point for a standing wave and/or a transition location between forced and free long waves.

It is hypothesized that some of the often observed discrepancies with present short wave dynamical models occurring in the inner surf zone are due to the interaction between the incident waves and the infragravity waves. The derived expressions for energy and momentum fluxes are utilized to study wave setup, longshore current and sediment transport in the inner surf zone.

Wave setup calculations show an increase in the mean water level compared with setup due to the short wave only. This is because the breaking short waves are depth controlled and the depth is slowly varying due to the presence of the long waves. Consequently, energy at side bands is generated and the setup is increased.

A steady longshore current driven by oblique short waves riding on cross-shore long period waves, is found to be finite at the shoreline due to the presence of finite side band energy. The model, in general, predicts smaller currents than Longuet-Higgins' (1970a) model because of the relative increase in bed shear stress due to the presence of long waves. In the derived analytical expression, contributions by the short waves and side bands can be identified. It is shown that the cross-shore long wave does not contribute to the forcing term, $\partial S_{yx} / \partial x$, since it is averaged out.

It is more general to consider an unsteady longshore current. The analytical solution for an unsteady longshore current shows three major terms: a transient term that vanishes after a few long wave periods, a steady term similar to the one obtained in the steady model, and an unsteady term which oscillates at the long wave frequency, but driven by the momentum changes at the side band frequencies, and acts closer to the shore line. This unsteadiness is attributed to the side band formation.

An improved longshore current model is necessary to improve the longshore sediment transport formulation. Based on the sediment transport model by Bailard (1981) and using the developed steady longshore current model, a longshore sediment transport distribution is calculated. The model predicts sediment transport maxima at

the shoreline and the breakerline. The results Qualitatively, the results compare favorably with various field data by Zenkovich (1960); Kraus et al., (1981), and White and Inman (1986).

It is recommended to include the wave setup in the longshore current models. Numerical solution for the unsteady longshore current including the large angle of wave incidence and assuming a strong current is of interest. Numerical solutions can be compared with the obtained analytical results. Actual depth profiles are recommended to use in computing the longshore sediment transport rate to compare quantitatively with the data.

LIST OF REFERENCES

- Abdelrahman, S.M., *Longshore sand transport distribution across the surf zone due to random waves*, M.S. Thesis, Naval Postgraduate School Monterey, CA, June 1983.
- Abramowitz, M., and I. Stegun, *Handbook of mathematical functions*, New York: Dover Publications, 1046 pages, 1964.
- Bagnold, R.A., *Mechanics of marine sedimentation, In the sea: Ideas and Observations*, 3, New York, Interscience, New York, 1963.
- Bagnold, R.A., *An approach to the sediment transport problem from general physics*, U.S. Geological Survey, professional paper no. 422-1, 1966.
- Bailard, J.A., *An energetics total load sediment transport model for a plane sloping beach*, J. Geophys. Res., 86, (C11), 10938-54, 1981.
- Bailard, J.A. and D.L. Inman, *An energetics bed load model for a plane sloping beach, Part I: Local transport*, J. Geophys. Res., 86, (C3), 2035-2043, 1981.
- Battjes, J.A., *Set-up due to irregular waves*, proc. of the 13th Conf. on Coastal Engineering, 1933-2004, 1972.
- Battjes, J.A., *Surf Similarity*, proc. of the 14th Conference on Coastal Engineering, 466-479, 1974.
- Battjes, J.A. and J.P.F.M. Janssen, *Energy loss and set-up due to breaking of random waves*, proc. of the 16th conference on Coastal Engineering, 569-587, 1978.
- Battjes, J.A. and M.J.F. Stive, *Calibration and verification of a dissipation model for random breaking waves*, J. Geophys. Res., 90 (C25), 9159-9167, 1985.
- Bijker, E.W., *Longshore transport computations*, J. of Waterways, Harbors, and Coastal Engineering Division, Proc. of ASCE, NY, WW4, 687-701, 1971.
- Bowen, A.J., *The generation of longshore currents on a plane beach*, J. Mar. Res., 27, 206-215, 1969.
- Bowen, A.J., *Simple models of nearshore sedimentation beach profiles and longshore bars in the coastline of Canada*, Geological Survey of Canada, 21-30, 1980.
- Bowen, A.J. and R.T. Guza, *Edge waves and surf beat*, J. Geophys. Res., 83 (C4), 1913-20, 1978.
- Bowen, A.J. and D.A. Huntley, *Waves, long waves and nearshore morphology*, Marine Geology, 60, 1-13, 1984.
- Bowen, A.J., D.L. Inman, and V.P. Simmons, *Wave set-down and set-up*, J. Geophys. Res., 73(8), 2569-2577, 1968.
- Bowen, A.J. and D.L. Inman, *Edge waves and crescentic bars*, J. Geophys. Res., 76(36), 8662-8671, 1971.
- Bradshaw, M.P., *Topographic control of run-up variability*, proc. of the 17th conf. on Coastal Engineering, 1091-1105, 1980.
- Collins, J.I., *Probabilities of breaking wave characteristics*, Proc. 13th Coastal Engineering Conf., New York, Amer. Soc. Civil Eng., 399-412, 1970.

- Dorrestein, R., *Wave set-up on a beach*, paper presented at 2nd Technical Conference on Hurricanes, Beach Erosion Board, 1961.
- Downing, J.P., *Suspended sand transport on a dissipative beach*, Proc. of 19th Coastal Engineering Conference, 1765-1781, 1984.
- Eckart, C., *Surface waves on water of variable depth*, wave report 100, University of California, Scripps Inst. of Oceanography, La Jolla, CA, 99 pp., 1951.
- Elgar, S.L., *Shoaling surface gravity waves*, Ph.D. dissertation, Scripps Institute of Oceanography, University of California, La Jolla, CA, 1985.
- Elgar, S.L. and R.T. Guza, *Observations of bispectra of shoaling surface gravity wave*, J. Fluid Mech., 161, 425-448, 1985.
- Fredrichs, K.O., *Water waves on a shallow sloping beach*, Comm. Proc., of Appl. Math., 1, 109, 1948.
- Gable, C.G., Editor, Report on data from the nearshore sediment transport study experiment at Torrey Pines Beach, California, November to December 1978, IMR reference No. 79-8, Institute of Marine Resources, La Jolla, CA, 1979.
- Gable, C.G. (Editor), Report on data from the Nearshore sediment transport study experiment at Leadbetter Beach, Santa Barbara, CA, January to February 1980, IMR reference No. 80-5, Institute of Marine Resources, La Jolla, CA, 1980.
- Gallagher, B., *Generation of surf beat by non-linear wave interactions*, J. Fluid Mech., 49(1), 1-20, 1971.
- Galvin, C.J. and P.S. Eagleson, *Experimental study of longshore currents on a plane beach*, U.S. Army Coastal Engineering Research Center, Technical memo 10, 1965.
- Garrett, C. and J. Smith, *On the interaction between long and short surface waves*, J. Phys. Oceanogr., 6, 925-930, 1976.
- Goda, Y., *Irregular wave deformation in the surf zone*, Coastal Eng. in Japan, 18, 13-27, 1975.
- Guza, R.T. and A.J. Bowen, *Finite amplitude edge waves*, J. Mar. Res., 34 (1), 269-293, 1976.
- Guza, R.T. and A.J. Bowen, *The Resonant instabilities of long waves obliquely incident on a beach*, J. Geophys. Res., 80(33), 4529-4534, 1975.
- Guza, R.T. and D.L. Inman, *Edge waves and beach cusps*, J. Geophys. Res., 80(21), 2997-3012, 1975.
- Guza, R.T. and E.B. Thornton, *Variability of longshore currents*, Proc. 16th Conf. on Coastal Engineering, ASCE, 1(756-775), 1978.
- Guza, R.T. and E.B. Thornton, *Local and shoaled comparisons of sea surface elevations, pressures, and velocities*, J. Geophys. Res., 85(C3), 1524-1530, 1980.
- Guza, R.T. and E.B. Thornton, *Wave set-up on a natural beach*, J. Geophys. Res., 86(C5), 4133-4137, 1981.
- Guza, R.T. and E.B. Thornton, *Swash oscillations on a natural beach*, J. Geophys. Res., 87(C1), 483-491, 1982.
- Guza, R.T. and E.B. Thornton, *Observations of surf beat*, J. Geophys. Res., 90(C2), 3161-3172, 1985a.
- Guza, R.T. and E.B. Thornton, *Velocity moments in nearshore*, J. of Waterway, Port, Coastal and Ocean Engineering, 111(2), 235-256, 1985b.
- Guza, R.T., E.B. Thornton, N. Christensen, *Observations of steady longshore currents in the surf zone*, submitted to J. Physical Oceanography, 1986.

- Guza, R.T., E.B. Thornton, and R.A. Holman, *Swash on steep and shallow beaches*, Proc. of the 19th conference on Coastal Engineering, 48, 708-723, 1984.
- Guza, R.T. and R.E. Davis, *Excitation of edge waves by waves incident on a beach*, J. Geophys. Res., 79(9), 1285-1290, 1974.
- Holman, R.A., *Infragravity energy in the surf zone*, J. Geophys. Res., 86(C7), 6442-6450, 1981.
- Holman, R.A. and A.J. Bowen, *Bars, bumps, and holes: models for the generation of complex beach topography*, J. Geophys. Res., 87(C1), 457-468, 1982.
- Holman, R.A. and A.J. Bowen, *Longshore structure of infragravity wave motions*, J. Geophys. Res., 89(C4), 6446-6452, 1984.
- Holman, R.A., D.A. Huntley, and A.J. Bowen, *Infragravity waves in storm conditions*, Proc. of the 16th conf. on Coastal Eng., ASCE, 1978.
- Holman, R.A. and A.H. Sallenger, *Set-up and swash on a natural beach*, J. Geophys. Res., 90 (C1), 945-953, 1985.
- Hunt, I.A., *Design of seawalls and breakwaters*, Proc. Am. Civil Eng., 85, 123-152, 1959.
- Huntley, D.A., *Long periods waves on a natural beach*, J. Geophys. Res., 81(36), 6441-6449, 1976.
- Huntley, D.A. and A.J. Bowen, *Comparison of the hydrodynamics of steep and shallow beaches*, J.R. Hails and A. Carr (Editors), *Nearshore sediment dynamics and sedimentation*, Wiley, New York, NY, 316 pp., 1975a.
- Huntley, D.A. and A.J. Bowen, *Field observations of edge waves and their effect on beach material*, J. Geol. Soc. London, 131, 69-81, 1975b.
- Huntley, D.A. and A.J. Bowen, *Beach cusps and edge waves*, Proc. of the 16th conference on Coastal Eng., 1378-1393, 1978.
- Huntley, D.A., R.T. Guza, and A.J. Bowen, *A universal form for shoreline run-up spectra*, J. Geophys. Res., 82(18), 2577-2581, 1977.
- Huntley, D.A., R.T. Guza and E.B. Thornton, *Field observations of surf beat, 1. progressive edges waves*, J. Geophys. Res., 86(C7) 6451-6466, 1981.
- Huntley, D.A. and C.S. Kim, *Is surf beat forced or free ?*, Proc. of the 19th Conference on Coastal Engineering, 9, 1659-1676, 1984.
- Inman, D.L., *Mechanics of sediment transport by waves and currents*, SIO Ref. Ser, 68-10, Scripps Inst. of Ocean., La Jolla, CA, 1968a.
- Inman, D.L., *Mechanics of sediment transport by waves and currents*, SIO Ref. Ser, 68-26, Scripps Inst. of Ocean., La Jolla, CA, 1968b.
- Inman, D.L. and R.A. Bagnold, *Littoral processes, In the Sea: Ideas and Observations*, 3, Intersciences publishers, New York, NY, 529-533, 1963.
- Jonsson, I.G., O. Skovgaard, and T.S. Jacobsen, *Computation of longshore currents*, Proc. 14th conference on Coastal Engineering, ASCE, 699-714, 1974.
- Kana, T.W. and L.G. Ward, *Nearshore suspended sediment load during storm and post-storm conditions*, Proc. of the 17th conf. on Coastal Engineering, 1158-1174, 1981.
- Komar, P.D., *Beach and sand transport: distribution and total drift*, Harbors and Coastal Engineering Division, American Society of Civil Engineers Waterways, WW2, 255-239, 1977.
- Komar, P.D., *The relative significance of suspension versus bed-load on beaches*, J. Sed. Petrology, 48, 921-932, 1978.

- Komar, P.D. and D.L. Inman, *Longshore sand transport on beaches*, J. of Geophys. Res., 75(30), 5914-5927, 1970.
- Kraus, N.C., R.S. Farinato and K. Horikawa, *Field experiments on Longshore sand transport in the surf zone*, Coastal Engineering in Japan, 24, 171-194, 1981.
- Lamb, H., *Hydrodynamics*, 6th ed., Art, 185, Dover, NY, 738 pp., 1932.
- Liu, P.L.F. and R.A. Dalrymple, *Bottom frictional stresses and longshore currents due to waves with large angles of incidence*, J. Marine Res., 36(2), 357-375, 1978.
- Longuet-Higgins, M.S., *On the wave-induced difference in mean sea-level between the two sides of a submerged breakwater*, J. Marine Res., 148-153, 1967.
- Longuet-Higgins, M.S., *Longshore currents generated by obliquely incident sea waves, 1*, J. Geophys. Res., 75, 6778-6789, 1970a.
- Longuet-Higgins, M.S., *Longshore currents generated by obliquely incident sea waves, 2*, J. Geophys. Res., 75, 6790-6801, 1970b.
- Longuet-Higgins, M.S., Recent progress study of longshore currents, in R.E. Meyer (Editor), *Waves on beaches and resulting sediment transport*, Academic Press, New York, NY, 203-248, 1972.
- Longuet-Higgins, M.S. and R.W. Stewart, *Changes in the form of short gravity waves on long waves and tidal currents*, J. Fluid Mech., 8, 565-583, 1960.
- Longuet-Higgins, M.S. and R.W. Stewart, *The changes in amplitude of short gravity waves on steady non-uniform currents*, J. Fluid Mech., 34(10), 529-549, 1961.
- Longuet-Higgins, M.S. and R.W. Stewart, *Radiation stress and mass transport in gravity waves with application to surf beats*, J. Fluid Mech., 13, 481-504, 1962.
- Madsen, O.S. and W.D. Grant, *Sediment transport in the coastal zone*, MIT, Department of Civil Engineering, Ralph M. Parsons Laboratory, Report No. 241, 105 pp., 1976.
- Madsen, O.S., D.W. Ostendorf, and A.S. Reyman, *A longshore current model*, proc. coastal zone 78, ASCE, 3, 2332-2341, 1978.
- Mase, H. and Y. Iwagaki, *Run-up of random waves on gentle slopes*, Proc. of 19th Conf. of Coastal Engineering, American Society of Civil Engineers, 1, 593-609, 1984.
- Meadows, G.A., *Time dependents fluctuations in longshore currents*, Proc. of the 15th Coastal Engineering Conference, 660-680, 1976.
- Mei, C.C., *Applied dynamics of ocean surface waves*, Wiley Interscience, 1983.
- Miche, A., *Exposes a l'action de la houle*, Ann. Ponts Chaussees, 121, 285-319, 1951.
- Miller, I. and J.E. Freund, *Probability and statistics for engineers*, 2nd edition, Prentice Hall, Inc., Englewood Cliffs, New Jersey, 1977.
- Moraes, C. de C., *Experiments of wave reflexion on impermeable slopes*, in proc. of the 12th conference on Coastal Engineering, ASCE, 509-521, New York, NY, 1970.
- Munk, W.H., *Surf beats*, Trans. Amer. Geophys. Un., 30, 849-854, 1949.
- Oltman-Shay, J. and R.T. Guza, *Infragravity edge wave observations on two California beaches*, submitted to J. Geophys. Res., 1986.
- Ostendorf, D.W. and O.S. Madsen, *An analysis of longshore current and associated sediment transport in the surf zone*, report 241, Parsons Laboratory, Dept. of Civil Engineering, MIT, 1979.
- Panter, P.F., *Modulation, Noise, and Spectral Analysis*, McGraw-Hill, Inc., 1965.
- Phillips, O.M., *The dynamics of the upper ocean*, Cambridge University Press, 1966.

- Sasaki, T. and K. Horikawa, *Nearshore current system on a gently sloping bottom*, Coastal engineering in Japan, 18, 123-142, 1975.
- Sasaki, T. and K. Horikawa, *Observation of nearshore current and edge waves*, Proc. 16th Int. Conf. on Coastal Engineering, 791-809, 1978.
- Sawaragi, T. and I. Deguchi, *Distribution of sediment transport rate across the surf zone*, Proc. 16th Conf. on Coastal Engineering, 1596-1613, 1979.
- Sawaragi, T. and K. Iwata, *On wave deformation after breaking*, Proc. of the 14th Conf. on Coastal Engineering, 481-498, 1974.
- Short, A.D., *Multiple offshore bars and standing waves*, J. Geophys. Res., 80(27), 3838-3840, 1975.
- Sternberg, R.W., N.C. Shi, and J.P. Downing, *Field investigations of suspended sediment transport in the nearshore zone*, Proc. 19th Coastal Engineering conference, 1782-98, 1984.
- Stokes, G.G., Report on recent researchs in hydrodynamics, Brit. Ass. Rep., (papers, i.167), 1846.
- Suhayda, J.N., *Standing waves on beaches*, J. Geophys. Res., 79(21), 3065-3071, 1974.
- Suhayda, J.N. and N.R. Pettigrew, *Observations of wave height and wave celerity in the surf zone*, J. Geophys. Res., 82(9), 1419-1424, 1977.
- Svendsen, I.A., P.A. Madsen, and J.B. Hansen, *Wave characteristics in the surf zone*, proc. of the 16th conference on Coastal Engineering, 521-539, 1978.
- Swart, D.H., *Predictive equations regarding coastal transports*, in proc. of the 15th conference on Coastal Engineering, ASCE, 1976.
- Symonds, G., *Long waves on beaches and dynamics of surf zone forcing*, Ph.D. thesis, Dalhousie University, Halifax, Nova Scotia, Canada, 1982.
- Symonds, G., D.A. Huntley, and A.J. Bowen, *Two-dimensional surf beat: long wave generation by a time-varying breakpoint*, J. Geophys. Res., 87(C1), 492-498, 1982.
- Thornton, E.B., *Variation of lonshore current across the surf zone*, Proc. of the 12th Conf. on Coastal Engineering, New York, ASCE, 291-308, 1970.
- Thornton, E.B., *Distribution of sediment transport across the surf zone*, In proc. of the 12th Int. conference on Coastal Engineering, ASCE, 1049-1068, 1973.
- Thornton, E.B., *Energetics of breaking waves within the surf zone*, J. Geophys. Res., 84, 4931-4938, 1979.
- Thornton, E.B. and R.T. Guza, *Longshore currents and bed shear stress*, proc. conf. on directional wave spectra application, New York, ASCE, 147-164, 1981.
- Thornton, E.B. and R.T. Guza, *Energy saturation and phase speeds measured on a natural beach*, J. of Geophys. Res., 87(C12), 9499-9508, 1982.
- Thornton, E.B. and R.T. Guza, *Transformation of wave height distribution*, J. of Geophys. Res., 88(C10), 5925-5938, 1983.
- Thornton, E.B. and R.T. Guza, *Surf zone longshore currents and random waves: Field data and models*, J. Phys. Oceanography, in press, 1986.
- Tucker, M.J., *Surf beats: sea wave of 1 to 5 minute period*, Proc. Royal Soc. London, Ser. A., 202, 565-573, 1950.
- Unna, P.J., *Waves and tidal streams*, Nature, London, 149, 219-220, 1942.
- Unna, P.J., *Sea waves*, Nature, London, 159, 239-242, 1947.
- Ursell, F., *Edge waves on a sloping beach*, Proc. Roy. Soc. A, 214, 79-97, 1952.

- Ursell, F., *Steady wave patterns on a non-uniform steady fluid flow* J. Fluid Mech., 9, 333-346, 1960.
- Van Dorn, W.G., *Set-up and run-up in shoaling breakers*, proc. of the 15th conference on Coastal Engineering, 739-751, 1976.
- Waddel, E., *Dynamics of swash and implication to beach response*, Coastal studies Institute, Tech. Rep. 139, Louisiana State Univ., 49 pp., 1973.
- Watts, G.M., *A study of sand movement at South Lake Worth inlet, Florida*: U.S. Army Corps of Engineers, Beach erosion board, Tech. Memo. No. 42, 24 pp., 1953.
- White, T.E. and D.L. Inman, *Measuring longshore transport with tracers*, Chapter 13 in NSTS Report, (in press).
- Whitham, G.B., *A note on group velocity*, J. Fluid Mech., 9, 347-352, 1960.
- Wood, W.L. and G.A. Meadows, *Unsteadiness in longshore currents*, J. Geophys. Res. letters, 2,(11), 1975.
- Wright, L.D., *Field observations of long-period of surf-zone standing waves in relation to contrasting beach morphologies*, Aust. J. Mar. Freshwater Res., 33, 181-201, 1982.
- Wright, L.D., B.G. Thom, and J. Chappell, *Morphological variability of high energy beaches*, Proc. of the 16th Coastal Engineering conference, 1180-1194, 1978.
- Wright, L.D., J. Chappell, B.G. Thom, M.P. Bradshaw, and P.J. Cowell, *Morphodynamics of reflective and dissipative beach and inshore systems: Southeastern Australia*, Marine Geology, 32, 105-140, 1979.
- Wright, L.D., R.T. Guza, and A.D. Short, *Dynamics on a high energy dissipative beach*, Marine Geology, 45, 41-62, 1982.
- Wu, C.S. and P.L.-F. Liu, *Effects of non-linear forces on nearshore currents*, Coastal Engineering, 8, 15-32, 1984.
- Wu, C.S., E.B. Thornton, and R.T. Guza, *Waves and longshore currents: comparison of a numerical model with field data*, J. Geophys. Res., 90, 4951-4958, 1985.
- Zenkovich, V.P., *Fluorescent substances as tracers for studying the movement of sand on the sea bed*, Experiments conducted in the U.S.S.R., Dock and Harbour Authority, 40, 280-283, 1960.

INITIAL DISTRIBUTION LIST

	No. Copies
1. Defense Technical Information Center Cameron Station Alexandria, VA 22304-6145	2
2. Library, Code 0142 Naval Postgraduate School Monterey, CA 93943-5002	2
3. Chairman, Department of Oceanography Code 68Tm Naval Postgraduate School Monterey, CA 93943-5000	1
4. Chairman, Department of Meteorology Code 63Rd Naval Postgraduate School Monterey, CA 93943-5000	1
5. Prof. E.B. Thornton Code 68Tm Department of Oceanography Naval Postgraduate School Monterey, CA 93943-5000	2
6. Dr. C.S. Wu Code 68Wu Naval Postgraduate School Monterey, CA 93943-5000	1
7. Saad M. Abdelrahman code 68Ad Department of Oceanography Naval Postgraduate School Monterey, CA 93943-5000	2
8. Office of Naval Research (Code 420CS) Naval Ocean Research and Development Activity 800 N. Quincy Street Arlington, VA 22217	1
9. Director Naval Oceanography Division, Naval Observatory 34th and Massachusetts Avenue NW Washington, DC 20390	1
10. The Director U.S. Army Coastal Engineering Research Center Kingman Building Ft. Belvoir, VA 22060	1
11. Library School of Oceanography Oregon State University Corvallis, OR 97331	1
12. Ports And Lighthouses Administration Civil Engineering Department Attn. Dr. Helmy Awad Ras El-Tin, Elgomrok, Gate # 1 Alexandria, Egypt	1

- | | | |
|-----|-----------------------------------------------------------------------------------------------------------------------|---|
| 13. | Commander
Naval Oceanography Command
NSTL station
Bay St. Louis, MS 39522 | 1 |
| 14. | Ministry of Maritime Transport
Attn: Admiral Wassfi Abbas
4 Battalsa street
Alexandria, Egypt | 1 |
| 14. | The Commanding Officer
Naval Oceanographic office
NSTL station
Bay St. Louis, MS 39522 | 1 |
| 15. | The Commanding Officer
Fleet Numerical Oceanography Center
Monterey, CA 93940 | 1 |
| 16. | The Commanding Officer
Naval Ocean Research and
Development Activity
NSTL station
Bay St. Louis, MS 39522 | 1 |
| 17. | Chairman, Oceanography Department
U. S. Naval Academy
Annapolis, MD 21402 | 1 |
| 18. | Scientific Liaison Office
Office of Naval Research
Scripps Institution of Oceanography
La Jolla, CA 92037 | 1 |
| 19. | Library
Department of Oceanography
University of Washington
Seattle, WA 98105 | 1 |
| 20. | Library
CICESE
P. O. Box 4803
San Ysidro, CA 92073 | 1 |
| 21. | Library
Scripps Institution of Oceanography
P. O. Box 2367
La Jolla, CA 92037 | 1 |
| 22. | Commander
Oceanographic Systems Pacific
Box 1390
Pearl Harbor, HI 96860 | 1 |
| 23. | Commanding officer
Naval Environmental Prediction
Research Facility
Monterey, CA 93940 | 1 |
| 24. | Chief of Naval Research
800 N. Quincy Street
Arlington, VA 22217 | 1 |

END

1-87

DTIC